



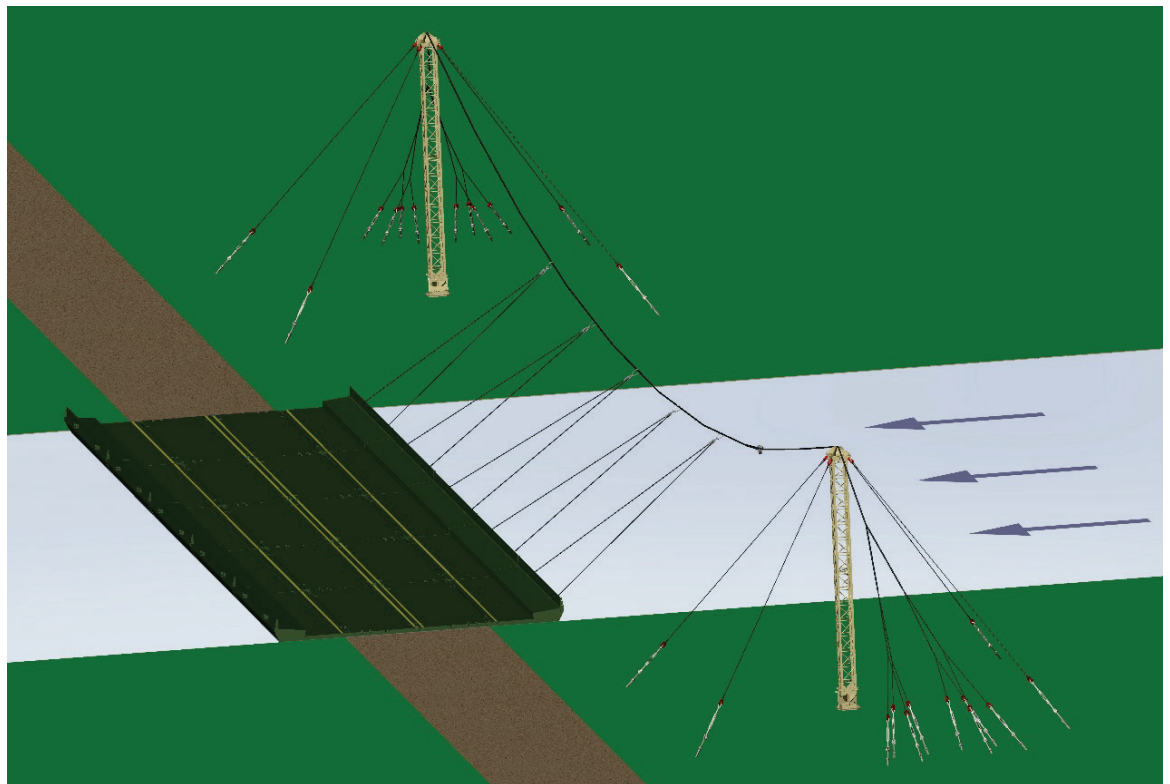
**US Army Corps
of Engineers®**
Engineer Research and
Development Center



Modernization and Structural Evaluation of the Improved Overhead Cable System

M. Wesley Trim, Matthew P. Murray, and C. Kennan Crane

March 2021



The U.S. Army Engineer Research and Development Center (ERDC) solves the nation's toughest engineering and environmental challenges. ERDC develops innovative solutions in civil and military engineering, geospatial sciences, water resources, and environmental sciences for the Army, the Department of Defense, civilian agencies, and our nation's public good. Find out more at www.erdclibrary.on.worldcat.org/discovery.

To search for other technical reports published by ERDC, visit the ERDC online library at <http://www.erdclibrary.on.worldcat.org/discovery>.

Modernization and Structural Evaluation of the Improved Overhead Cable System

M. Wesley Trim, Matthew P. Murray, and C. Kennan Crane

*Geotechnical and Structures Laboratory
U.S. Army Engineer Research and Development Center
3909 Halls Ferry Road
Vicksburg, MS 39180-6199*

Final report

Approved for public release; distribution is unlimited.

Prepared for U.S. Army, PdM Bridging
6501 East 11 Mile Road
Warren, MI 48397-5000

Under MIPR 11326139

Abstract

A modernized Overhead Cable System (OCS) prototype for a 689 ft (210 m) Improved Ribbon Bridge (IRB) crossing was designed, assembled, and structurally tested. Two independent structural tests were executed, i.e., a component-level compression test of the BSS tower was performed to determine its load capacity and failure mode; and a system-level ‘dry’ test of the improved OCS prototype was conducted to determine the limit state and failure mode of the entire OCS. In the component-level compression test of the BSS tower, the compressive capacity was determined to be 102 kips, and the failure mode was localized buckling in the legs of the tower section. During system-level testing, the prototype performed well up to 40.5 kips of simulated drag load, which corresponds to a uniformly distributed current velocity of 10.7 ft/s. If a more realistic, less conservative parabolic velocity distribution is assumed instead, the drag load for an 11 ft/s current is 21.1 kips. Under this assumption, the improved OCS prototype has a factor of safety of 1.9, based on a 689-ft crossing and 11-ft/s current. The OCS failed when one of the tower guy wires pulled out of the ground, causing the tower to overturn.

Contents

Abstract	ii
Figures and Tables	v
Preface	viii
1 Introduction	1
1.1 Background.....	1
1.2 Objective.....	3
1.3 Approach	3
2 Improved OCS prototype development	5
2.1 Design procedure	5
2.1.1 Main Anchor (Catenary) Cable	6
2.1.2 Bridle line connections	9
2.1.3 BSS towers	11
2.1.4 Anchorage	13
2.1.5 Catenary tensioning.....	22
2.2 Prototype design summary	23
3 Component-level testing of the BSS tower	29
3.1 Overview of BSS tower	29
3.2 BSS tower testing methodology.....	30
3.2.1 Test arrangement.....	30
3.2.2 Instrumentation and data collection.....	33
3.2.3 Test procedure	37
3.3 BSS tower test results and discussion.....	37
3.3.1 Time history data.....	37
3.3.2 BSS tower capacity and compressive failure mode.....	41
3.4 Component-level testing summary and conclusions.....	43
4 System-level testing of the improved overhead cable system prototype	44
4.1 Full-scale OCS testing methodology	44
4.1.1 Testing approach	44
4.1.2 Test arrangement and procedure	46
4.1.3 Instrumentation.....	48
4.2 OCS test results and discussion.....	53
4.2.1 Failure mode	62
4.2.2 BSS tower load analysis	65
4.3 Loading equivalents for uniform versus parabolic river current distributions.....	68
4.4 System-level testing summary and conclusions.....	71
5 Summary and conclusions	72

5.1	Summary of unresolved issues with the improved OCS prototype.....	72
5.1.1	<i>Helical anchors unable to penetrate all soil types</i>	72
5.1.2	<i>Synthetic rope constructional elongation</i>	73
5.1.3	<i>BSS tower modifications</i>	74
5.1.4	<i>Differing bank heights</i>	79
5.1.5	<i>Approach guys and downstream anchorage</i>	80
5.1.6	<i>Optimal OCS configurations for various crossings</i>	80
5.1.7	<i>Effects of vehicular loading on the OCS</i>	81
5.1.8	<i>OCS scalability</i>	81
5.2	Conclusions.....	82
	References	85
	Unit Conversion Factors	86
	Report Documentation Page	

Figures and Tables

Figures

Figure 1. Typical short-term IRB anchorage. Adapted from (Headquarters 2003b).	1
Figure 2. Typical IRB shore guy anchorage for 0–3 ft/s currents. Adapted from (Headquarters 2003b).....	2
Figure 3. Typical IRB overhead cable system for 3–11 ft/s currents. Adapted from (Headquarters 2003b).....	2
Figure 4. Plan and elevation views of an OCS.	6
Figure 5. OCS design worksheet provided in (Headquarters 2003b).	7
Figure 6. Table for determining cable size and number of cables from (Headquarters 2003b).....	7
Figure 7. Bridle line connector from (Headquarters 2003b).	10
Figure 8. Prototype bridle line connection detail.	10
Figure 9. BSS tower assembly from (Headquarters 2003b).	11
Figure 10. Possible tower heights from (Headquarters 2003b).	12
Figure 11. Deadman from (Headquarters 2003b).	13
Figure 12. Deadman systems tested in unpacked sand (Mejias-Santiago 2018).	14
Figure 13. Diagram showing load transfer from helical anchor bearing plates into surrounding soil.	15
Figure 14. Models of anchor array connections using tension-distributing pulley arrangements.....	15
Figure 15. Example of v-bridle concept.	16
Figure 16. Method used to connect eight anchors to the single catenary line.....	16
Figure 17. V-bridle rope sizes used to connect the catenary to the helical anchors in the prototype OCS.....	17
Figure 18. Prototype v-bridle rope assembly.....	18
Figure 19. Anchor layout for modernized OCS prototype.	19
Figure 20. Anchor array layout procedure (Steps 1-2).....	19
Figure 21. Anchor array layout procedure (Steps 3-5).....	20
Figure 22. Installation of the helical anchor deadman system.	21
Figure 23. Modernized OCS anchorage components.	22
Figure 24. Catenary tensioning method.	23
Figure 25. Improved OCS prototype assembly.....	24
Figure 26. (a) Assembled BSS tower and (b) exploded view of tower components used to support the OCS.....	29
Figure 27. Overview of the BSS Tower compression testing arrangement on the strong-floor.	30
Figure 28. Tower Cap modification for compressive load testing.	31
Figure 29. Modified cap to actuator connection.	31

Figure 30. BSS tower baseplate to strong-floor connection.	32
Figure 31. Fully assembled BSS tower.....	32
Figure 32. Strain gauge rosette locations.	34
Figure 33. Axial strain gauge locations.....	35
Figure 34. Displacement potentiometer locations.....	36
Figure 35. Load time history data.	38
Figure 36. Displacement time history data.....	39
Figure 37. Strain gauge rosette time history data.	40
Figure 38. Axial strain gauge time history data.	41
Figure 39. Compressive load versus displacement response of the BSS tower.....	42
Figure 40. Initial buckling of tower section leg near the top of the tower at 102 kips.	42
Figure 41. Secondary buckling of tower section legs near the base of the tower at 130 kips.....	43
Figure 42. (a) Photograph and (b) schematic of the actual IRB/OCS arrangement.	45
Figure 43. Mechanical loading concept.	45
Figure 44. OCS test site with overlaid topography.....	46
Figure 45. Plan and elevation views of the full-scale OCS test setup.....	47
Figure 46. Plan view of OCS showing gauge locations and identifiers.....	49
Figure 47. Bridle line tension measurement. Gauge B1 is shown; gauges B2 - B30 are similar.....	50
Figure 48. Helical ground anchor load measurement. Instrumented anchors for tower 2 are shown; tower 1 anchors were identically instrumented.....	51
Figure 49. Catenary tension measurement. Gauge C1 is shown; gauge C2 was symmetrically located on the other end of the catenary near tower 2.....	52
Figure 50. Tower tilt measurements. Tower 2 inclinometers are shown; tower 1 inclinometers were similar.....	53
Figure 51. Calculated and actual drag loads versus uniform current velocity.	57
Figure 52. Catenary tension measurements from load cells C1 and C2.....	58
Figure 53. Tower guy anchor load data: (a) guy #1 for tower 1 and 2, (b) guy #2 for tower 1 and 2. Guys #3 and #4 are not plotted as they remained slack (tension=0).	59
Figure 54. Anchor array load data: (a) A1-1 and A2-1, (b) A1-2 and A2-2, (c) A1-3 and A2-3, (d) A1-4 and A2-4, (e) A1-5 and A2-5, (f) A1-6 and A2-6, (g) A1-7 and A2-7, (h) A1-8 and A2-8.	61
Figure 55. Tower tilt angle data: (a) tower 1 and 2 tilt in X- (crossing) direction, and (b) tower 1 and 2 tilt in Z- (downstream) direction.	62
Figure 56. Tower 1 failure progression: (a) initial state, $v=0$ ft/s, (b) $v=9$ ft/s, (c) $v=10$ ft/s, and (d) failure at $v=10.7$ ft/s.	63
Figure 57. Tower 1 failure photographs.	64
Figure 58. Maximum forces on tower 1.....	65

Figure 59. Diagram showing the resultant catenary load on tower 1 obtained by vector addition.....	66
Figure 60. Free-body diagram used to determine the reaction force at the base of the tower 1.....	67
Figure 61. Parabolic and uniform velocity profiles for an 11 ft/s current.....	68
Figure 62. Equivalent drag forces for uniform versus parabolic current distributions.....	70
Figure 63. Chance ROCK-IT™ helical lead section designed to penetrate rocky soils.....	72
Figure 64. Loss of catenary tension: (a) initial sag and (b) sag after 3 days.....	73
Figure 65. Load versus elongation chart for 1.75-in.-diam EverSteel™-X rope provided by Samson Inc.....	74
Figure 66. BSS tower baseplate modification.	75
Figure 67. Post-test photographs of (a) tower 1 and (b) tower 2 baseplates.	76
Figure 68. Tower cap rope departure angle issue.....	77
Figure 69. BSS tower cap modification concept.	78
Figure 70. Catenary tensioning issue.	79

Tables

Table 1. Rope assemblies and COTS connectors (items RA-1 through RA-8, CS-1, and BL-1).....	25
Table 2. Tower assembly (items T-1 through T-11).....	27
Table 3. Helical anchor assembly (items H-1 through H-5).....	28
Table 4. BSS tower instrumentation summary.....	33
Table 5. OCS test load matrix.....	48
Table 6. OCS test instrumentation package.	49
Table 7. OCS test pull #1 data.....	55
Table 8. OCS test pull #2 data.	56
Table 9. Drag force on each IRB bay for a 689 ft (210 m), 11 ft/s crossing assuming the river has a parabolic velocity profile.....	69

Preface

This study was conducted for Product Manager, Bridging (PdM Bridging), under MIPR 11326139.

This work was performed by the Structural Engineering Branch (GSS) and the Structural Mechanics Branch (GSM) of the Geosciences and Structures Division (GS), U.S. Army Engineer Research and Development Center, Geotechnical and Structures Laboratory (ERDC-GSL). At the time of publication, Mrs. Mariely Mejias-Santiago was Chief, GSS; Mr. Brad Steed was Chief, GSM; Mr. James L. Davis was Chief, GSD; and Mr. Nicholas Boone, GZI, was the Technical Director for Force Projection and Maneuver Support. The Deputy Director of ERDC-GSL was Mr. Charles W. Ertle II, and the Director was Mr. Bartley P. Durst.

COL Teresa A. Schlosser was the Commander of ERDC, and Dr. David W. Pittman was the Director.

1 Introduction

1.1 Background

The Improved Ribbon Bridge (IRB) Operator's Manual (Headquarters 2003a) is the foremost source of information regarding IRB operations. The manual covers all IRB operations such as launching, bridge construction, maintenance, etc. Bridge anchorage is covered in work package (WP) 0035 of the IRB Operator's Manual (Headquarters 2003b). WP0035 provides anchorage information based on how long the bridge is to remain in place and the current velocity of the river being crossed.

If a bridge is needed only for a short time, a temporary system of anchorage that utilizes Bridge Erection Boats (BEBs) and approach guys (cables) is used to hold the bridge, as shown in Figure 1. If the IRB is to remain for an extended period of time, the manual (Headquarters 2003b) states that for currents between 0 and 3 ft/s, BEBs can be replaced with upstream and downstream anchorage using shore guys. Shore guy anchorage is illustrated in Figure 2. For currents between 3.1 and 11 ft/s, an overhead cable system (OCS) must be used according to the manual. The OCS is the focus of the present work. A typical OCS is shown in Figure 3.

Figure 1. Typical short-term IRB anchorage. Adapted from (Headquarters 2003b).

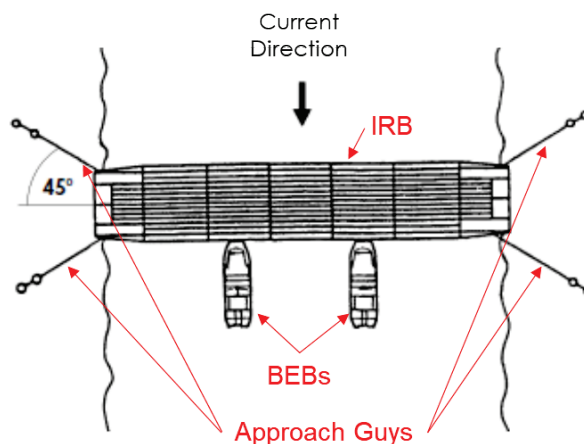


Figure 2. Typical IRB shore guy anchorage for 0–3 ft/s currents. Adapted from (Headquarters 2003b).

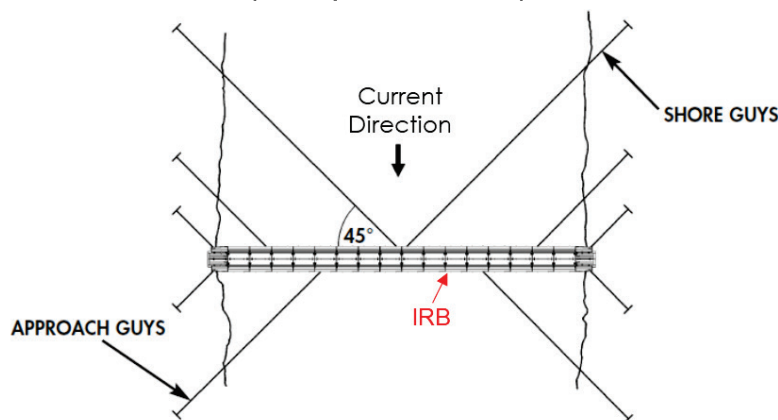
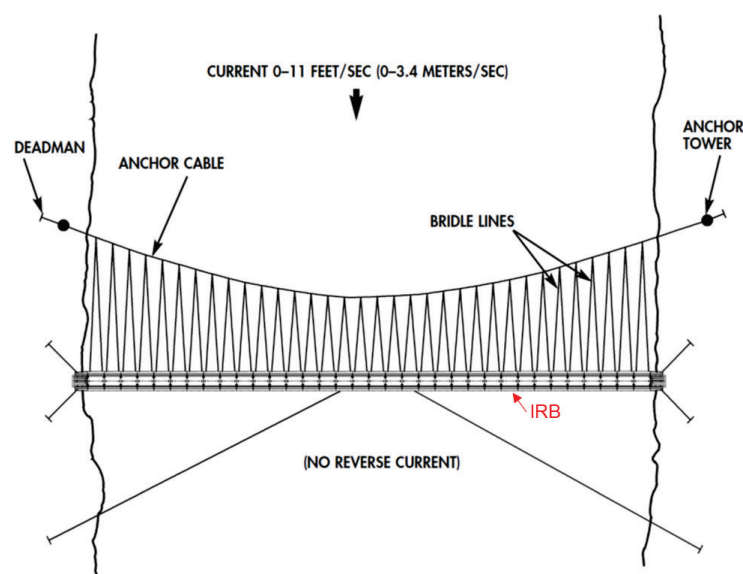


Figure 3. Typical IRB overhead cable system for 3–11 ft/s currents. Adapted from (Headquarters 2003b).



The IRB manual (Headquarters 2003b) states that the components necessary to install the standard overhead cable system are supplied in the IRB supplemental set SC-5420-97-CL-E51. This is also referred to as the Bridge Supplemental Set or BSS. The majority of the materials and tools in that supply catalog, which was originally published in 1974, are obsolete by today's standards. This has left a capability gap within the Multi-Role Bridge Company (MRBC) to conduct sustained gap-crossing operations. A Capability Production Document (CPD) for the BSS was issued with the intention of modernizing the BSS. The CPD (MSCoE 2014) reads

“The BSS will have modernized and standardized tools needed to construct, repair and or reduce obstacles for bridging sites from present to 2041. BSS resolves or reduces capability gaps throughout the entire range of military operations and provides unrestricted functionality while facilitating troop labor intensive tasks pertaining to bridge construction. The BSS provides the MRBC with a float bridge anchorage capability.”

The BSS CPD also specifies that in order to meet threshold requirements, the OCS must anchor 689 ft (210 m) of IRB in currents up to 11 ft/s. The maximum gap and current speed that the legacy OCS was ever previously tested to was 420 ft (128 m) and 4 ft/s (ATEC 2003, 2002). In March 2019, the Office of the Product Manager (PdM) Bridging tasked the ERDC with developing and testing a modernized overhead cable system that met this threshold requirement. The BSS project was placed on an accelerated schedule because of impending programmatic deadlines. The BSS program was slated to enter the production and deployment (PD) phase in FY20.

1.2 Objective

This report documents the development and structural testing of the improved OCS prototype kit. The objectives of this work were to design a modernized OCS, build a prototype, and structurally evaluate the prototype to verify that it met the BSS CPD threshold requirements for IRB anchorage.

1.3 Approach

Previous work conducted by ERDC (Bryant et al. 2019, Trim and Padula 2020), which related water current velocity to IRB drag loading, was leveraged to estimate design loads for the OCS. The OCS was redesigned to accommodate the expected loading. Several of the legacy OCS materiel solutions were replaced with modern alternatives. However, several major aspects of the design were not revised due to the limited amount of time and resources available to meet imminent programmatic deadlines associated with entering the PD phase at Milestone C. An improved OCS prototype for a 689 ft (210 m) IRB crossing was then built at ERDC using the revised OCS design. A full-scale ‘dry’ test of the prototype was executed where the fluid-induced drag load was simulated with mechanical loading. This allowed for a safe, controllable test with directly measurable load inputs while eliminating the need for massive volumes of fast-moving water. The improved OCS prototype was tested to failure in order to determine the limits of the system.

In this final report, Chapter 2 describes the improved OCS prototype and its development. Chapters 3 and 4 pertain to the structural testing and evaluation that was performed to ensure the improved OCS prototype met requirements. Finally, Chapter 5 provides a summary of the work, documents key lessons learned, and consolidates conclusions.

2 Improved OCS prototype development

The design of a float bridge anchorage system is influenced by a multitude of factors, including:

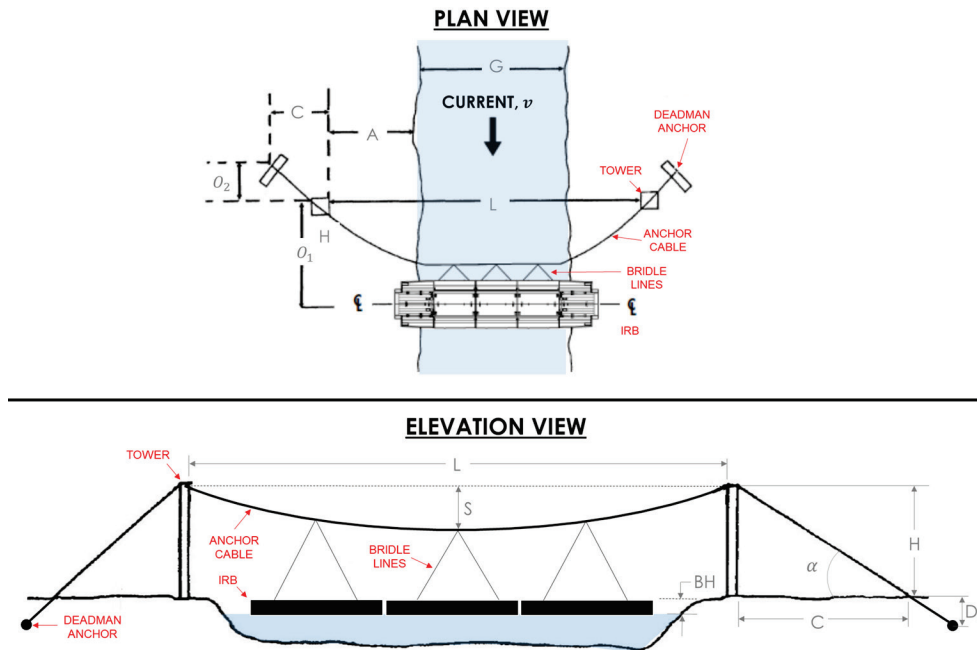
- Available equipment
- Available personnel
- Available construction time
- Crossing duration
- Depth of the groundwater table
- Drag characteristics of the float bridge
- Height and slope of the river banks
- River current velocity
- River width
- River depth
- River bottom conditions
- Soil conditions at ground anchor locations

Each of these factors was considered in the development of a modernized, improved overhead cable anchorage system for the IRB. Section 2.1 outlines the improved OCS prototype design procedure. The initial prototype assembly is detailed in section 2.2. There, an assembly schematic is provided along with a list of all components required to construct the improved OCS.

2.1 Design procedure

The procedure provided in the IRB Operator's Manual (Headquarters 2003b) was followed as closely as possible to design an OCS for a 689 ft crossing with 11 ft/s current, i.e. the threshold requirement crossing defined in the BSS CPD. Figure 4 shows a schematic of the overhead cable system. The major components of the system are labeled along with the various dimensions used in the design procedure.

Figure 4. Plan and elevation views of an OCS.



2.1.1 Main Anchor (Catenary) Cable

The IRB Operator's Manual provides the worksheet shown in Figure 5 for the OCS designer to complete. The first step is to determine the number and size of the master cable(s). For this, the manual instructs the designer to use the table shown in Figure 6. The table refers to 'normal' and 'reinforced' bridge types. These are legacy float-bridge types that do not apply to the IRB. This discrepancy was investigated, and it was found that the table shown in Figure 6 was taken directly from TC 5-210, Appendix C (Headquarters 1988). This poses a problem because those legacy float bridges have drastically dissimilar fluid drag characteristics compared to the IRB. The drag loads that an OCS must resist are decidedly different for a Class 60 float bridge and an IRB. The fact that the table used to size the OCS for the IRB was taken directly from another type of bridge immediately raised concerns.

Figure 5. OCS design worksheet provided in (Headquarters 2003b).

1. CABLE DATA	
Number of master cables	_____
Size of master cable(s) (C_D)	_____
Length of master cable(s) (C_L)	_____
Number of clips at each end of cable	_____
Spacing of cable clips	_____
Initial sag (S)	_____
2. TOWER DATA	
Actual tower height (H)	_____
Near shore	_____
Far shore	_____
Tower-waterline distance (A)	_____
Near shore	_____
Far shore	_____
Tower-bridge offset (O_1)	_____
Near shore	_____
Far shore	_____
3. DEADMAN DATA	
Depth of deadman (D_D)	_____
Near shore	_____
Far shore	_____
Tower-deadman distance (C)	_____
Near shore	_____
Far shore	_____
Tower-deadman offset (O_2)	_____
Near shore	_____
Far shore	_____
Deadman face (D_f)	_____
Deadman thickness (D_t)	_____
Deadman length (D_L)	_____
Near shore	_____
Far shore	_____
Bearing plate thickness (x)	_____
Bearing plate length (y)	_____

Figure 6. Table for determining cable size and number of cables from (Headquarters 2003b).

Wet gap width (G) (feet)	Type bridge assembly	Size (inches) and number of cables for specified river velocities											
		5 FPS			7 FPS			9 FPS			11 FPS		
		Single	Dual	Triple	Single	Dual	Triple	Single	Dual	Triple	Single	Dual	Triple
200	Normal	1/2	3/8	3/8	5/8	1/2	1/2	3/4	5/8	1/2	7/8	3/4	5/8
	Reinforced	5/8	1/2	3/8	3/4	5/8	1/2	7/8	3/4	5/8	1-1/8	7/8	3/4
400	Normal	5/8	1/2	1/2	3/4	5/8	1/2	1	7/8	5/8	1-1/4	1	3/4
	Reinforced	3/4	5/8	1/2	1	3/4	5/8	1-1/4	1	3/4	1-1/2	1-1/4	7/8
600	Normal	3/4	5/8	1/2	1	3/4	5/8	1-1/4	1	3/4	1-1/2	1-1/4	7/8
	Reinforced	1	3/4	5/8	1-1/8	1	3/4	1-1/2	1-1/4	7/8	*	1-1/2	1-1/8
800	Normal	7/8	3/4	5/8	1-1/8	7/8	3/4	1-3/8	1-1/8	7/8	*	1-1/2	1-1/8
	Reinforced	1-1/8	7/8	3/4	1-3/8	1-1/8	7/8	*	1-3/8	1	*	*	1-1/4
1000	Normal	1	7/8	3/4	1-1/4	1	7/8	1-1/2	1-3/8	1	*	*	1-1/4
	Reinforced	1-1/4	1	3/4	1-1/2	1-1/4	1	*	*	1-1/8	*	*	1-3/4
1200	Normal	1-1/8	7/8	3/4	1-3/8	1-1/8	7/8	*	1-1/2	1-1/8	*	*	1-3/8
	Reinforced	1-3/8	1-1/8	7/8	*	1-3/8	1	*	*	1-1/4	*	*	*

Notes.
 1. All values are based upon Improved Plough Steel cable and a 2 percent initial sag.
 2. Asterisks (*) indicate that it is unsafe to construct that system.

Another issue with the cable sizing table shown in Figure 6 is that it relies on the use of improved plough steel (IPS) cable. In the past 30 yr, since that table was developed, technological advances in synthetic cables have produced modern alternatives with properties superior to those of IPS cable. Thus, in an effort to modernize the OCS, a decision was made to replace the legacy steel cable with a modern synthetic rope.

To appropriately size the new cable, the anticipated drag load on the OCS had to be estimated. Research performed by Bryant et al. (2019) was leveraged. In that study, the hydrodynamic characteristics of the IRB were quantified via extensive flume testing using scaled models. An empirical equation was developed that related current velocity, v (ft/s) to IRB drag force, F_{drag} (lbf). Assuming there is no vehicular traffic on the bridge, the drag force on an IRB bay can be calculated for a given velocity using

$$F_{\text{drag.bay}} \text{ (lbf)} = 44.9e^{0.3184v(\text{ft/s})} \quad (1)$$

If the velocity of the river current is uniform across the entire width, the drag force on each IRB bay will be equal. So, the total drag force on the whole bridge is

$$F_{\text{drag}} \text{ (lbf)} = n_{\text{bays}} \times F_{\text{drag.bay}} \text{ (lbf)} \quad (2)$$

where, n_{bays} is the number of interior IRB bays required to span a crossing of width G (ft), which can be found from

$$n_{\text{bays}} = \frac{G-45 \text{ ft}}{22 \text{ ft}} \quad (3)$$

Assuming the current in the river is uniform across the width is a conservative assumption. The actual velocity profile across a river will vary based on many factors such as bathymetry, bottom conditions, flow rates, etc. Rivers typically flow fastest in the center and the current progressively slows toward the banks. Assuming the velocity is constant across the entire gap is effectively a ‘worst-case’ condition, so using it to develop a design load is a logical approach.

Substituting the CPD threshold requirement velocity, $v = 11$ ft/s into Eq. 1, we find that the drag force on each IRB bay is approximately 1,490 lbf (1.49 kips). For the CPD threshold requirement gap, $G=689$ ft, and Eq. 3 indicates that 30 IRB interior bays are required. Therefore, assuming a

uniform current velocity, the total drag load on the IRB is 44.7 kip (by Eq. 2). This was the design load used to size the master cable.

To ensure the towers that support the cable in the air are an adequate distance away from the river, the IRB Operator's Manual states that the distance between the towers, L , should be

$$L = 1.1G + 100 \text{ ft} \quad (4)$$

Based on the CPD threshold requirement gap, $G = 689$ ft, Eq. 4 gives $L = 858$ ft. This was the unsupported length of the main catenary used to design the improved OCS prototype.

EverSteel™-X rope (Samson Rope Technologies EverSteel-X 2020) was chosen as the replacement for standard IPS cable. EverSteel™-X has a 12-strand braided design using Dyneema® Max DM20 fiber material to achieve superior creep performance for improved service life in applications where creep results from long-term static loads. The greatest advantage of the EverSteel™-X synthetic rope is its strength-to-weight ratio, which is about 9× that of IPS cable. Another useful property of the EverSteel™-X is its low density, which allows it to float on water. Additional properties of EverSteel™-X include extremely low stretch, a low friction coefficient, superior flex fatigue, length stability over time, and excellent wear resistance (Samson Rope Technologies EverSteel-X 2020).

For the main cable size, a diameter of 1.75 in. was chosen. This size was selected based on the design load; it was also a size that would work with the existing BSS tower design. Manufacturer specifications indicate the 1-3/4 in. EverSteel™-X rope has a minimum breaking strength of 306 kips and an average breaking strength of 340 kips. Based on the design load, the maximum tension in the catenary was conservatively estimated to be 105 kips. Thus, the main cable has a safety factor against breaking of approximately 3.

2.1.2 Bridle line connections

Next, the bridle line attachment was addressed. The IRB Operator's Manual specifies that a custom bridle line connector be used. The connector, shown in Figure 7, features a pulley designed to ride along the catenary. This pulley was no longer needed because synthetic rope has a much lower friction coefficient than steel cable. So, the

modernized OCS did not require the custom pulley connectors, which could only be used with one cable size. For the improved OCS prototype, a replacement connector assembly was sourced.

Figure 7. Bridle line connector from (Headquarters 2003b).

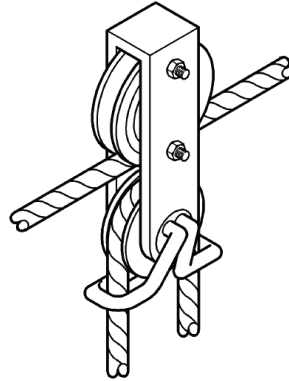
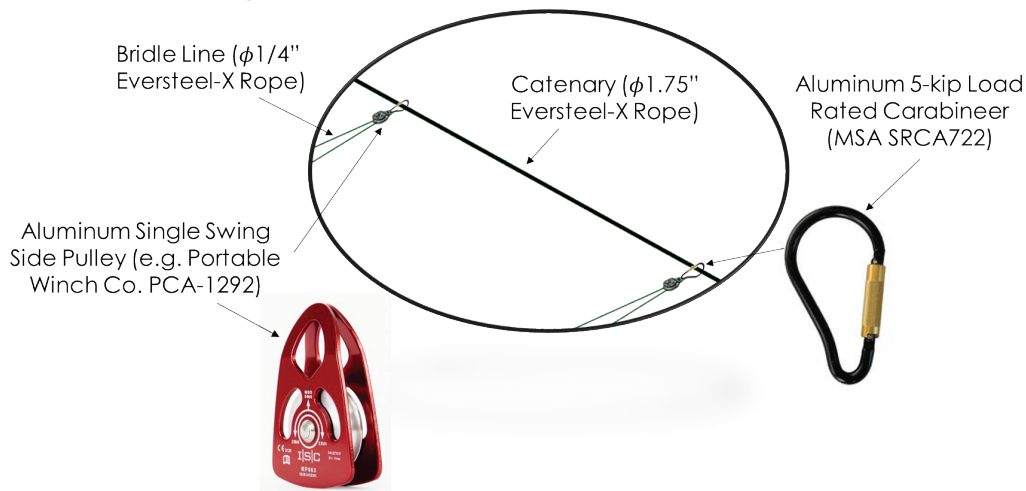


Figure 8 shows the new bridle line connection. The simple assembly uses two commercial-off-the-shelf (COTS) components i.e., one MSA model SRCA722 carabineer and one single swing side pulley, e.g. Portable Winch Co. model PCA-1292. Both components are fully aluminum to reduce the hanging weight on the catenary. For the bridle line, which feeds through the pulley and connects each IRB bay to the OCS, $\frac{1}{4}$ -in.-diam EverSteel™-X rope was chosen. The MSA SRCA722 carabineer has a gate opening of 2.1 in., so it could be used with up to 2-in.-diam main cable. The pulley can accommodate bridle lines with diameters ranging from $\frac{1}{4}$ in. to $\frac{1}{2}$ in.

Figure 8. Prototype bridle line connection detail.



The SRCA722 carabineer has a minimum breaking strength of 5 kips. The PCA-1292 pulley is rated for 11.2 kips, and the $\frac{1}{4}$ in. EverSteel™-X

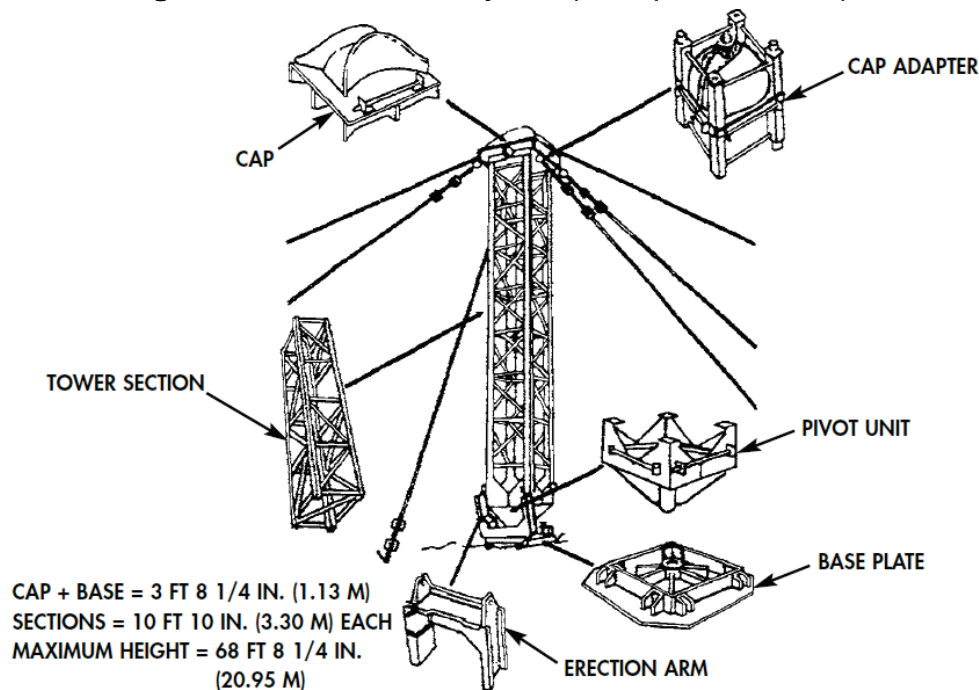
rope has a minimum strength of 7.7 kips. Therefore, the carabineer drives the safety factor of the bridle line connection. Based on the anticipated drag load per IRB bay, 1.5 kips (from Eq. 1 with $v = 11$ ft/s), the factor of safety on the bridle connection is 3.3.

2.1.3 BSS towers

Next, attention was turned to the towers that support the main catenary cable. The IRB Operator's Manual (Headquarters 2003b) states:

“When installing an overhead cable system, towers are used to ensure that the master cable remains at least 3 ft (0.9 m) above the water level. The tower components are provided and located in the Ribbon Bridge Supplemental Set. The tower assembly is made up of a tower base, a pivot unit, six tower sections, a tower cap, a cap adapter, and two wire rope slings. [Refer to Figure 9]”

Figure 9. BSS tower assembly from (Headquarters 2003b).



The towers are the primary structural members in the OCS. Due to impending programmatic deadlines, a significant tower redesign was not feasible. Therefore, a decision was made to use the legacy BSS towers in the prototype. Fabrication drawings (Amato 2012) were obtained and used to generate a 3-D CAD model of the tower.

To ensure the main catenary hangs at least 3 ft above the water, the IRB Operator's Manual instructs the designer to calculate the required height of the tower using

$$H_{req} = 3 \text{ ft} + S - BH \quad (5)$$

where, S is the initial sag in the catenary due to self-weight, and BH is the bank height. The manual specifies that a 2 percent sag (or less) is desired, i.e.,

$$S = 0.02L \quad (6)$$

For design purposes, a bank height, $BH = 0$ ft was assumed. This maximized the required height of the tower, producing a 'worst-case' condition. For the CPD threshold requirement crossing, $L = 858$ ft (from Eq. 4). Therefore, the required tower height is $H_{req} = 17.2$ ft. The IRB Operator's Manual provides the table shown in Figure 10 to determine the actual tower height, H , which is adjusted by adding or removing tower sections. Since, $H_{req} = 17.2$ ft, two tower sections were needed for the CPD threshold requirement crossing. The height of the resulting tower was $H = 25.4$ ft.

Figure 10. Possible tower heights from (Headquarters 2003b).

NUMBER OF TOWER SECTIONS	TOWER HEIGHT (H)
Cap, base, and pivot unit	3 ft 8 1/4 in. (1.13 m)
With 1 tower section	14 ft 6 1/4 in. (4.43 m)
With 2 tower sections	25 ft 4 1/4 in. (7.73 m)
With 3 tower sections	36 ft 2 1/4 in. (11.04 m)
With 4 tower sections	47 ft 1/4 in. (14.34 m)
With 5 tower sections	57 ft 10 1/4 in. (17.65 m)
With 6 tower sections	68 ft 8 1/4 in. (20.95 m)

Note that Figures 9 and 10 indicate that towers up to ~68 ft tall can be constructed. A 68-ft tower height corresponds to an unsupported span of 3,250 ft, assuming 2 percent cable sag and even bank heights. It is highly unlikely that an OCS would work for a gap of that magnitude. Uneven bank heights are beyond the scope of the current work, but future work to address the issue of differing bank heights is recommended.

No data could be found regarding the load capacity of the legacy BSS Class 60 towers. So, prior to conducting the full-scale OCS test, a component level test of a tower was performed to determine the capacity of the tower

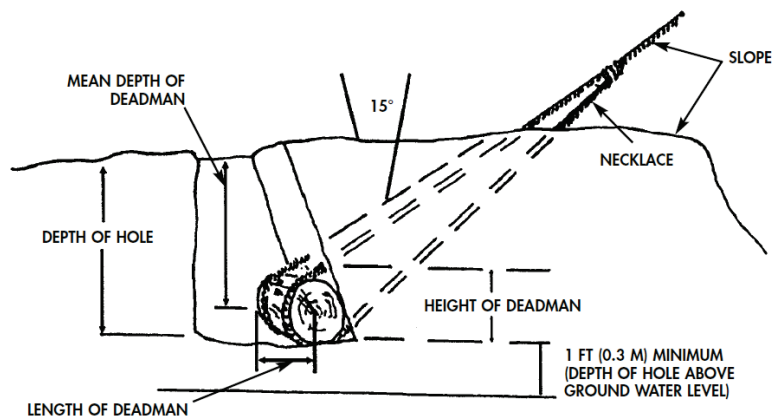
and its compressive failure mode. Chapter 3 discusses the details and results of the component level BSS tower test.

2.1.4 Anchorage

Finally, the last piece of the OCS that required design attention was the deadman anchor. Regarding the deadman, the IRB Operator's Manual (Headquarters 2003b) reads

“The use of a deadman on each shore is the preferred method of securing the overhead cable(s). [Refer to Figure 11]. These deadmen provide the holding power for the entire overhead cable system. Because of this, accurate deadman design is critical. Construct deadmen using logs, rectangular timber, steel beams, or similar objects buried in the ground with a guy line or sling attached to the deadman's center. The holding power of a deadman is affected by the frontal bearing area, mean (average) depth, angle of pull, deadman material, and soil conditions.”

Figure 11. Deadman from (Headquarters 2003b).

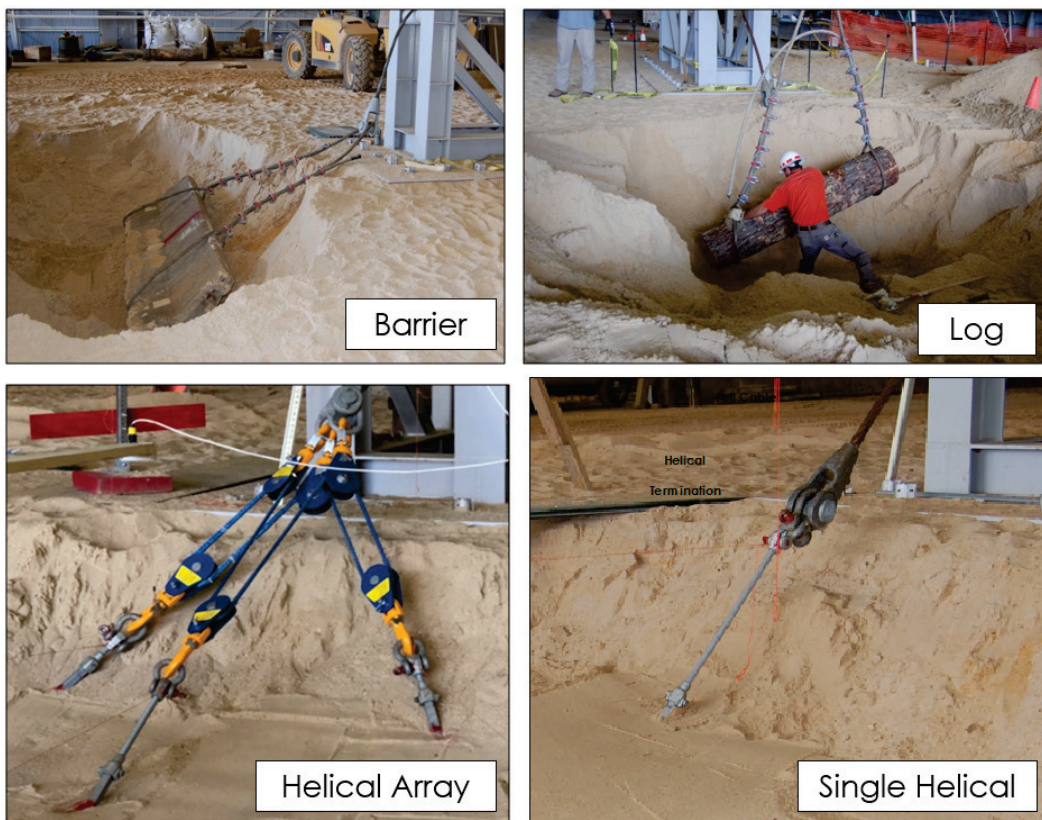


One of the main criticisms of the OCS received from user feedback was regarding the deadman installation procedure. The excavation and burying processes were considered tedious and time-consuming. So, an alternative means of anchorage was investigated for the improved OCS prototype. For design, using the CPD threshold requirement, the new anchor solution needed to resist 105 kips of catenary tension.

Previous research conducted by Mejias-Santiago (2018) quantified the load capacity of conventional log- and barrier-type deadman systems in extremely weak clay and loose-sand soils (“worst-case” scenarios). An array of helical anchors, which are commonly used for earth retention and foundation

applications, was also tested as a potential replacement to the conventional deadman systems. Figure 12 shows the various deadman systems that were evaluated. Experimental results indicated that the maximum load capacity in the loose sand soil was approximately 36, 68, and 69 kips for the log-type, barrier-type, and helical array (3 anchors) deadman systems, respectively (Mejias-Santiago 2018). The barrier-type and anchor array deadman systems were then tested in clay soil. Results indicated that the maximum load capacity in weak clay soil was approximately 57 kips for the barrier-type, 36 kips for the three helical anchor array, and 19 kips for a single helical deadman system (Mejias-Santiago 2018).

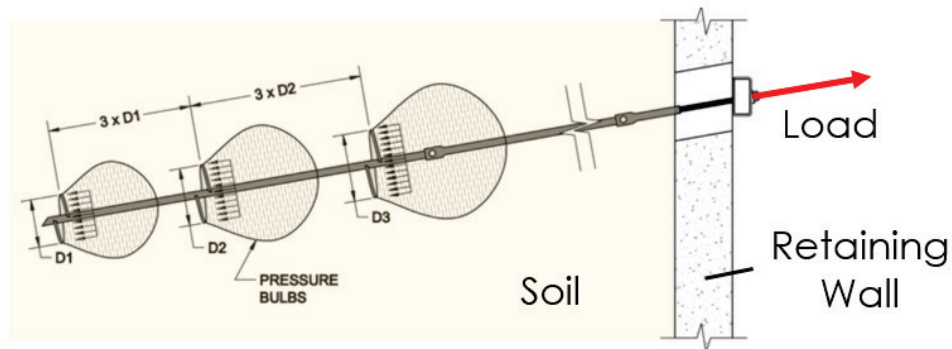
Figure 12. Deadman systems tested in unpacked sand (Mejias-Santiago 2018).



None of the systems evaluated provided the required deadman capacity of 105 kips; however, the helical anchor array was easily scaled by increasing the number of anchors used within the array. Helical anchors resist pullout by transferring forces to the soil through the helical bearing plates, as shown in Figure 13. The pulley system used to connect the helical array evaluated by Mejias-Santiago (2018) allowed for tension to be evenly distributed throughout the helical anchors under load; therefore, the individual load capacity of the anchors within the assumed, ‘worst-case’

soil conditions (weak clay) was roughly 12 kips, based on the results from the 3-anchor array. A minimum of nine anchors were therefore required to achieve the 105-kip capacity needed.

Figure 13. Diagram showing load transfer from helical anchor bearing plates into surrounding soil.



The difficulty of implementing such a system resides within the method used to connect each individual anchor to the catenary in order to transfer the tension of the OCS into the soil. Attempts were made to implement a self-correcting pulley arrangement to distribute tension evenly throughout the system. Models were constructed using wooden representations of correctly sized and spaced pulleys and helical anchors (shown in Figure 14). The system required a total of 18 high-capacity snatch blocks (pulleys) and connecting shackles. The result was a highly congested and unwieldy solution that would be nearly impossible to construct in the field due to the combined weights of the individual components.

Figure 14. Models of anchor array connections using tension-distributing pulley arrangements.



To reduce complexity, weight, and field-installation time, an alternative connection solution was developed. The new design, shown in Figure 15, was based on a v-bridle concept that is often implemented in high-load, maritime towing operations. This method allowed a stepwise reduction of load from the single catenary into eight smaller lines attached to the exposed ends of the helical anchors, as shown in Figure 16. Since an even number of anchors had to be employed to achieve a balanced system, larger (1.5 in. compared to 1.25 in.) helical anchors were selected to account for the reduction in capacity attributed with removing one of the required anchors from the array.

Figure 15. Example of v-bridle concept.

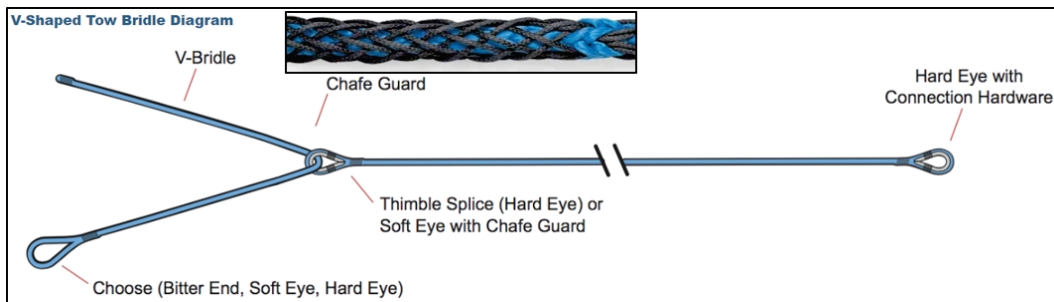
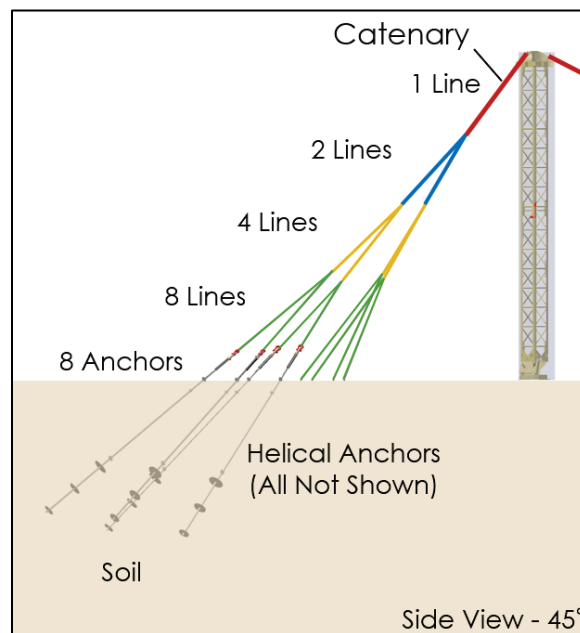


Figure 16. Method used to connect eight anchors to the single catenary line.



The v-bridle lines were made from EverSteel™-X rope of three different diameters, specifically chosen to provide the required strength of each bridle while minimizing the number of differently sized ropes used within

the modernized OCS. Figure 17 shows the number of v-bridles required for the catenary connection along with the diameter of each rope. The length of each v-bridle was minimized in order to position the Line 1 to catenary connection at the lowest possible height, which simplified installation. Each v-bridle contained an eye-splice at each end and a section of chafe guard that spanned the central section between the splices. HD Howzer thimbles were used to protect the soft eyes. The main advantage of using this model of thimble was that they could be easily installed/removed from properly sized eyes after the splices had been made, which also allowed for easier installation of the catenary connection. Figure 18 shows the various components of the v-bridle lines. Additional details regarding the rope assemblies are provided in section 2.2.

Figure 17. V-bridle rope sizes used to connect the catenary to the helical anchors in the prototype OCS.

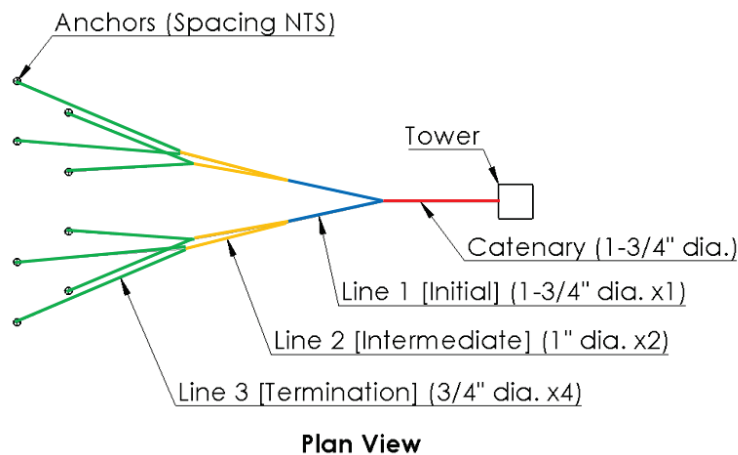
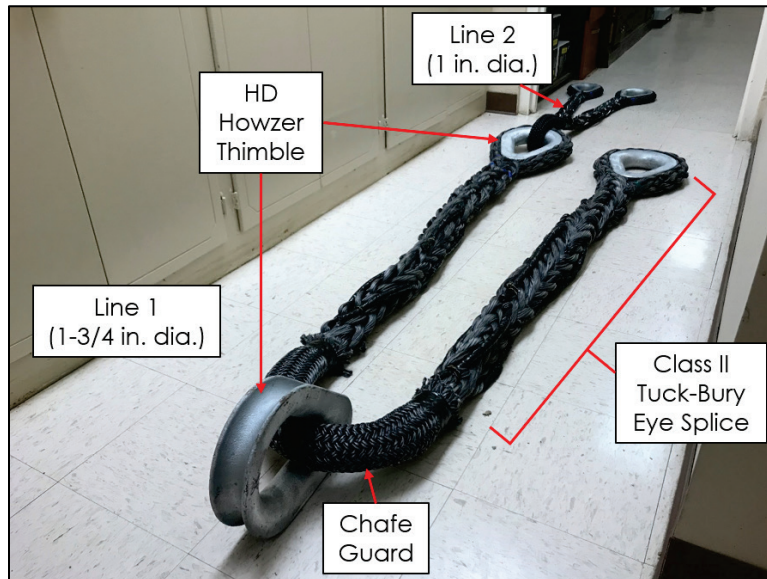


Figure 18. Prototype v-bridle rope assembly.



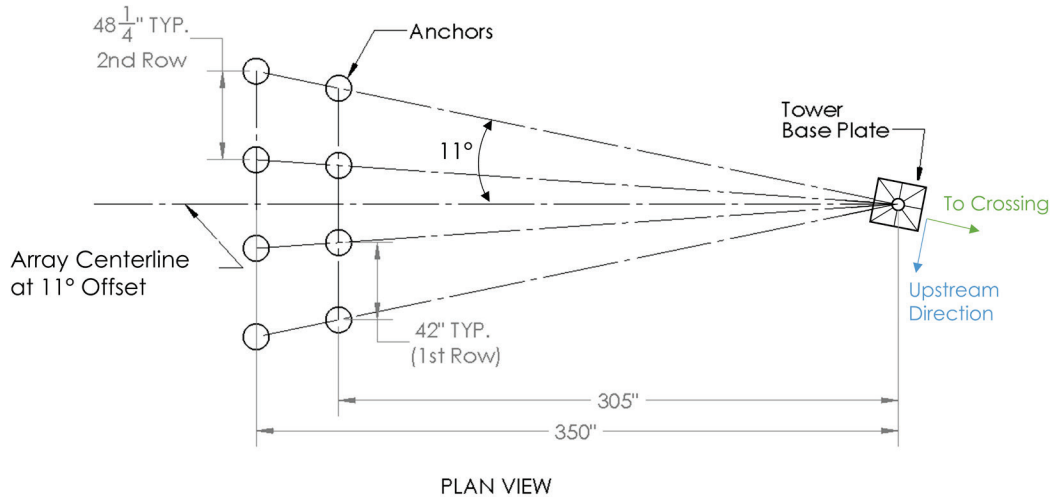
A downside to the v-bridle method was that the number of anchors, n , used to construct the array had to be a power of two, i.e., 2^n . If a larger deadman capacity was required, the next available increment of a system such as this would call for $2^4=16$ anchors. Also, the space between the ground and the top of the tower would have to be increased in order to fit the split from 8 to 16 lines, adding even more complexity into the system.

The manufacturer-recommended spacing between helical anchors is five times the largest helical diameter; however, the absolute minimum spacing was stated to be 3 ft. The model of helical chosen for the deadman system consisted of a triple-helical design with 10, 12, and 14 in. diam; therefore, the minimum recommended spacing between the anchors was 70 in. The anchor footprint required to achieve the recommended spacing would provide excessively large v-bridle angles that would increase the force on each anchor; therefore, spacing was compromised to attain smaller forces on the anchors. The compromise was justifiable since the anchors were not to be installed vertically, but rather at an angle. Once driven into the soil, the space between the subsurface helixes would be spaced adequately apart from each other.

A simple pattern was devised to minimize the ground area required to implement the 8-anchor system. The chosen spacing exceeded the absolute minimum spacing between the anchors and remained within the maximum allowable tower-to-deadman slope (45°) provided within the IRB Operator's Manual. The spacing also reduced the amount of force that

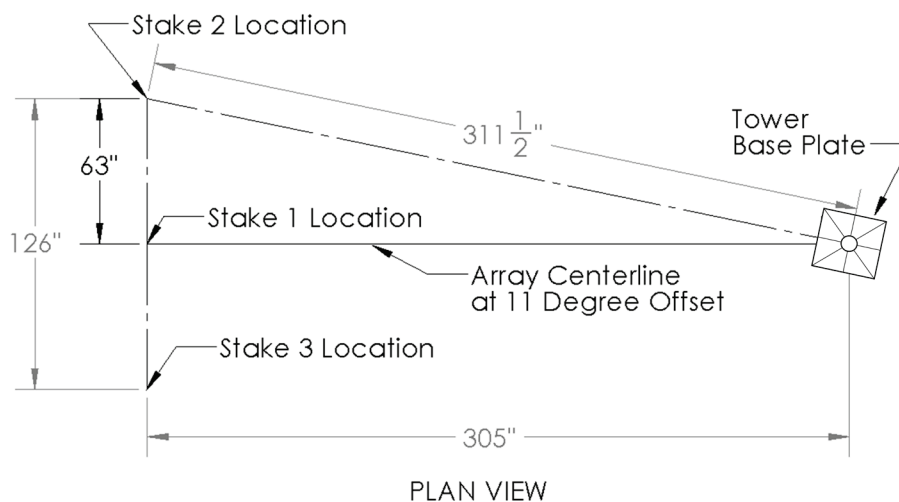
was added to each anchor due to load angle. The anchor layout for the prototype is shown in Figure 19.

Figure 19. Anchor layout for modernized OCS prototype.



The pattern utilized a layout that was simple to construct in the field. Marking the layout required three individuals with string-line, stakes, and a tape measure. The anchor array layout procedure follows. (1) The centerline of the anchor array was first marked using the upstream offset angle of 11° , which was provided by the IRB Operator's Manual. (2) Three stakes were driven along the pattern shown in Figure 20.

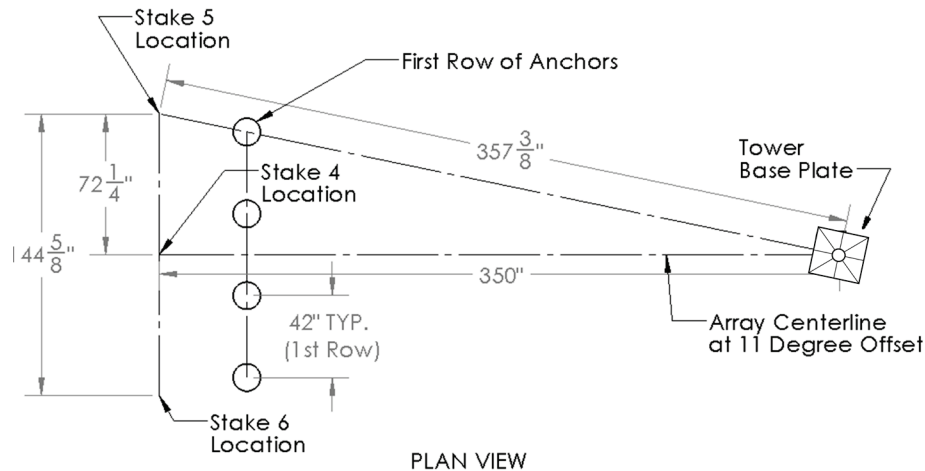
Figure 20. Anchor array layout procedure (Steps 1-2).



(3) The positions for the four anchors comprising the first row were located by drawing a line between stakes 2 and 3. Then, the ground was

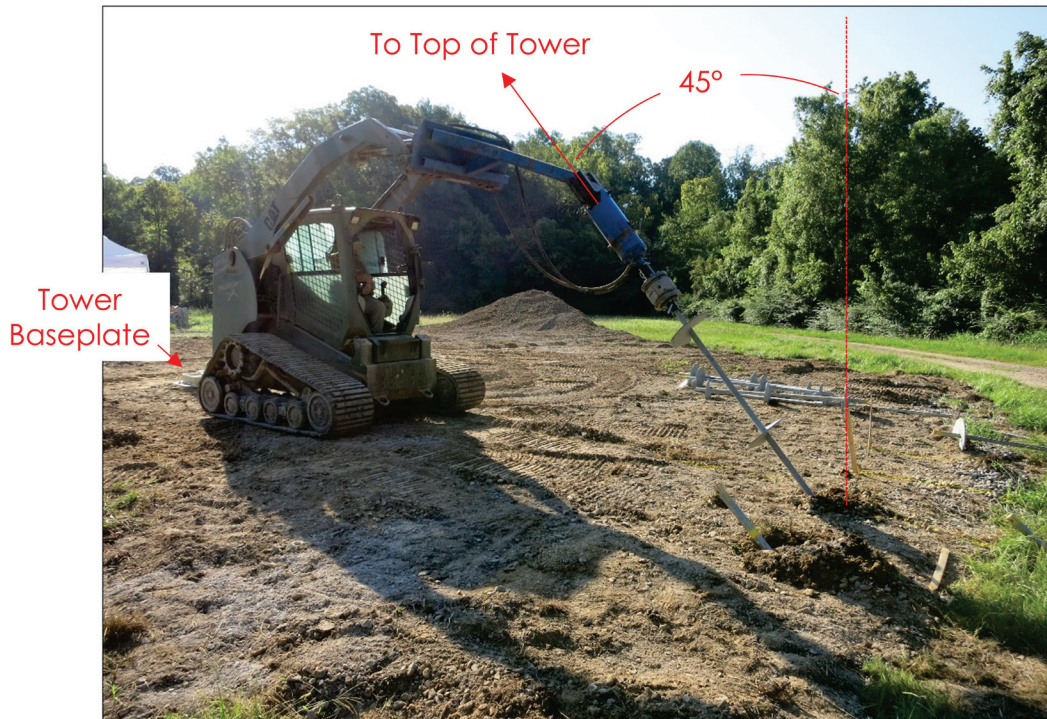
marked at the location of stakes 2 and 3 along with two additional marks on that same line such that the spacing between each of the four stakes was 42 in. (4) Stakes 4, 5, and 6 were installed to lay out another line at the distances shown in Figure 21. (5) Lastly, the positions for the second row of four anchors was marked using the point of stakes 5 and 6 and two additional points with spacing of 48.25 in., providing the final layout shown above in Figure 19.

Figure 21. Anchor array layout procedure (Steps 3-5).



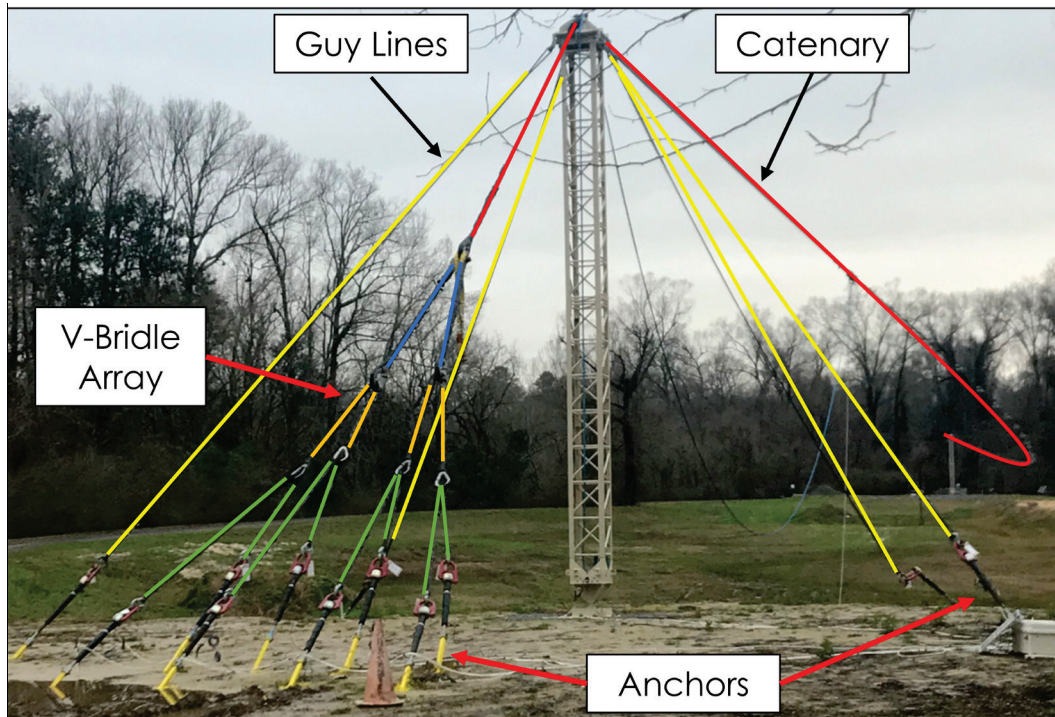
With the locations marked, the helical anchors were driven into the ground at a 45° angle, with the exposed end of each anchor pointing toward the top of the tower, as shown in Figure 22. Each anchor consisted of a lead section that contained the three helices, followed by two extension bars. Details regarding the anchors and supplemental hardware are provided in section 2.2. Approximately 12 in. of each extension rod was left exposed aboveground to facilitate supplementary hardware attachment.

Figure 22. Installation of the helical anchor deadman system.



Individual helical anchors were used to anchor the guy lines of each tower. The guy lines were also set at a 45° angle to the ground and attached to the four corners of the tower cap. The complete anchorage system for the modernized OCS is shown in Figure 23. The ‘weakest link’ within the anchorage was the single helical anchor used for the guy lines. As drag force is increasingly applied to the catenary, the tops of the towers are pulled toward the IRB, increasing the load on the guy lines’ anchors. If load onto the system continues to rise, the guy anchor will begin to pull out of the soil, and the tower will begin to noticeably lean. Further loading of the system will pull the anchor completely from the soil, and the tower will fall to the ground. This method of failure has several advantages: (1) The visible leaning of the tower before failure provides a visual indicator that the system is near maximum capacity. (2) All of the main anchorage remains in place, preventing loss of the bridge downstream. (3) Although the toppling of the tower would be considered hazardous, pullout of the anchor from the soil is rather graceful, i.e., there is no shrapnel from fracturing of metallic load-bearing components. The intent of the design was to allow the safest form of failure in the event that the modernized OCS was overloaded. Also, repair of the system after such a failure would require only a single helical anchor to be reinstalled before setting back up the toppled tower.

Figure 23. Modernized OCS anchorage components.

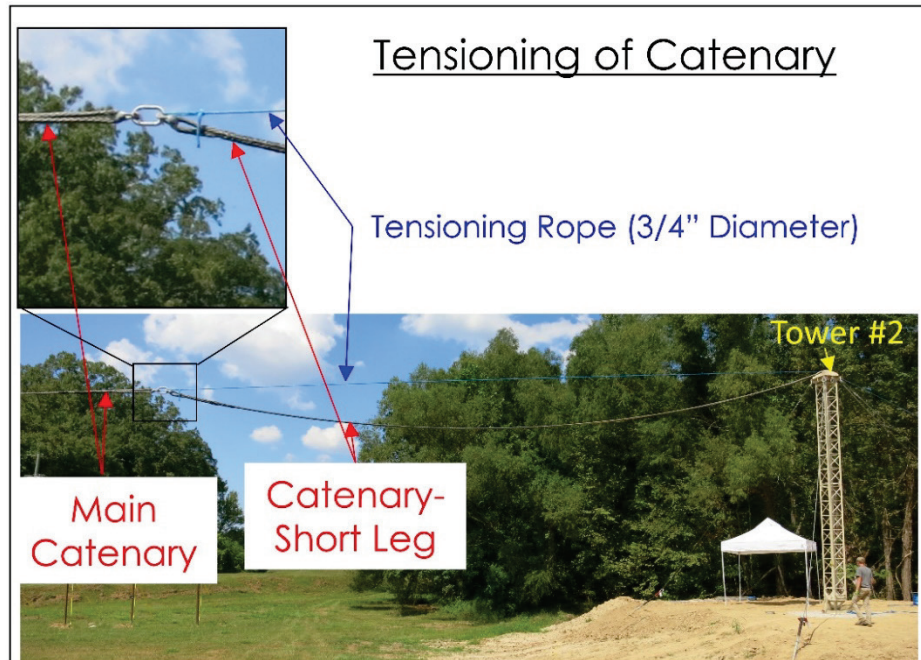


2.1.5 Catenary tensioning

With the anchorage installed on both shores, the next issue addressed was how to connect the main cable to each anchor while ensuring the cable was sufficiently tensioned to hang as a catenary. Every crossing would require a unique length of cable. If the cable was too long, there would be too much slack in the system, and the OCS would be ineffective. If the cable was too short, it would be impossible to connect all of the tension components. A cable tensioning procedure was devised to address this issue.

To accommodate tensioning, the catenary was split into two legs of rope. The main catenary rope was made to end 50 ft. before tower #2. And, a shorter leg of the catenary was made to go over tower #2 and terminate at the anchor array. This allowed for a 3/4-in.-diam 'tensioning rope' to be connected as shown in Figure 24.

Figure 24. Catenary tensioning method.



While the system was completely slack, all of the connections were made on the tower #1 side. Then, the tensioning rope could be used to pull the slack out of the system and hold the tension so the second (short) leg of the catenary could be fed over tower #2 and connected to the anchor array. This was accomplished by tying the tensioning rope to the shackle that connected the two catenary ropes. The tensioning rope was routed over the top of the tower down to a bulldozer equipped with a 10-kip capacity winch. The winch had to be located as near to the centroid of the anchor array as possible to give the correct catenary departure angle (typically 45°). Finally, the tensioning rope was released, transferring the tension to the short leg of the catenary.

2.2 Prototype design summary

An assembly schematic of the improved OCS prototype is shown in Figure 25. Many of the synthetic ropes required chafe guards, eye splices, and/or thimbles. These rope assemblies and connectors are tabulated in Table 1. The parts comprising each tower assembly are listed in Table 2. Table 3 specifies the components of each helical anchor assembly.

Figure 25. Improved OCS prototype assembly.

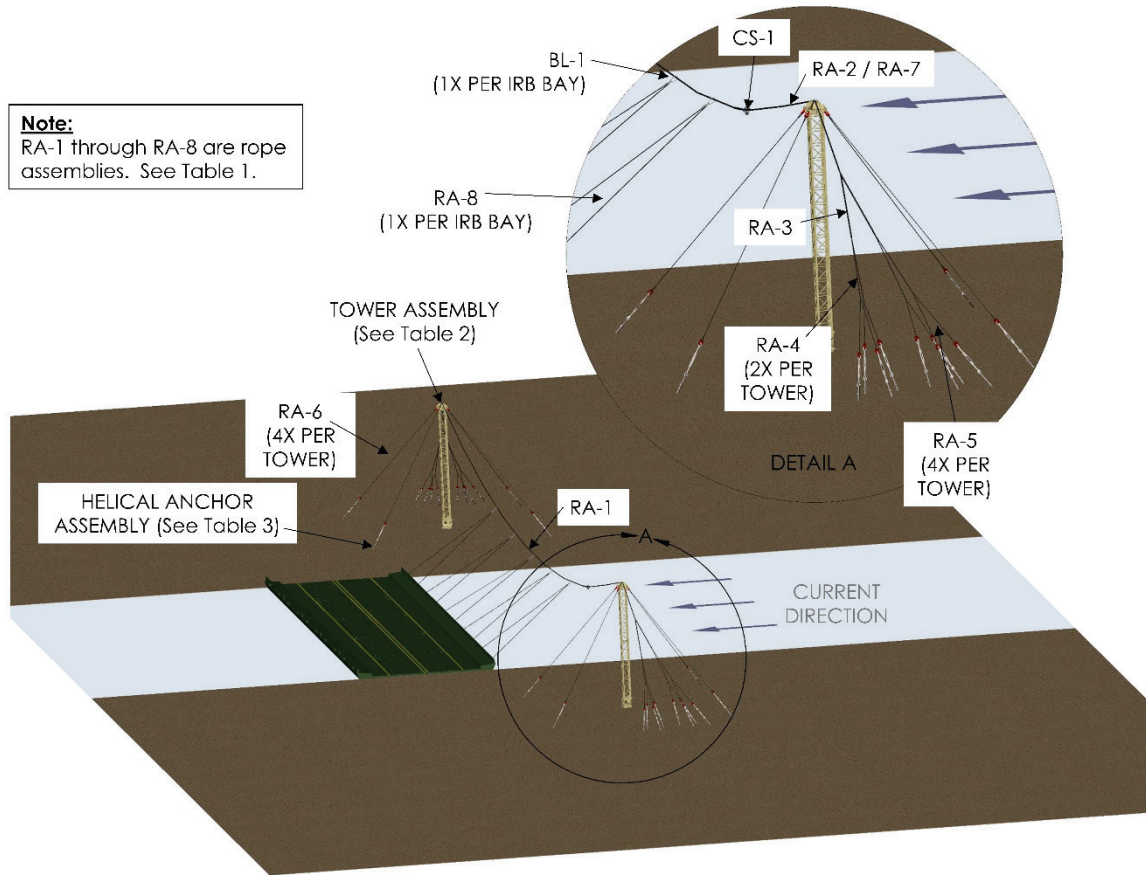
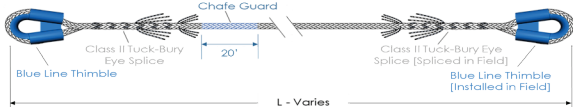
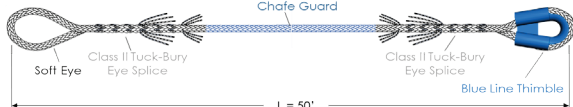
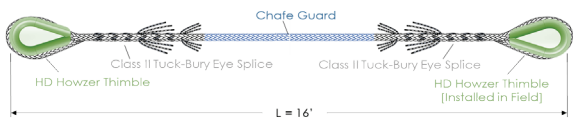
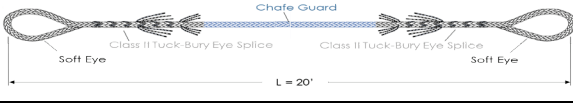
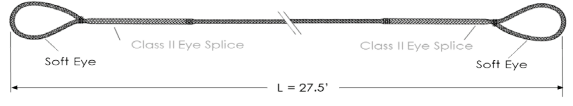
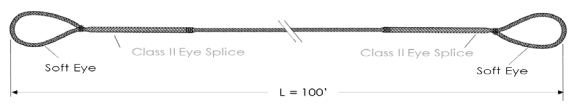
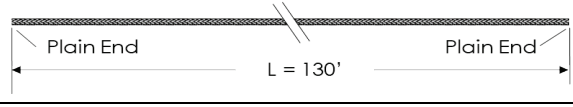


Table 1. Rope assemblies and COTS connectors (items RA-1 through RA-8, CS-1, and BL-1).

ROPE ASSEMBLIES					
Item #	Description	Rope Diameter, D	Final Rope Length, L	Qty	Rope Assembly Schematic
RA-1	Catenary - Main Leg	1-3/4"	1000'	1	
RA-2	Catenary - Fixed Leg	1-3/4"	50'	1	
RA-3	Anchor Array - Line 1	1-3/4"	16'	2	
RA-4	Anchor Array - Line 2	1"	16'	4	
RA-5	Anchor Array - Line 3	3/4"	20'	8	
RA-6	Tower Guys	3/4"	27.5'	8	
RA-7	Tensioning Rope	3/4"	100'	1	
RA-8	IRB Bridles	1/4"	130'	30	
COTS CONNECTORS					
Item #	Description	Manufacturer & Model	Qty	Reference	
CS-1	Catenary Shackle	Crosby 1021285	1	https://www.thecrosbygroup.com/html/en-US/pdf/pgs/83.pdf	
BL-1	Bridle Line Carabineer & Pulley	MSA SRCA22 CARABINEER & PCA-1292 PULLEY	30	Figure 8	

Rope Assembly (RA) Notes:

1. Potential Vendor for Rope Assemblies: SWOS (swos.net).
2. All ropes shall be constructed from Samson Eversteel™-X (12-strand Class 2, HMPE): Samson product code 844.
3. All rope shall be tensioned to 70% MBS (minimum breaking strength) for minimum of 10 cycles to remove constructional elongation prior to terminating.
4. All splices to follow manufacturer's recommended procedure for 12-strand Class II rope: Items 1-5 require Tuck-Bury eye splices. Items 6-7 require normal eye splices.
5. All thimbles and chafe guards to be sized per manufacturer's recommendations for the rope being terminated.
6. Blue Line Thimbles: Samson product code 930.
7. HD Howzer Thimbles: Samson product code 933.
8. Chafe Guard: Samson product code 706

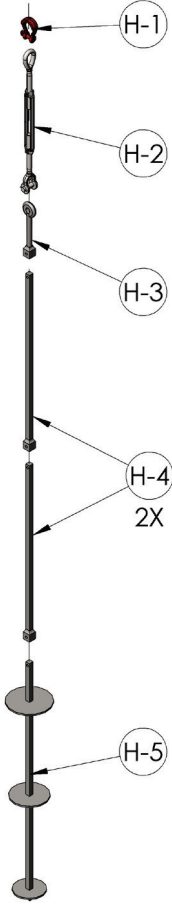
Table 2. Tower assembly (items T-1 through T-11).

Tower Assembly Diagram	Item #	Description	Manufacturer Description / Part No.	Qty per Assembly
	T-1	Base Plate <i>(Note 2)</i>	DWG: (Amato 2012) / PN: 12565626	1
	T-2	Erection Arm	DWG: (Amato 2012) / PN: 12565631	1
	T-3	Pivot Unit	DWG: (Amato 2012) / PN: 12565627	1
	T-4	Tower Section <i>(Note 3)</i>	DWG: (Amato 2012) / PN: 12565628	2
	T-5	Tower Cap <i>(Note 4)</i>	DWG: (Amato 2012) / PN: 12565630	1
	T-6	Erection Arm to Pivot Unit Pin	DWG: (Amato 2012) / PN: 12565644	3
	T-7	Erection Arm to Base Plate Pin	Loop-Grip Clevis Pin, 3/4" Dia. / McMaster-Carr PN: 91594A325	2
	T-8	Bolt	3/4"-10 x 14-1/2" Grade 5 Plain Finish Hex Cap Screw / Fastenal PN: 0157970	20
	T-9	Nut	3/4"-10 Grade 5 Plain Finish Steel Security Heavy Hex - Steel Insert Lock Nut / Fastenal PN: 37537	20
	T-10	Base Plate Anchor Screw	American Earth Anchors 18" Penetrator Screw Anchors/ AEA PN: PE18	8
	T-11	Shackles for Guy Lines	Crosby G2169/S2169 Alloy Screw Pin Wide Body Shackles, 12.5t WLL / Crosby PN: 1021673	4

Tower Assembly Notes:

1. 2x Tower Assemblies required per BSS.
2. Item T-1, the 8x thru holes have a 1.5" diameter per (Amato 2012). The holes must be enlarged to 1.875" to accommodate screw anchors (item T-10).
3. Item T-4, to accommodate different bank heights and/or crossing spans, additional tower sections may be required. These issues were considered out of scope during rapid prototype development.
4. Item T-5, when fabricated per (Amato 2012), any rope departure angle over ~37° causes the rope to contact the lip of the tower cap, which is undesirable. The tower cap may need to be redesigned and/or the departure angle may need to be increased

Table 3. Helical anchor assembly (items H-1 through H-5).

Anchor Assembly Diagram	Item #	Description	Manufacturer Description / Part No.	Qty per Assembly
	H-1	Shackle for Synthetic Rope	Crosby G2169/S2169 Alloy Screw Pin Wide Body Shackle, 12.5t WLL / Crosby PN: 1021673	1
	H-2	Turnbuckle	Crosby HG-227 Jaw & Eye Turnbuckles 1-1/2"x18" / Crosby PN: 1032331	1
	H-3	Ovaleye Adapter	AB Chance 1.5" Square Shaft Ovaley Adapter / Chance PN: C1100041	1
	H-4	Helical Anchor Extension	AB Chance SS150 5ft Extension / Chance PN: C1500145	2
	H-5	Helical Anchor Lead Section	AB Chance SS150 10/12/14x7ft Helical Lead Section / Chance PN: C1500163	1
<p>Helical Anchor Assembly Notes:</p> <p>1. 30x Helical Anchor Assemblies are recommended per BSS. 16x are required to anchor the catenary. A minimum of 8x tower guy lines are required, however, additional guy lines may be needed (14x max).</p>				

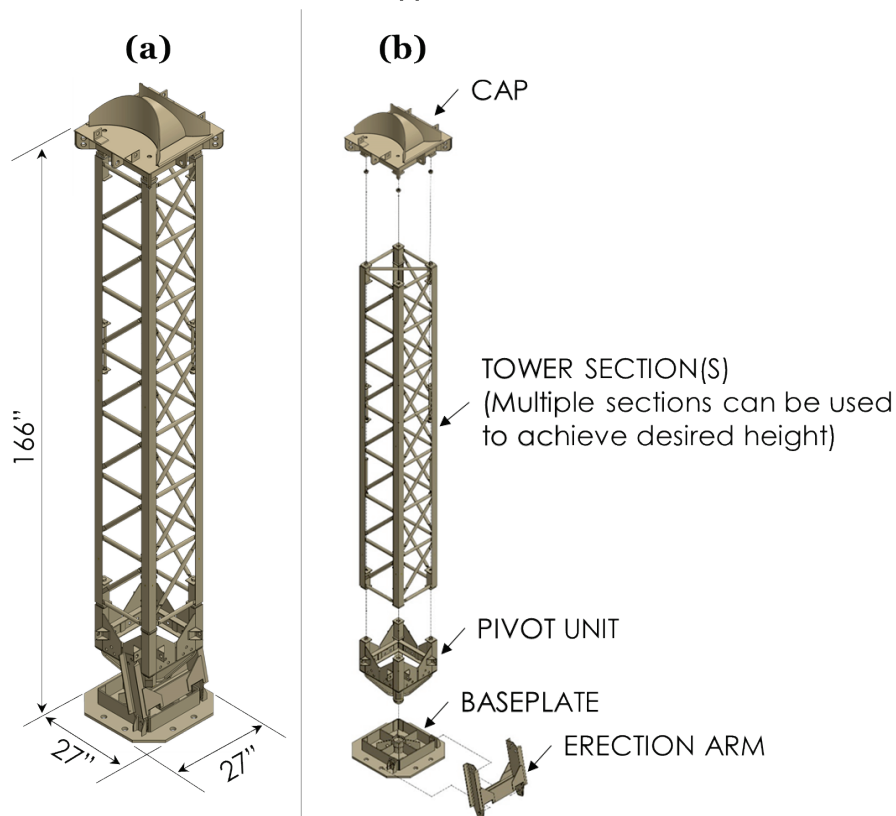
3 Component-level testing of the BSS tower

This chapter describes the legacy BSS Class 60 tower that is used to support the OCS and the component-level compression testing that was performed to determine the compressive load carrying capacity of the tower. Section 3.1 provides an overview of the BSS tower. Section 3.2 describes the testing methodology, and section 3.3 presents and discusses the test results. Finally, section 3.4 provides a summary with key conclusions.

3.1 Overview of BSS tower

The legacy BSS tower was originally designed for Class 60 float bridges (Headquarters 1988), which have drastically different fluid drag characteristics than the current generation IRB. The BSS tower has a modular design, comprising several steel weldments that can be quickly assembled with just a few bolts. Figure 26 shows assembled and exploded views of the tower. The 3-D solid model of the tower shown in the figure was generated from drawings by (Amato 2012).

Figure 26. (a) Assembled BSS tower and (b) exploded view of tower components used to support the OCS.



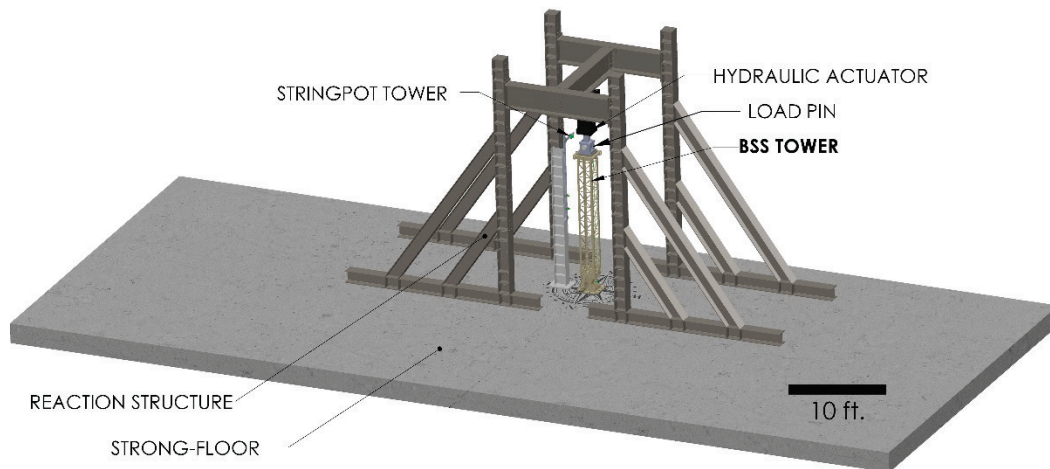
3.2 BSS tower testing methodology

This section describes the BSS Tower compression testing methodology. Section 3.2.1 details the test arrangement. Instrumentation specifics are provided in section 3.2.2. The test procedure is outlined in section 3.2.3.

3.2.1 Test arrangement

Figure 27 shows a schematic overview of the BSS Tower compression testing arrangement, as tested on the ERDC strong-floor. Compressive loading was applied to the BSS Tower via a single-ended hydraulic actuator (MTS Model No. 243.90T), with a 600-kip compressive load capacity and 20-in. stroke. The actuator was connected to a large, preexisting, steel reaction structure, which was in turn bolted to the reinforced concrete strong-floor.

Figure 27. Overview of the BSS Tower compression testing arrangement on the strong-floor.



To apply a uniform compressive load to the tower, the tower cap had to be modified by removing the pieces of steel comprising the rope guide. Figure 28 illustrates the modification made to the tower cap. The modified tower cap was connected to the hydraulic actuator as shown in Figure 29.

Figure 28. Tower Cap modification for compressive load testing.

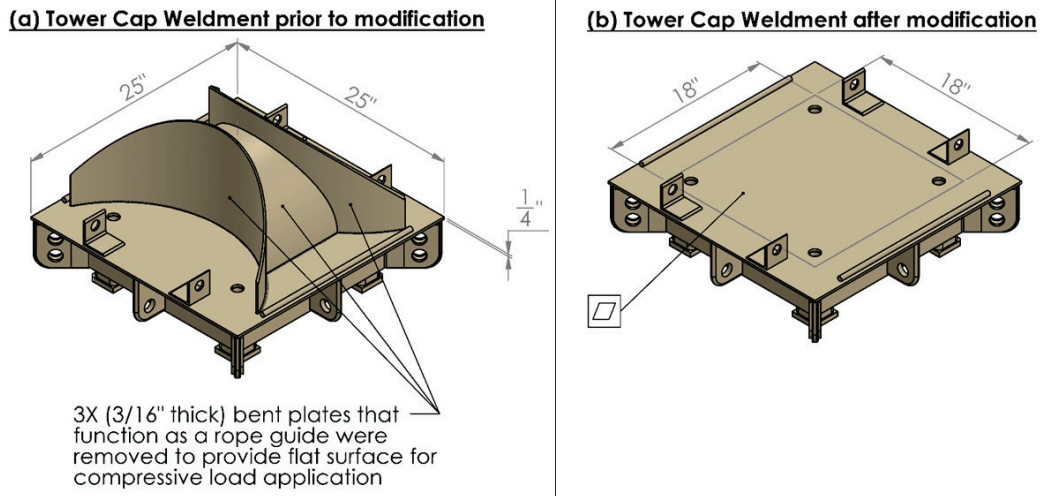
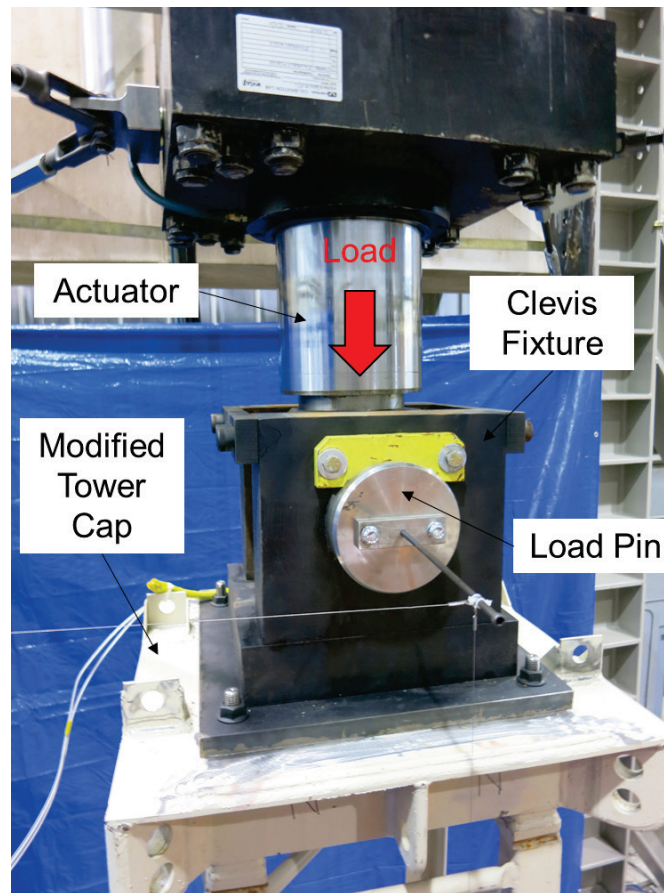


Figure 29. Modified cap to actuator connection.



At the base of the tower, a 1-in.-thick steel adaptor plate was used to connect the base of the tower to the concrete strong-floor, as shown in Figure 30. Next, the pivot unit, tower section, and cap were placed atop

the baseplate. Figure 31 shows the fully assembled BSS tower. Note the erection arm was removed prior to testing.

Figure 30. BSS tower baseplate to strong-floor connection.

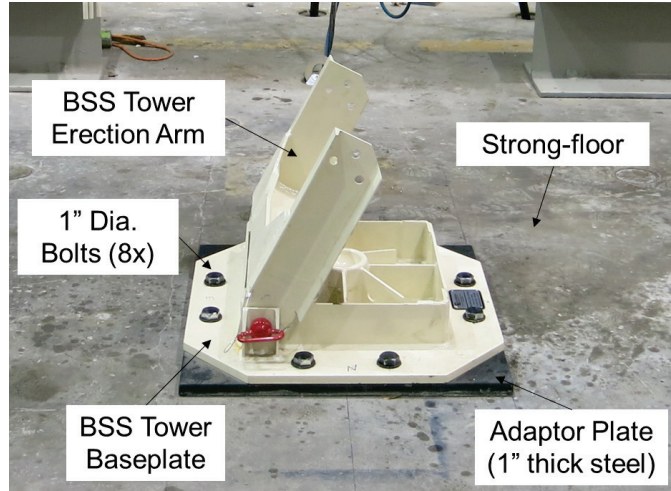


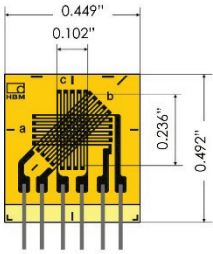
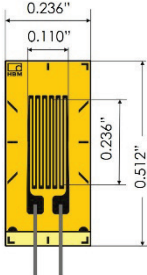


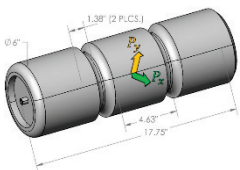
Figure 31. Fully assembled BSS tower.



3.2.2 Instrumentation and data collection

Table 4 details the BSS tower instrumentation package. Four strain gauge rosettes, eight axial strain gauges, and four displacement potentiometers (‘string-pots’) were used to measure structural response. A biaxial clevis load pin was used to measure the load applied by the hydraulic actuator.

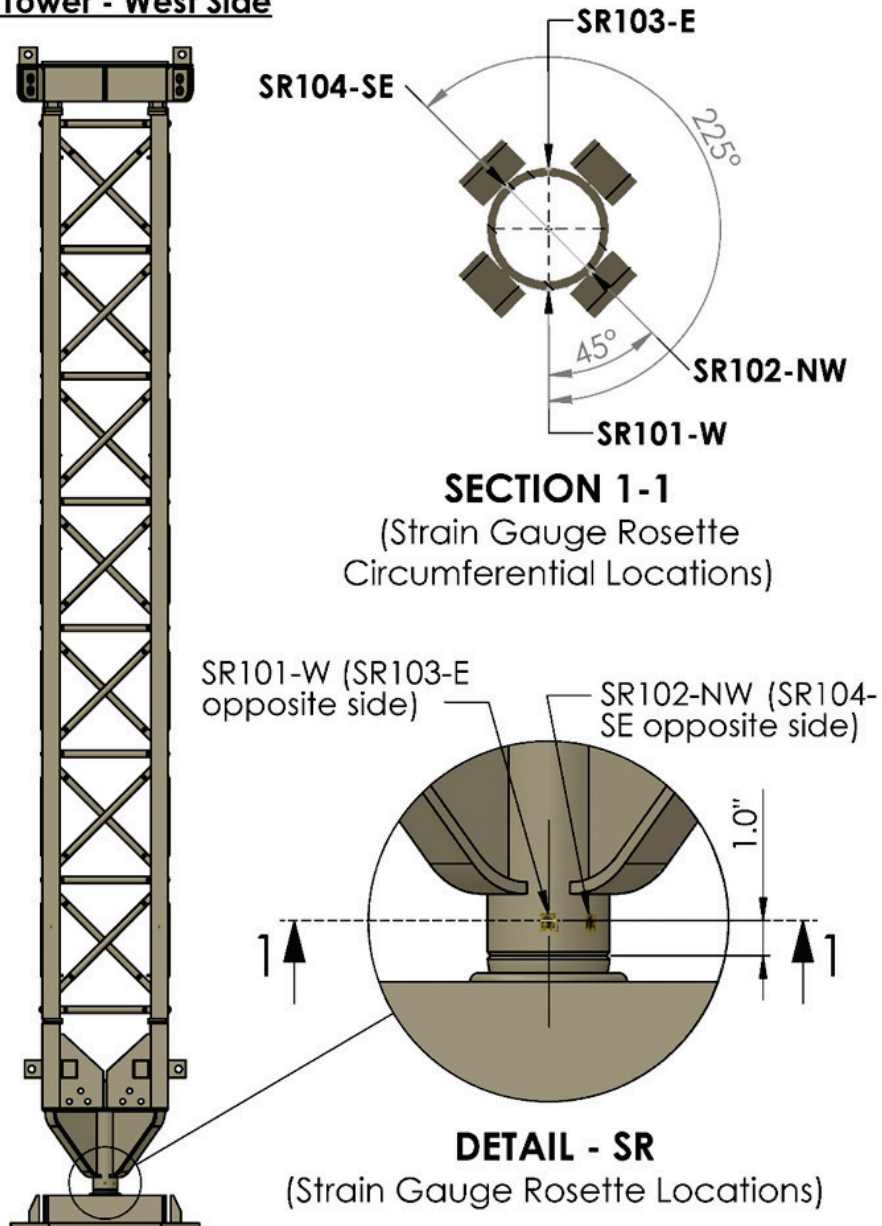
Table 4. BSS tower instrumentation summary.

Gauge Type, Make, & Model No.	Gauge ID	Gauge Orientation	Gauge Schematic	Gauge Locations
Strain Gauge Stacked Rosette (SR) HBM 1-RY91-6/350	SR101-W-a SR101-W-b SR101-W-c	Horizontal 45° Vertical		Figure 32
	SR102-NW-a SR102-NW-b SR102-NW-c	Horizontal 45° Vertical		
	SR103-E-a SR103-E-b SR103-E-c	Horizontal 45° Vertical		
	SR104-SE-a SR104-SE-b SR104-SE-c	Horizontal 45° Vertical		
Axial Strain Gauge (SA) HBM 1-LY11-6/350	SA201-SW	Vertical		Figure 33
	SA202-NW	Vertical		
	SA203-NE	Vertical		
	SA204-SE	Vertical		
	SA301-SW	Vertical		
	SA302-NW	Vertical		
	SA303-NE	Vertical		
	SA304-SE	Vertical		
Displacement Potentiometer Unimeasure PA-20-S10-N1S-10K	D101V-N	Vertical		Figure 34
	D102H-E	Horizontal		
Displacement Potentiometer Unimeasure LX-PA-20-S1N-1PN	D201H-E	Horizontal		Figure 34
	D202-E	45°		
Biaxial Clevis Load Pin Strainsert SPA-400	P _x	Horizontal		
	P _y	Vertical		

Finite element analysis was used to determine optimal gauge locations. The four strain gauge rosettes were installed on the pivot unit just above the ball and socket joint as shown in Figure 32. Each of the four rosettes were in the same plane, only their circumferential locations differed. SR101 and SR103 were installed in between gussets, while SR102 and SR104 were in-line with the gussets. Each rosette was oriented such that grid 'a' was horizontal, grid 'b' was at 45 deg, and grid 'c' was vertical.

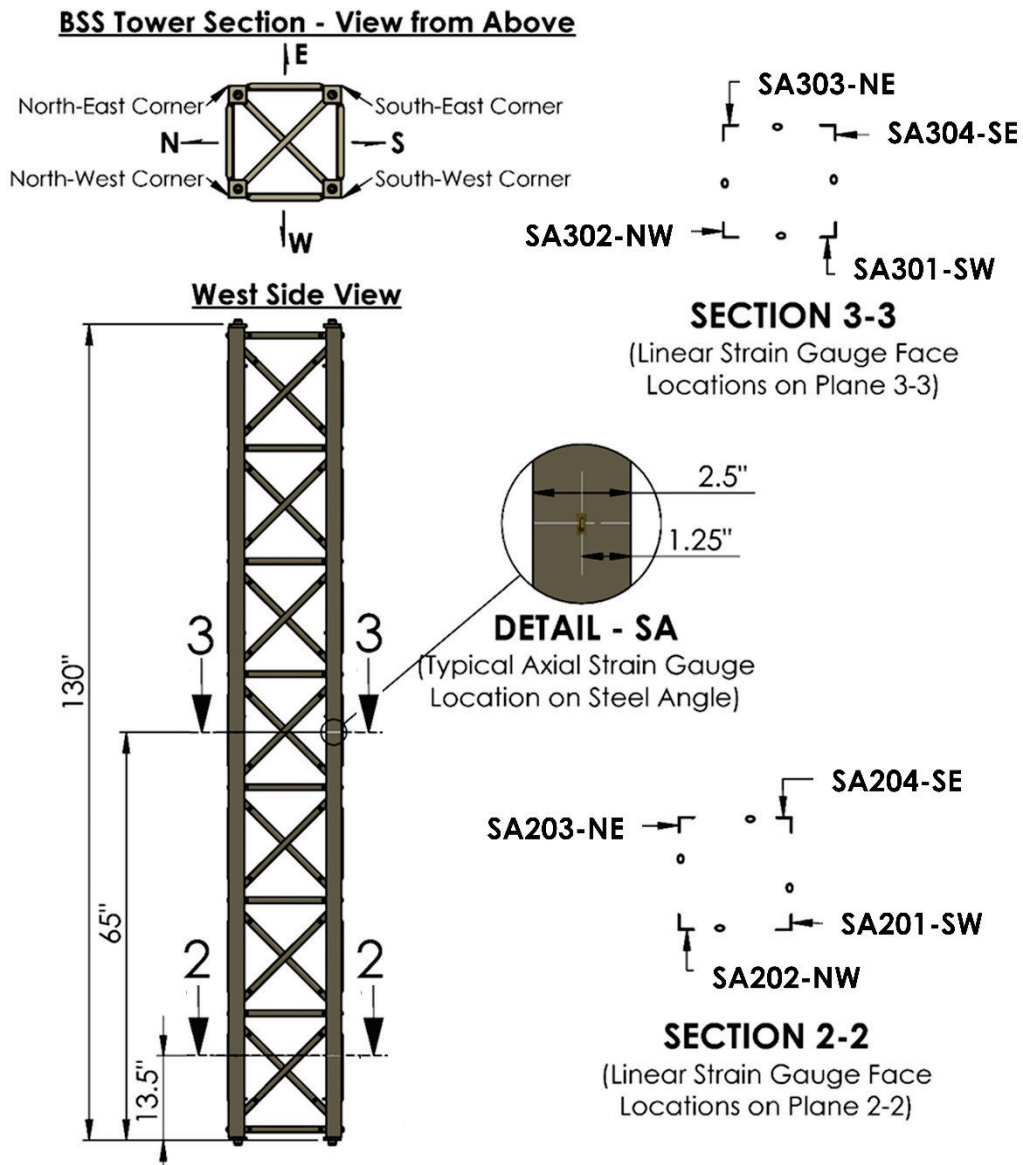
Figure 32. Strain gauge rosette locations.

BSS Tower - West Side



The eight uniaxial strain gauges were installed on the tower section, as shown in Figure 33. The four coplanar SA20x gauges were installed near the base of the tower section in an unsupported section of the corner steel angle, which was a suspected buckling location. The four SA30x gauges were also coplanar, located at the midpoint of the tower section. All of the uniaxial strain gauges were oriented vertically, i.e., in line with the compressive load.

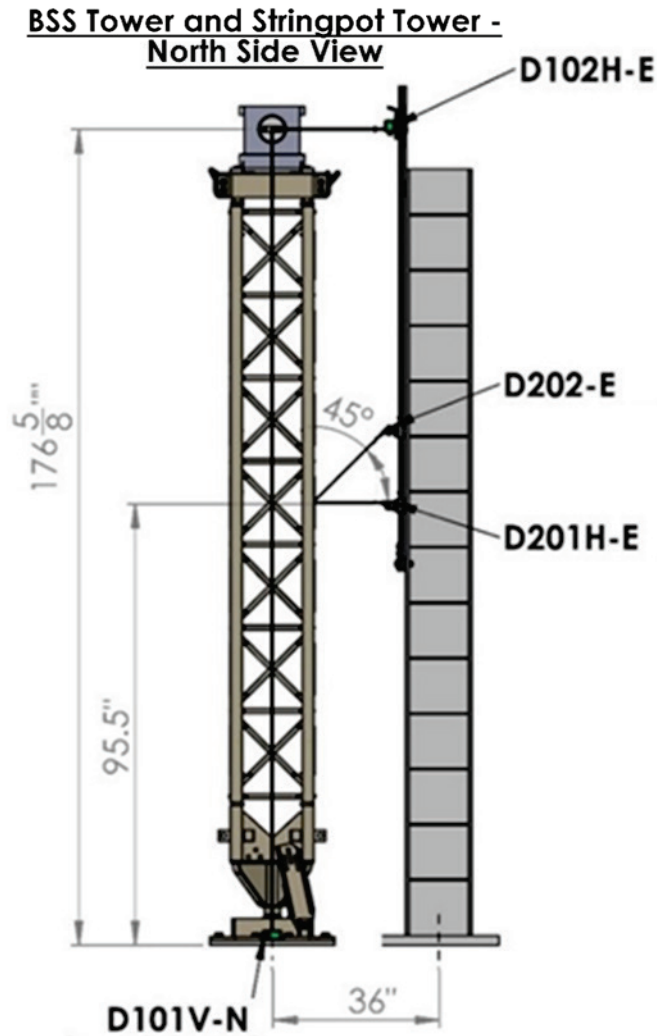
Figure 33. Axial strain gauge locations.



The locations of the four string-pots used to measure tower displacement are shown in Figure 34. D101 and D102 were used to measure global tower

displacement. D201 and D202 were attached to the tower mid-height to capture any global buckling deformation.

Figure 34. Displacement potentiometer locations.



Applied load was measured with a biaxial load pin, which was shown in Figure 29. The P_y axis was oriented vertically and the P_x axis was oriented horizontally. The resultant applied load, P , was calculated by

$$P = \sqrt{P_x^2 + P_y^2} \quad (7)$$

A National Instruments SCXI-1001 data acquisition system was used to collect the 26 channels of data. The data sampling rate was set at 5 Hz. Post-test filtering of the data was deemed unnecessary.

3.2.3 Test procedure

Quasi-static, monotonic, displacement controlled compressive loading was applied to the BSS tower via hydraulic actuator. A constant displacement rate of 0.0005 in./s was used. The tower was compressed until a drastic loss of stiffness occurred, at which point displacement was manually stopped. The actuator was then retracted, unloading the structure.

3.3 BSS tower test results and discussion

The BSS tower compression test was executed on 22 April 2019 at the ERDC strong-floor testing facility. In section 3.3.1, the time history data are presented. The compressive load capacity and failure mode of the BSS tower are given in section 3.3.2.

3.3.1 Time history data

Figure 35 shows the vertical (P_y) and horizontal (P_x) force components measured by the biaxial load pin. The resultant force (P), which was calculated using Eq. 7, is also plotted. The resultant force was driven by the vertical load component, which was expected based on the boundary conditions of the simple compression test. The horizontal load component was negligible.

The load was initially increased from 0 to 12.5 kips to preload the structure. From $t=250$ s to $t=650$ s, the structure was allowed to settle. At $t=650$ s, loading was resumed and the test ran under a constant displacement rate until $t=1,340$ s. At that time, the test was paused to examine buckling damage occurring in the tower section. At $t=1,650$ s, loading resumed at the constant displacement rate of 0.0005 in./s. The test was terminated at $t=2,400$ s after a significant amount of buckling had occurred. At $t=2,500$ s, the actuator was reversed, unloading the tower.

Figure 35. Load time history data.

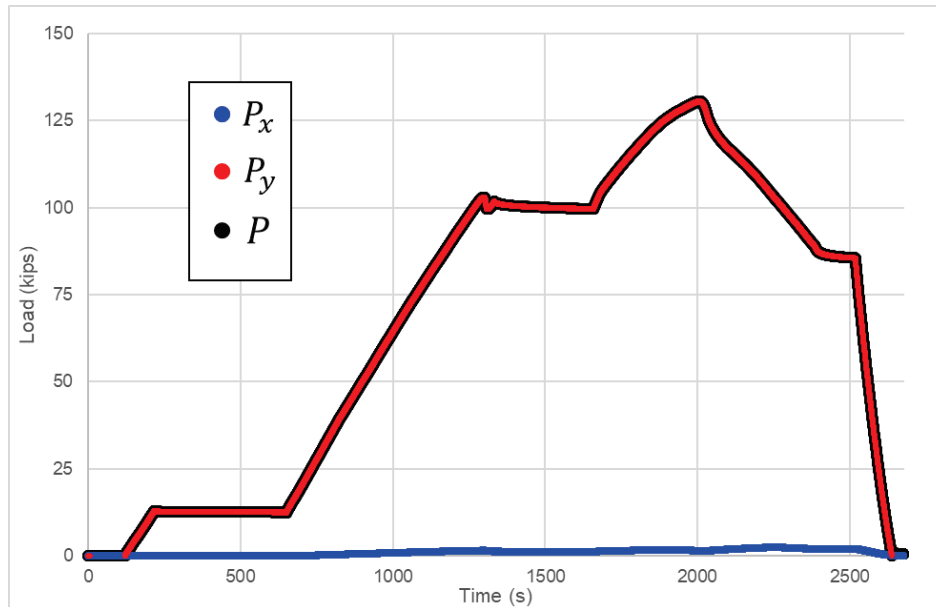


Figure 36 shows the time histories of the displacement gauge data. From Figure 36(a), the vertical displacement during the test peaked at 0.77 in., and the top of the tower displaced a total of 0.67 in. The horizontal displacement at mid-height of the tower was about 0.5 in. As seen from Figure 36(b), the majority of that displacement occurred between $t=2,000$ s and $t=2,400$ s as the tower section was buckling.

Figure 36. Displacement time history data.

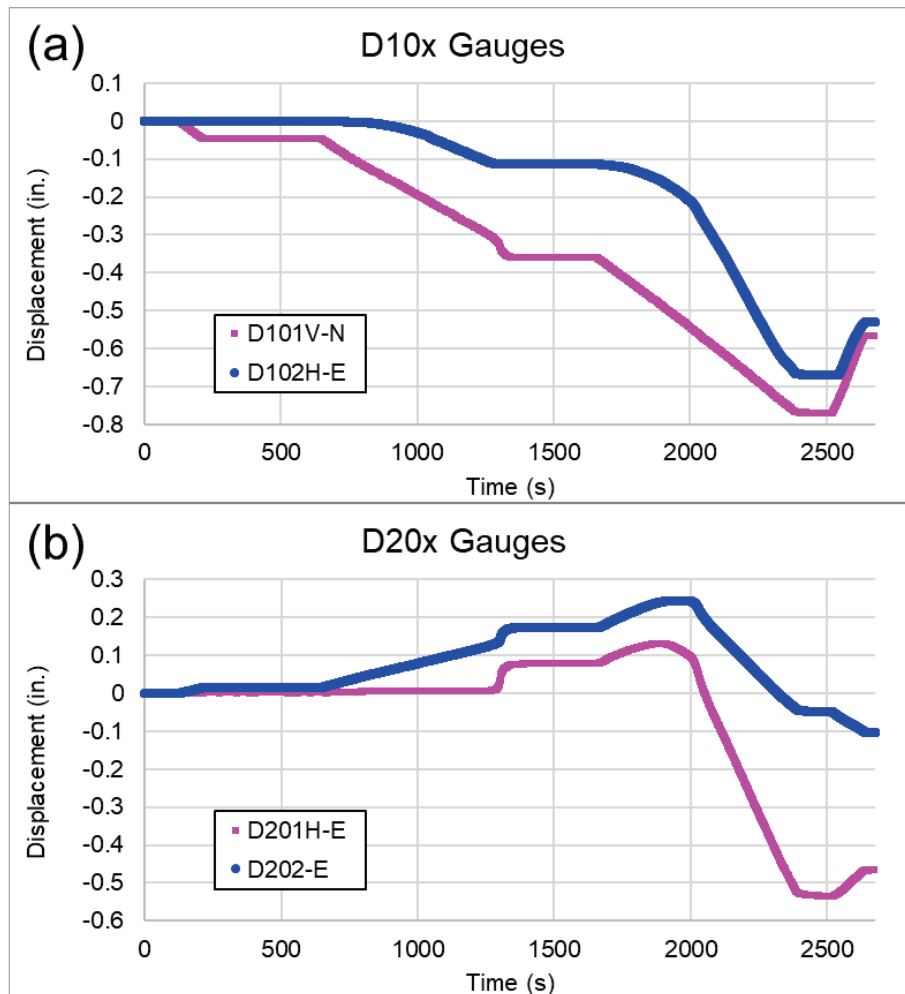


Figure 37 shows the strain gauge rosette time history data. Two of the rosettes had issues. First, SR101 (shown in Figure 37[a]) stopped transmitting reliable data at $t=820$ s. All of the SR101 data beyond that were unreliable, so it was removed. Second, no data from the SR102 gauge were recorded, as shown in Figure 37(b).

SR103 and SR104 were located on the opposite side from SR101 and SR102, respectively. Thus, SR101 and SR103 were expected to give similar responses. This is supported by the strong correlation between the first 820 s of data from SR101 and the corresponding data from SR103. Similarly, SR102 and SR104 should have given comparable readings.

The elastic strain limit for the steel comprising the BSS tower can be estimated as

$$\varepsilon_y = \frac{1.5S_y}{E} \approx 1,800 \mu\varepsilon \quad (8)$$

where, S_y = tensile yield strength ≈ 36 ksi, and
 E = elastic modulus $\approx 30,000$ ksi.

Since none of the SR10x gauges exceeded $\sim 1,800 \mu\varepsilon$, no plastic deformation occurred in the pipe at the base of the tower where those gauges were affixed.

Figure 37. Strain gauge rosette time history data.

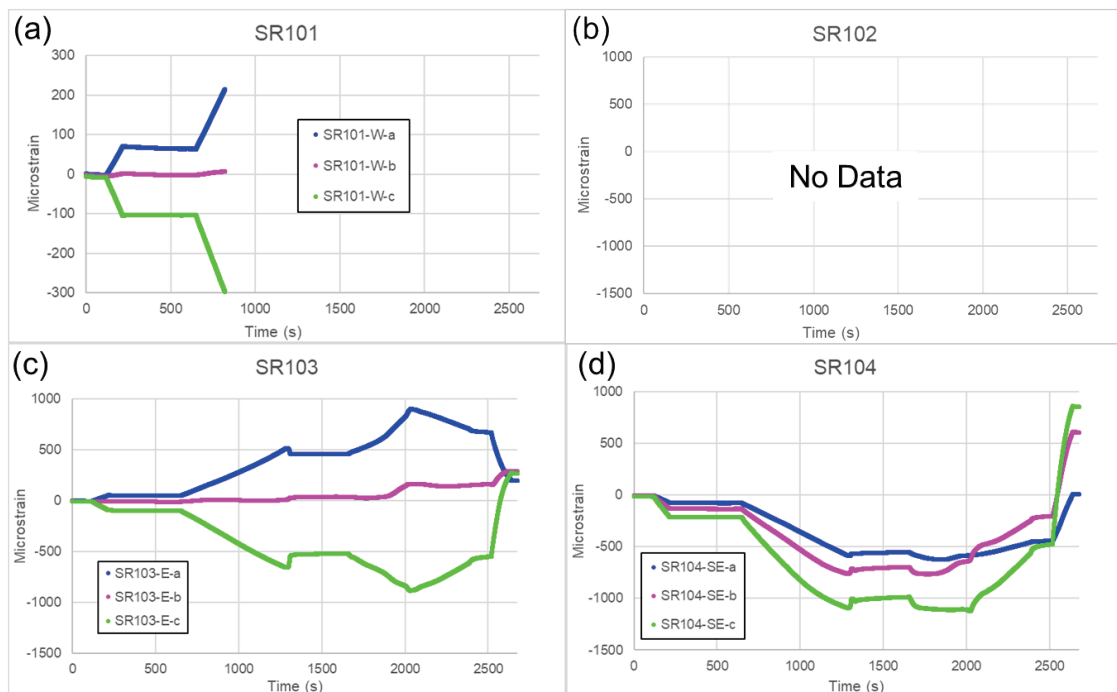
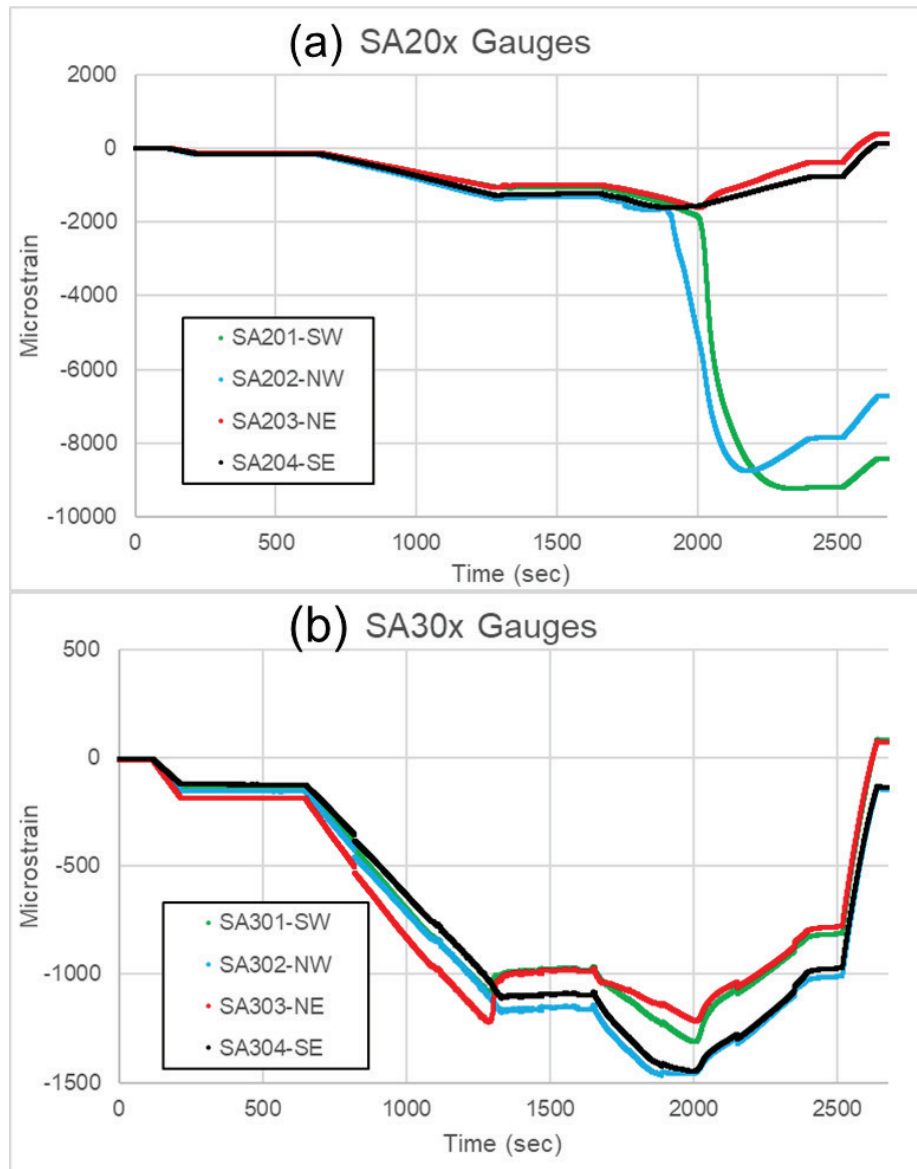


Figure 38(a) and (b) show the time history responses of the SA20x and SA30x gauges, respectively. All of these strain gauges were located on the tower section weldment. The SA20x gauges were located 13.5 in from the bottom of the tower section. Finite element analysis predicted this to be a region of concern and rightfully so. As seen in Figure 38(a), at $t=1,900$ s, SA202 began to show a significant increase in strain once the magnitude reached $-1,900 \mu\varepsilon$. At $t=2,000$ s, SA201 followed suit. Localized buckling did occur at these gauge locations. After being unloaded, SA201 and SA202 indicated $-8,400$ and $-6,700 \mu\varepsilon$ of plastic strain, respectively. The SA30x gauges, which were located mid-height on the tower, did not register plastic deformation. A peak strain magnitude of $1,450 \mu\varepsilon$ occurred at the SA302 and SA304 gauge locations.

Figure 38. Axial strain gauge time history data.



3.3.2 BSS tower capacity and compressive failure mode

Figure 39 shows compressive load versus vertical displacement for the BSS tower. The tower responded linear elastically up to 102 kips. At that point, one of the legs in the tower section began to buckle near the top of the tower. Subsequently, load redistributed to the remaining stable legs until the load peaked at 130 kips. Then, two of the other legs began to buckle, but this time, the localized buckling occurred on the opposite end of the tower section near the locations where the SA20x strain gauges were installed. No additional load was gained after this secondary buckling failure.

Figure 39. Compressive load versus displacement response of the BSS tower.

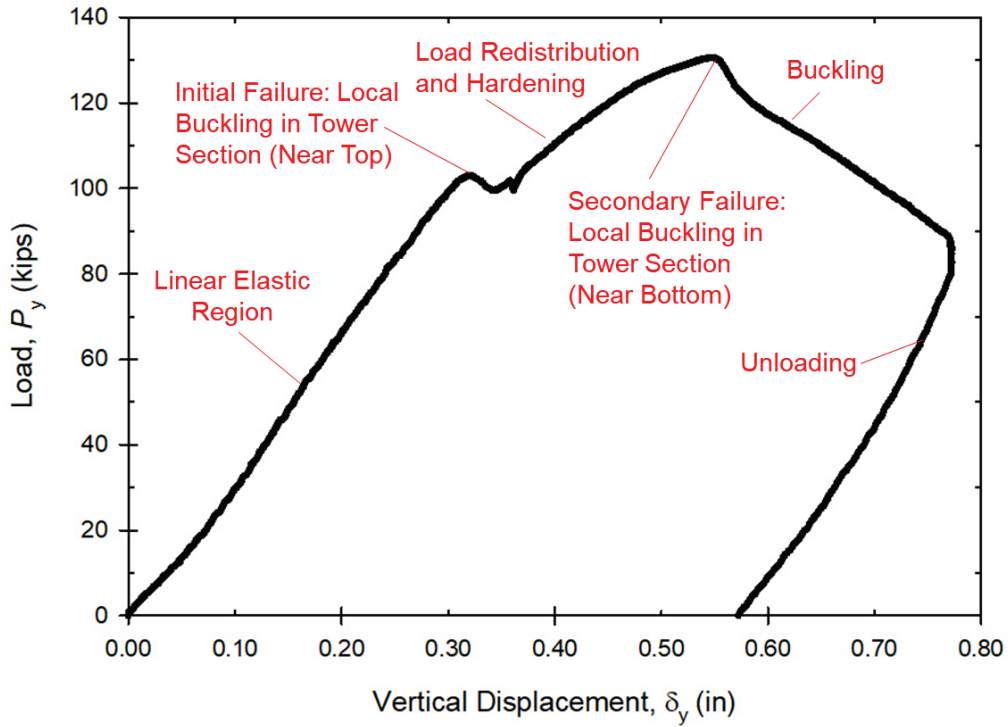


Figure 40 shows the initial buckling of tower section leg near the top of the tower that occurred when the load reached 102 kips. Figure 41 shows the secondary buckling failure that began at 130 kips. The secondary buckling occurred near the base of the tower section in the vicinity of the SA-201 and SA-202 strain gauges.

Figure 40. Initial buckling of tower section leg near the top of the tower at 102 kips.

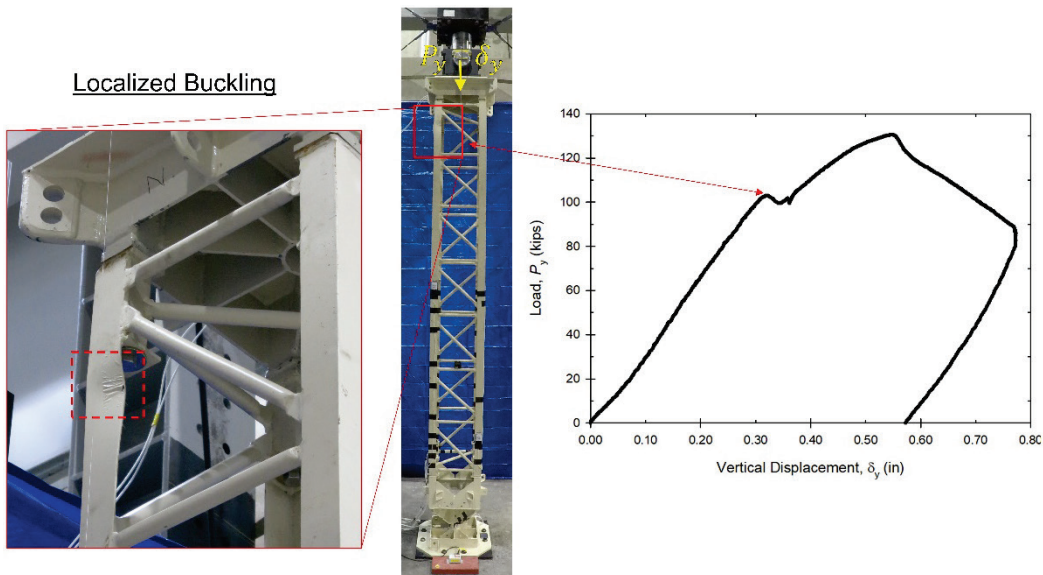
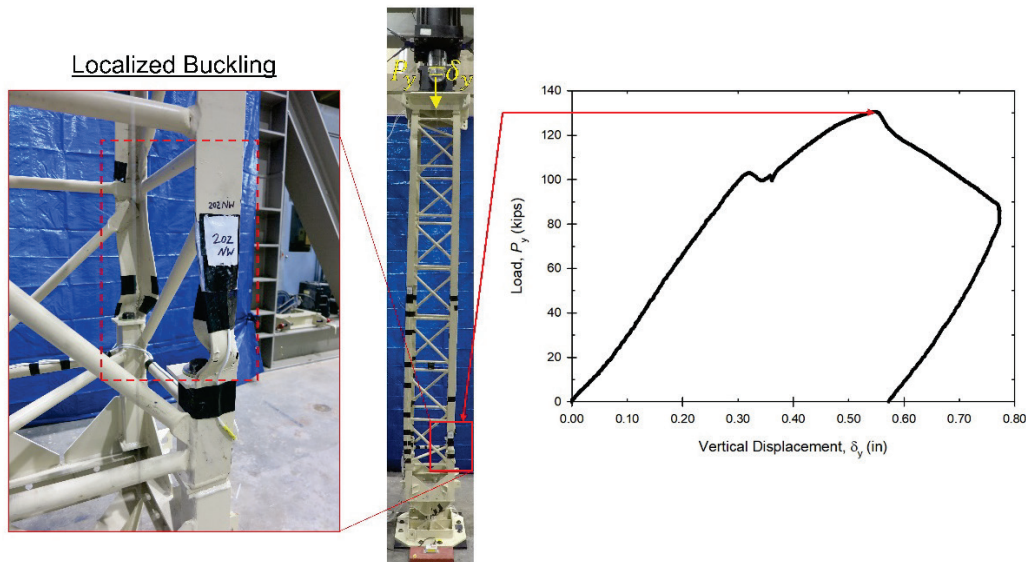


Figure 41. Secondary buckling of tower section legs near the base of the tower at 130 kips.



Based on these results, the compressive capacity of the BSS tower was determined to be 102 kips, which is the load at which the initial buckling failure occurred. Buckling is inherently unstable, so the load gained after the initial failure should not be considered in the capacity determination. The capacity is based on yield strength, not ultimate strength.

3.4 Component-level testing summary and conclusions

A component-level compression test of the legacy BSS Class 60 tower was executed on the ERDC strong-floor to determine its load capacity and failure mode. The compressive yield strength of the tower was determined to be 102 kips. The failure mode under simple compression loading was localized buckling in the legs of the tower section. The following caveats associated with this limited component-level testing should be noted.

- In this test, simplistic loading conditions were used. In fielded conditions, the loads on the BSS tower are more complex. Factors such as eccentric loading and influences from rope contact on the tower cap were omitted. If future testing is desired, it is recommended the test plan include an investigation into the effects of these loading complexities.
- Tower durability and fatigue were also not considered. The strength and failure mode of the tower could change after extended periods of use. Additional analysis to estimate the fatigue strength of the tower could be performed if personnel safety is of concern.

4 System-level testing of the improved overhead cable system prototype

This chapter provides the details of the system-level test of the improved OCS prototype that was described in chapter 2. The primary objective of this testing was to verify that the modernized OCS can sufficiently anchor a 689 ft (210 m) IRB crossing with 11 ft/s current. This would fulfill the threshold requirement for anchorage in the BSS CPD (MSCoE 2014). The testing methodology is described in section 4.1. The test results are reported and discussed in section 4.2. Loading equivalents for uniform versus parabolic current distributions are described in section 4.3. Finally, in section 4.4, the test series is summarized and key conclusions are drawn.

4.1 Full-scale OCS testing methodology

This section describes the full-scale OCS testing methodology. The approach is detailed in section 4.1.1. The test setup and procedure are described in section 4.1.2. And, instrumentation details are provided in section 4.1.3.

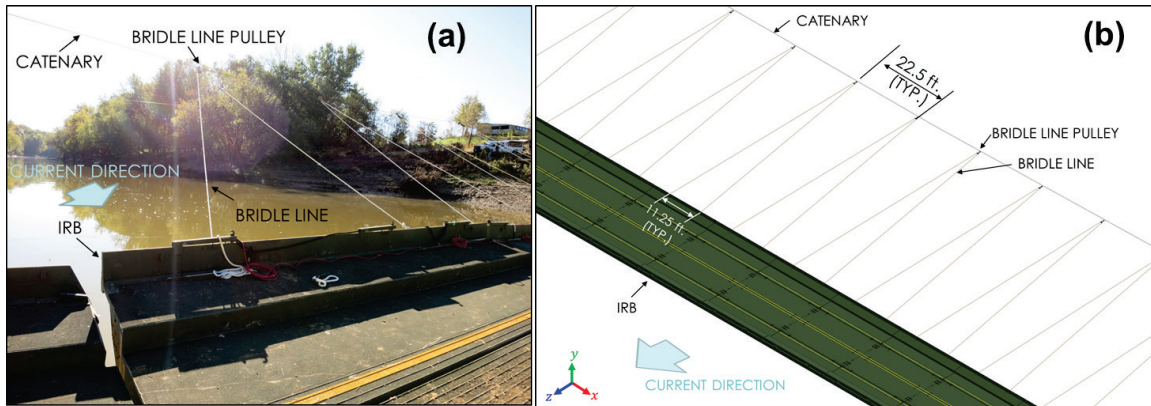
4.1.1 Testing approach

No facility or location existed with the vast, controllable volumes of water required to conduct a full-scale 689-ft, 11-ft/s test of the OCS. For this reason, an approach was devised to simulate the fluid-induced drag load with mechanical loading instead. This allowed for a safe, controllable test with directly measurable load inputs, while eliminating the need for massive volumes of fast-moving water.

The ERDC CHL conducted extensive small-scale hydrodynamic empirical testing to relate flow velocity to OCS cable tension via flume testing of small-scale physical models. The full details of that significant testing endeavor are published in Bryant et al. (2019). These empirical data were leveraged to conduct a ‘dry’ test, where hydrodynamic loads were simulated via mechanical devices to achieve appropriate cable tensions.

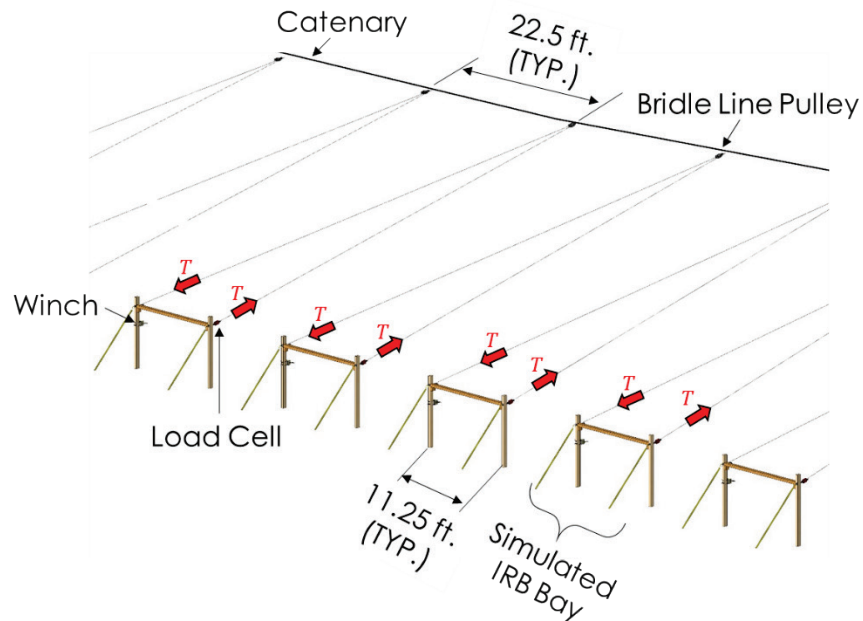
The actual IRB/OCS arrangement is shown in Figure 42. Each bridle line was routed through a pulley attached to the catenary, and each bridle line was tied to an IRB bay at two locations. These bridle lines transfer the fluid drag loading from the IRB to the OCS catenary.

Figure 42. (a) Photograph and (b) schematic of the actual IRB/OCS arrangement.



To mechanically simulate the hydrodynamic drag loading on the IRB, the concept shown in Figure 43 was devised. The apparatus used winches and pulleys to apply the load in lieu of moving water. Anchored posts, with spacing identical to that of the actual IRB/bridle line tie-down points, were used to represent the IRB. Tension was applied to each bridle line using a highly controllable winch, and that tension was monitored with a load cell.

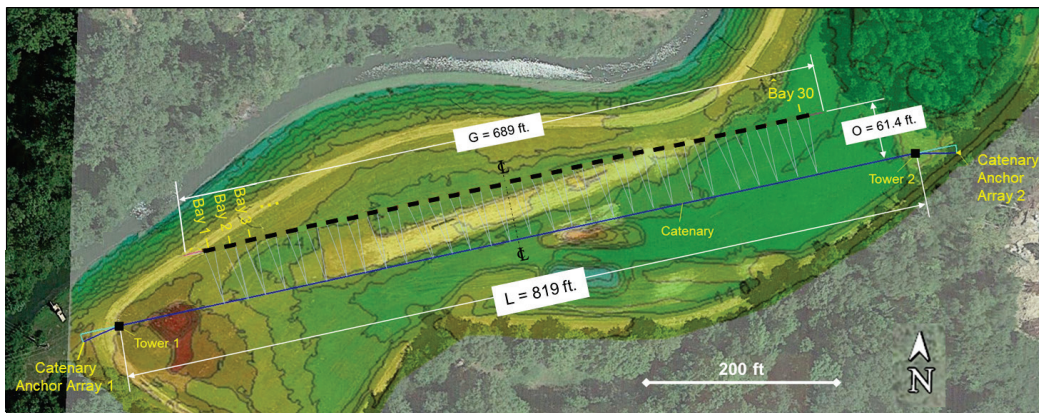
Figure 43. Mechanical loading concept.



4.1.2 Test arrangement and procedure

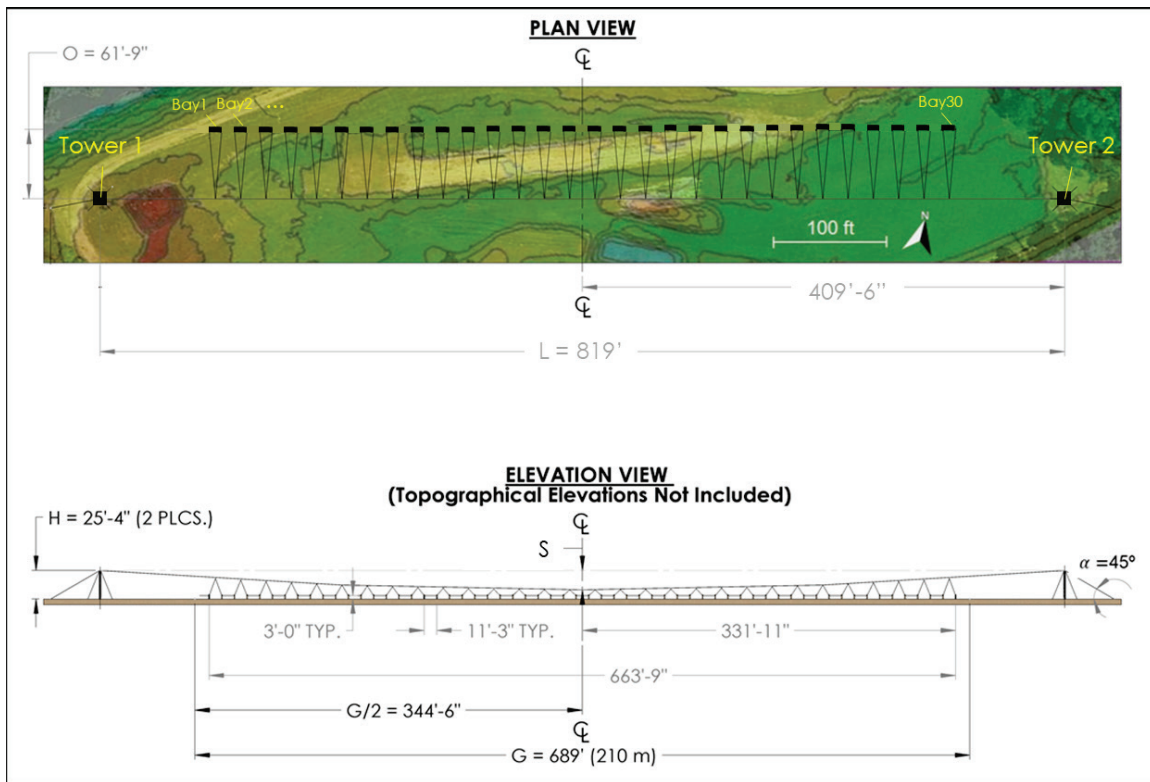
The test site for the full-scale OCS ‘dry’ test was located at the ERDC in Vicksburg, MS. Figure 44 shows an aerial view of the site with topography overlaid. The procedure provided in the IRB Operator’s Manual (Headquarters 2003b) was followed as closely as possible to set up the OCS prototype for a 689 ft (210 m) crossing with 11 ft/s current. Due to physical space limitations, the distance between the two towers had to be reduced from $L = 858$ ft. (per Eq. 4) to $L = 819$ ft for the test. Variances such as this will be common in the field as adjustments to terrain will need to be made frequently. Additional dimensions of the OCS setup are given in Figure 45.

Figure 44. OCS test site with overlaid topography.



As seen from the topography map in Figure 44, the elevation at the tower 2 location was lower than the elevation at the tower 1 location. In order to simulate equal bank heights, soil was brought in to build up the area where tower 2 was to be placed. The elevation at tower 2 was increased by about 6 ft, which made the elevations at tower 1 and 2 roughly equal. Since the soil around tower 2 had not fully settled, it was compacted with heavy equipment. Prior to erecting tower 2, a stable footing was formed by excavating a 6 ft × 6 ft area at the base of the tower, which was subsequently filled and compacted with a 4-in.-thick layer of crushed limestone. The soil at the tower 1 site was intentionally left undisturbed aside from mildly scraping the area to level it. The rationale was that if soil-bearing capacity was an issue, the effects would manifest at tower 1 but not at tower 2.

Figure 45. Plan and elevation views of the full-scale OCS test setup.



Two ‘dry’ pull tests on the OCS were executed. Test #1 was executed 22 Jan 2020. For test 1, loads were applied that corresponded to uniform currents of 3, 4, 5, 6, 7, and 8 ft/s. Test #2 was executed 29 Jan 2020. Test 2 also started at a uniform current of 3 ft/s, and load was increased again in increments corresponding to 1 ft/s uniform current increases until failure occurred. Before each test, the catenary was initially tensioned to achieve a desired level of sag, S .

The IRB Operator’s Manual specifies that an initial sag of $S=0.02L$ is desired (per Eq. 6). However, the manual also states that the overhead cable needs only to be 3 ft above the water level. For test #1 the initial sag in the main cable was set at $S_{test\ 1} = 0.02(819\text{ ft}) = 16.4\text{ ft}$. For test #2, the lower condition was used, 3 ft above water level. For test #2, the sag was set at $S_{test\ 2}=22.4\text{ ft}$.

Once the catenary was properly tensioned to achieve the desired initial sag, drag load could be applied via the bridle lines. The first load target corresponded with a 3 ft/s uniform current speed. Substitution of $v=3\text{ ft/s}$ and into Eq. 1 yields $F_{\text{drag,bay}}=117\text{ lbf}$. Plugging that into Eq. 2 along with $n_{\text{bays}}=30$ gives the total drag forces corresponding to a 3 ft/s current,

$F_{drag} = 3,501$ lbf. Since each IRB bay has two bridle line connection points, and the line is routed through a pulley, the tension in each bridle line for the 3 ft/s condition is $T_b = F_{drag,bay}/2 = 58$ lbf. Therefore, the first load target was to tension each bridle line to 58 lbf. These calculations were repeated to determine target loads corresponding to currents up to 11 ft/s in 1 ft/s increments. The resulting load matrix is given as Table 5.

Table 5. OCS test load matrix.

Uniform Current Speed (ft/s)	Total Drag Force on OCS, F_{drag} [Eq. 2] (lbf)	Drag Force per IRB Bay, $F_{drag,bay}$ [Eq. 1] (lbf)	Bridle Line Tension, $T_b = F_{drag,bay} / 2$ (lbf)
3	3,501	117	58
4	4,814	160	80
5	6,619	221	110
6	9,100	303	152
7	12,512	417	209
8	17,203	573	287
9	23,653	788	394
10	32,521	1,084	542
11	44,714	1,490	745

The 30 winches were simultaneously wound until each bridle line dynamometer read as close as possible to the target load corresponding to a particular current speed. Once the desired load was reached, winching ceased and the load was held for 3 to 5 min. After the hold period, winching commenced, ramping the load to the next target increment.

4.1.3 Instrumentation

Instrumentation for the full-scale OCS test comprised 56 load cells and 4 inclinometers. The location of each gauge is shown in Figure 46. The gauges surrounding tower 1 and 2 were labeled in a manner that took advantage of the mirror symmetry in the setup. For instance, gauge ‘G1-1’ corresponds to tower 1-guy 1 and ‘G2-1’ coincides with tower 2-guy 1. Because of symmetry, the loads in guy wire 1 on both towers should be roughly equal. The same is true for the ‘A’ prefixed gauges, which correspond to the 8 anchors in each anchor array. Gauges ‘C1’ and ‘C2,’ which measure tension in the catenary, were also symmetrically located

about the centerline such that their load measurements should correlate. These redundant gauges served to increase confidence in measurement accuracy. The entire instrumentation package for the full-scale OCS test is provided in Table 6.

Figure 46. Plan view of OCS showing gauge locations and identifiers.

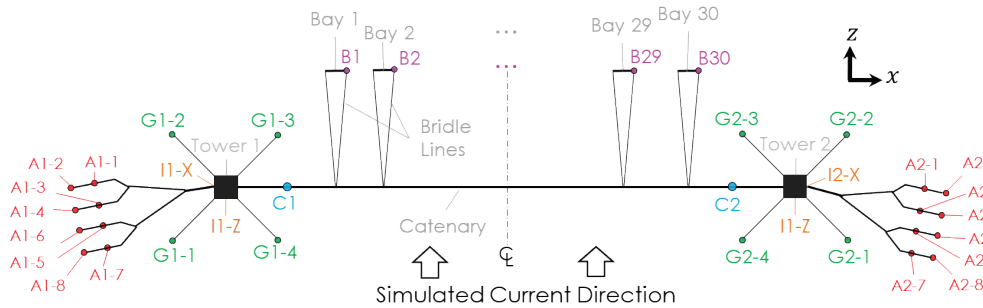


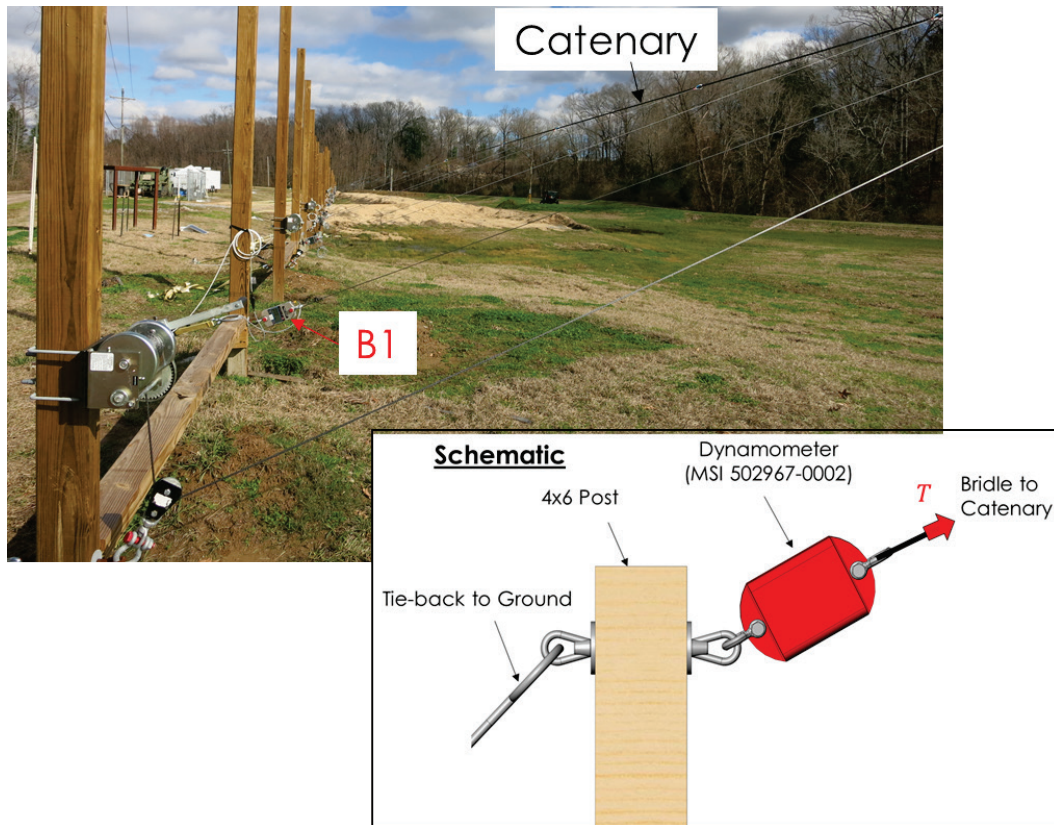
Table 6. OCS test instrumentation package.

Measurement Type	Gauge IDs		Gauge Make & Model	Qty.	Ref.
Bridle Line Tension	B1 - B30		MSI 502967-0002 Digital Tension Dynamometer	30	Figure 47
Tower Guy Load	Tower 1	Tower 2	Transducer Techniques TLL-50K Tension Link Load Cell	24	Figure 48
	G1-1 G1-2 G1-3 G1-4	G2-1 G2-2 G2-3 G2-4			
Array Anchor Load	A1-1 A1-2 A1-3 A1-4 A1-5 A1-6 A1-7 A1-8	A2-1 A2-2 A2-3 A2-4 A2-5 A2-6 A2-7 A2-8			
Catenary Tension	C1	C2	Omega LC-702-200K Tension Link Load Cell	2	Figure 49
Tower Tilt Angle (X is parallel and Z is perpendicular to crossing)	I1-X I1-Z	I2-X I2-Z	TE Connectivity G-NSDOG1-006 MEMS Inclinometer	4	Figure 50

Tension in each of the 30 bridle lines was measured with 30 identical, 2.5- kip capacity, digital tension dynamometers. These load cells were labeled B1 – B30, where B1 was the bridle line closest to tower 1, and B30 was the bridle that connected to the catenary closest to tower 2. Digital dynamometers (as opposed to analog load cells) were chosen because the

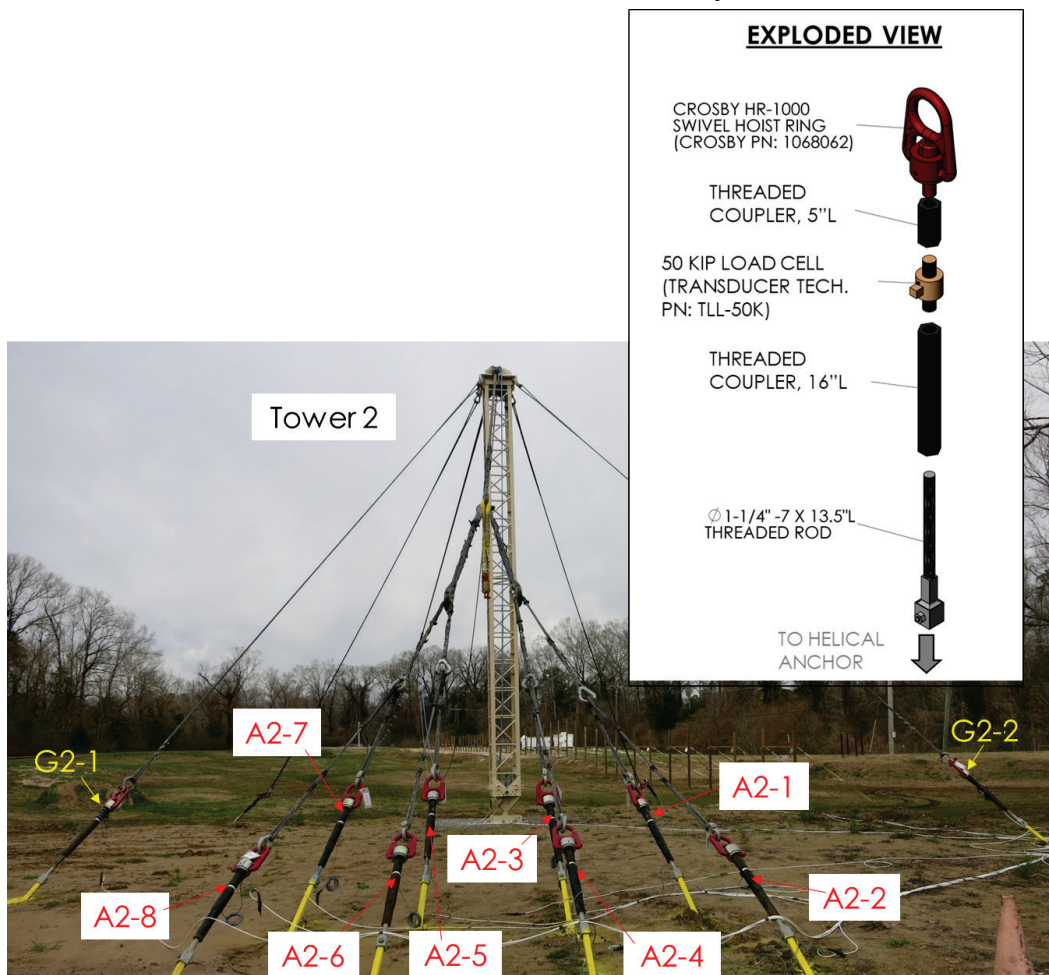
digital display gave the winch operator instant feedback on the bridle-line tension. This allowed for equal tension in each bridle line to be achieved despite each winch load being independently applied by 30 unique operators. Figure 47 illustrates the bridle line tension measurement.

Figure 47. Bridle line tension measurement. Gauge B1 is shown; gauges B2 - B30 are similar.

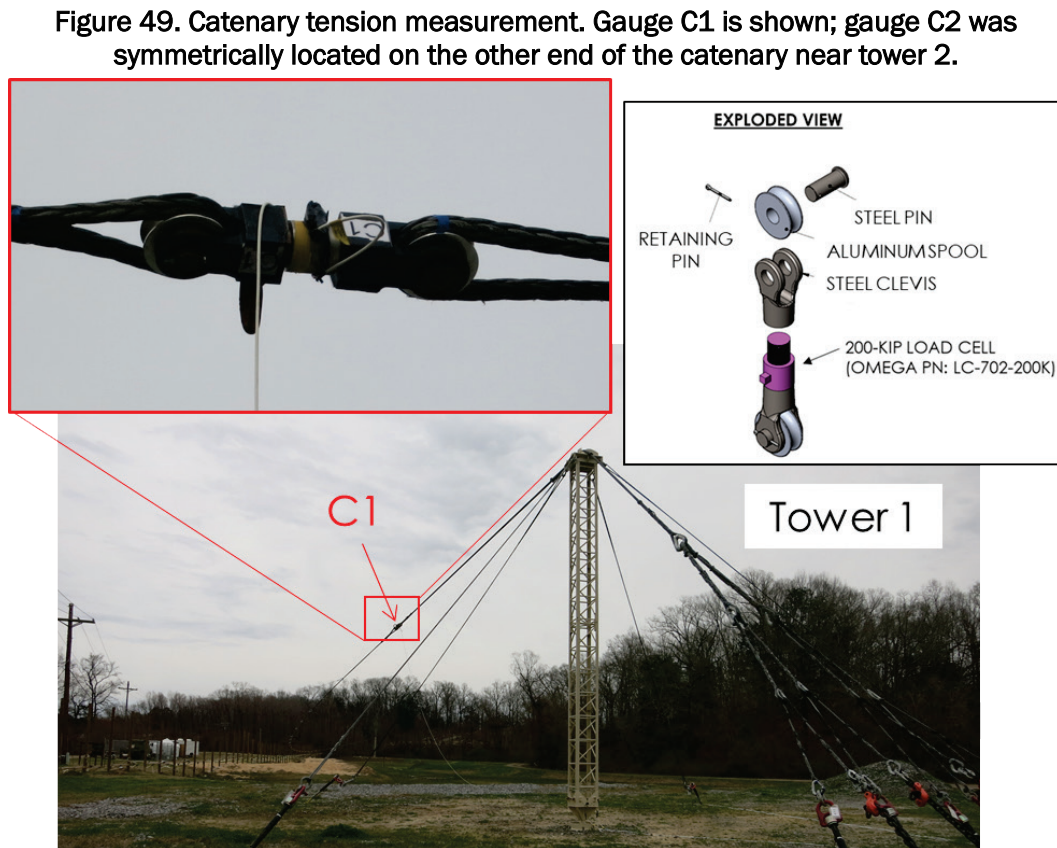


Each of the 24 helical ground anchors (12 per tower) was instrumented with an identical, 50-kip capacity, analog load cell. The load cells on each of the four guy line anchors attached to tower 1 were labeled 'G1-1' through 'G1-4.' Similarly, the guy line anchors for tower 2 were labeled 'G2-1' through 'G2-4.' The 8 main cable anchors in the tower 1 array were labeled 'A1-1' through 'A1-8'; the 8 main cable anchors in the tower 2 array were identified as 'A2-1' through 'A2-8.' Figure 48 shows the instrumented anchors of tower 2. Tower 1 was instrumented in a similar fashion.

Figure 48. Helical ground anchor load measurement. Instrumented anchors for tower 2 are shown; tower 1 anchors were identically instrumented.

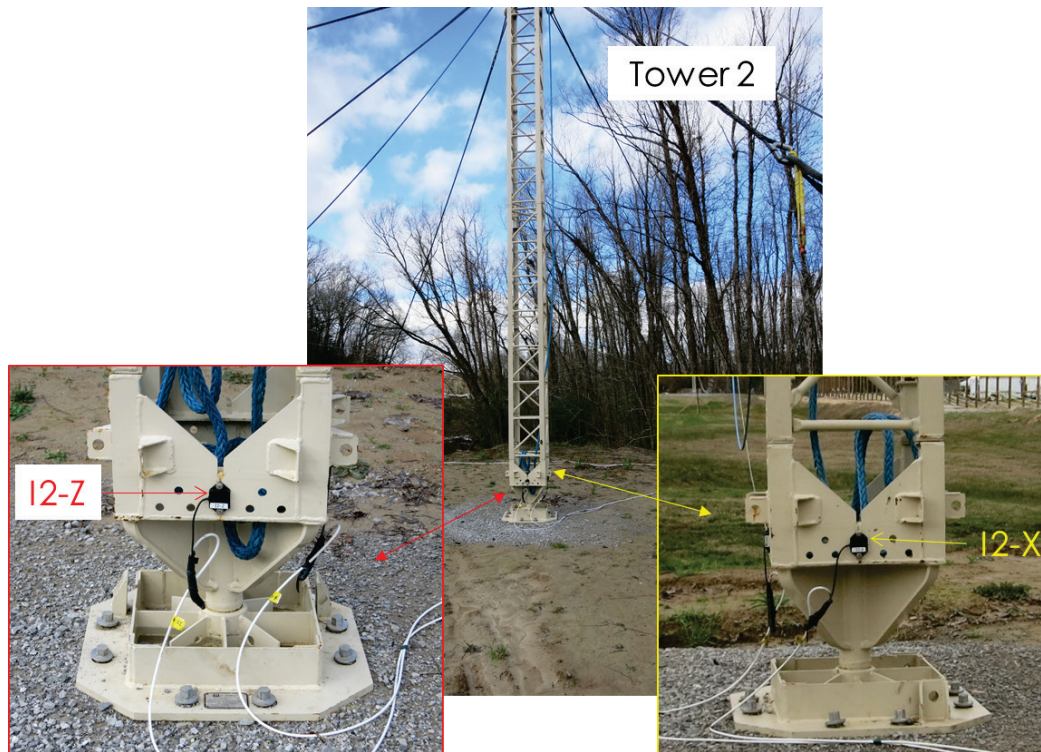


The tension in the main catenary cable was measured redundantly at two locations equidistant from the centerline of the crossing. These two, identical, 200-kip capacity load cells were labeled 'C1' and 'C2.' 'C1' was located on the catenary approximately midway between tower 1 and the first bridle line pulley. 'C2' was symmetrically located on the other end of the catenary between the last bridle line pulley and tower 2. 'C1' and 'C2' were about 75 ft from tower 1 and tower 2, respectively. Figure 49 shows a photograph of load cell 'C1,' located on the catenary near tower 1.



Two inclinometers were placed on each tower to measure angular rotation. The two inclinometers attached to tower 1 were labeled 'I1-X' and 'I1-Z.' Similarly, 'I2-X' and 'I2-Z' were affixed to tower 2. The gauges with the 'X'-suffix were attached to the x-face of each tower and measured tilt perpendicular to the river current direction. The 'Z' gauges measured tilt in the upstream-downstream direction. The inclinometers were calibrated to read 0° when plumb, i.e., vertically oriented. Figure 50 shows the tower 2 inclinometers. The other two inclinometers were similarly attached to tower 1. The inclinometers measure single-axis rotation about the axis where the cable exits the body of the inclinometer. From the views in Figure 50, the cables can be seen exiting the left side of the gauge.

Figure 50. Tower tilt measurements. Tower 2 inclinometers are shown; tower 1 inclinometers were similar.



Data from each gauge were recorded using a Campbell Scientific CR3000 data logger. A continuous sampling rate of 0.033 Hz was used. The data were not filtered. During testing, data were also wirelessly transmitted to a laptop to facilitate real-time load monitoring. The transient data were subsequently reduced to data points corresponding to each incremental flow rate in Table 5. The test to failure (test 2) was also recorded from multiple angles with video cameras.

4.2 OCS test results and discussion

The OCS test pull #1 and test pull #2 data are provided in Table 7 and Table 8, respectively. The data are also plotted in Figures 51-55. The magnitude of the applied load for each test was determined by multiplying each bridle line tension measurement, B_i , by 2 (to account for the doubling effect of the pulley), and summing over the 30 bridle lines, i.e.,

$$F_{\text{drag}} = \sum_{i=1}^{30} 2B_i \quad (9)$$

For test #1, tension was applied to the bridle lines to simulate current speeds of 3, 4, 5, 6, 7, and 8 ft/s. Once the load corresponding to the 8-

ft/s current was reached, the system was left in that tensioned state. After 4 days, the tension was released in preparation for test #2. Once the system was reset, test pull #2 was executed.

Test #2 was a test to failure that was intended to estimate the capacity of the entire overhead cable system. In test #2, tension was reapplied to the bridle lines, starting with the 3 ft/s condition again, just as in test #1. Load was increased in increments corresponding to 1 ft/s uniform current increases, and each load increment was held for a minimum of 3 min prior to proceeding to the next. Failure occurred while load was being ramped up from the 10 ft/s to the 11 ft/s current state. The maximum applied drag load was 40.5 kips at the time of failure, which corresponds to a uniform current velocity of 10.7 ft/s. The failure mode is discussed in detail in section 4.2.1. Section 4.2.2 presents a load analysis of the forces on the tower just prior to failure.

Table 7. OCS test pull #1 data.

		Simulated Uniform Current Velocity (ft/s)	3	4	5	6	7	8
		<i>Target Total Drag Load [Eq. 2] (kips)</i>	3.5	4.8	6.6	9.1	12.5	17.2
Bridle Tension	Total Applied Drag Load [Eq. 9] (kips)	3.7	4.6	6.3	8.7	12.0	17.0	
Catenary Tension	C1 (kips)	13.8	17.0	21.6	27.3	33.5	40.4	
	C2 (kips)	13.3	16.9	21.6	27.3	33.3	40.8	
Tower 1 Guy Tension	G1-1 (kips)	4.3	4.9	6.0	7.4	9.1	11.4	
	G1-2 (kips)	4.1	4.6	5.4	6.4	7.1	7.6	
	G1-3 (kips)	-0.3	-0.3	-0.3	-0.3	-0.3	-0.3	
	G1-4 (kips)	-0.2	-0.2	-0.2	-0.2	-0.2	-0.2	
Tower 2 Guy Tension	G2-1 (kips)	2.1	2.6	3.4	4.7	6.5	8.9	
	G2-2 (kips)	2.7	3.3	3.9	4.8	5.4	6.0	
	G2-3 (kips)	-0.1	-0.1	-0.1	-0.1	-0.1	-0.1	
	G2-4 (kips)	0.0	0.0	0.0	0.0	0.0	0.0	
Tower 1 Anchor Array Tension	A1-1 (kips)	1.2	1.8	2.6	3.5	4.4	5.2	
	A1-2 (kips)	1.1	1.4	1.9	2.5	3.3	4.2	
	A1-3 (kips)	3.4	3.9	4.5	5.3	6.2	6.9	
	A1-4 (kips)	1.2	1.6	2.1	2.8	3.5	4.5	
	A1-5 (kips)	2.3	3.1	4.0	5.0	6.1	7.2	
	A1-6 (kips)	1.3	1.7	2.3	3.1	4.1	5.4	
	A1-7 (kips)	1.6	2.1	2.8	3.6	4.5	5.6	
	A1-8 (kips)	1.0	1.4	1.9	2.7	3.6	4.8	
Tower 2 Anchor Array Tension	A2-1 (kips)	1.3	1.8	2.5	3.3	4.1	4.9	
	A2-2 (kips)	1.3	1.6	1.9	2.5	3.1	3.8	
	A2-3 (kips)	2.6	3.4	4.2	5.2	6.1	7.0	
	A2-4 (kips)	1.9	2.4	3.0	3.9	4.8	5.8	
	A2-5 (kips)	-	-	-	-	-	-	
	A2-6 (kips)	0.9	1.2	1.7	2.4	3.1	4.2	
	A2-7 (kips)	2.6	3.3	4.2	5.3	6.4	7.7	
	A2-8 (kips)	1.5	1.8	2.4	3.1	4.0	5.0	
Tower 1 Tilt	I1-X (deg)	-0.03	0.00	0.23	0.46	0.79	1.53	
	I1-Z (deg)	-0.03	-0.06	-0.01	0.12	0.24	0.49	
Tower 2 Tilt	I2-X (deg)	-0.04	0.00	0.14	0.23	0.44	0.96	
	I2-Z (deg)	0.03	0.00	0.02	-0.01	0.09	0.37	

Table 8. OCS test pull #2 data.

		Simulated Uniform Current Velocity (ft/s)	3	4	5	6	7	8	9	10	10.7†
		Target Total Drag Load [Eq. 2] (kips)	3.5	4.8	6.6	9.1	12.5	17.2	23.7	32.5	40.6
Bridle Tension	Total Applied Drag Load [Eq. 9] (kips)	3.8	4.9	6.8	8.9	12.3	16.8	23.7	31.9	40.5	
Catenary Tension	C1 (kips)	15.0	18.3	22.3	28.8	36.0	43.6	53.9	65.1	73.9	
	C2 (kips)	14.9	18.2	22.2	28.7	36.0	43.5	53.7	65.2	74.6	
Tower 1 Guy Tension	G1-1 (kips)	4.2	4.9	5.9	7.3	9.6	12.6	15.3	19.4	22.6	
	G1-2 (kips)	4.2	4.8	5.5	6.5	7.7	8.9	9.4	9.8	10.5	
	G1-3 (kips)	-0.2	-0.2	-0.2	-0.2	-0.2	-0.2	-0.2	-0.2	-0.3	-0.3
	G1-4 (kips)	-0.2	-0.2	-0.2	-0.2	-0.2	-0.2	-0.2	-0.2	-0.3	-0.3
Tower 2 Guy Tension	G2-1 (kips)	4.7	5.4	6.4	7.8	9.5	11.4	14.3	18.6	22.3	
	G2-2 (kips)	5.2	6.0	6.8	7.8	8.6	9.2	10.0	10.3	10.5	
	G2-3 (kips)	0.0	0.0	0.0	0.0	0.0	-0.1	-0.1	-0.1	-0.1	-0.1
	G2-4 (kips)	0.0	0.0	0.0	0.0	0.0	-0.1	-0.1	-0.1	-0.1	-0.1
Tower 1 Anchor Array Tension	A1-1 (kips)	1.9	2.3	2.9	3.8	4.6	5.4	6.6	7.4	7.2	
	A1-2 (kips)	1.6	2.0	2.5	3.2	4.0	4.9	6.2	8.0	9.2	
	A1-3 (kips)	1.7	2.2	2.9	3.9	5.0	5.9	7.3	8.4	8.9	
	A1-4 (kips)	2.2	2.7	3.3	4.3	5.2	6.2	7.6	9.6	11.4	
	A1-5 (kips)	1.9	2.5	3.2	4.3	5.5	6.7	8.6	10.1	11.0	
	A1-6 (kips)	1.3	1.8	2.3	3.3	4.3	5.7	7.7	10.3	13.0	
	A1-7 (kips)	1.9	2.4	3.0	3.9	4.9	6.0	7.3	8.4	9.9	
	A1-8 (kips)	2.1	2.7	3.3	4.3	5.3	6.5	8.1	10.5	13.3	
Tower 2 Anchor Array Tension	A2-1 (kips)	0.4	0.7	1.1	1.9	2.9	3.9	5.4	6.9	8.0	
	A2-2 (kips)	0.9	1.2	1.5	2.1	2.9	3.8	5.0	6.3	7.2	
	A2-3 (kips)	2.3	2.9	3.6	4.8	6.1	7.2	8.8	10.3	11.6	
	A2-4 (kips)	1.4	1.7	2.2	3.1	4.1	5.2	6.7	8.4	9.7	
	A2-5 (kips)	2.4	2.9	3.6	4.7	5.8	6.9	8.5	9.9	11.1	
	A2-6 (kips)	1.1	1.5	2.0	2.8	3.7	4.8	6.2	8.0	9.5	
	A2-7 (kips)	2.7	3.4	4.2	5.6	7.0	8.4	10.3	12.4	14.1	
	A2-8 (kips)	1.7	2.2	2.7	3.7	4.9	6.0	7.5	9.4	11.0	
Tower 1 Tilt	I1-X (deg)	0.50	0.62	0.82	1.04	1.28	1.86	2.43	3.91	5.38	
	I1-Z (deg)	0.02	0.04	0.16	0.14	0.25	0.24	0.38	0.84	1.62	
Tower 2 Tilt	I2-X (deg)	0.39	0.56	0.66	0.86	1.13	1.23	1.55	2.01	2.31	
	I2-Z (deg)	-0.11	-0.12	0.03	0.00	-0.03	-0.01	0.12	0.29	0.41	

†: Failure occurred prior to reaching the 11 ft/s uniform current condition.

Figure 51. Calculated and actual drag loads versus uniform current velocity.

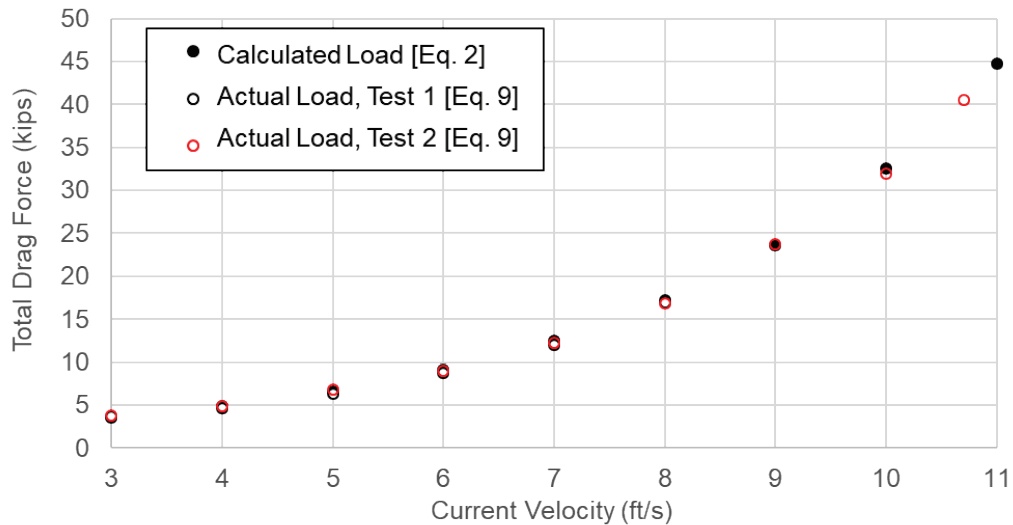


Figure 51 shows total drag load versus current velocity. The solid black dots represent the total drag load on a 210 m IRB in a uniformly distributed current. These were the target loads for each load test increment. The actual bridle load measurements from both tests (the empty circles) closely match the target loads in each case up to 10 ft/s. During test #2, as load was being increased from 10 ft/s to 11 ft/s, failure occurred when the total applied drag load equaled 40.5 kips. This load corresponds to a uniform current velocity of 10.7 kips. In Figures 52-55, uniform current velocity is plotted on the lower x-axis, and the corresponding drag force is shown on the upper x-axis for convenience.

Figure 52. Catenary tension measurements from load cells C1 and C2.

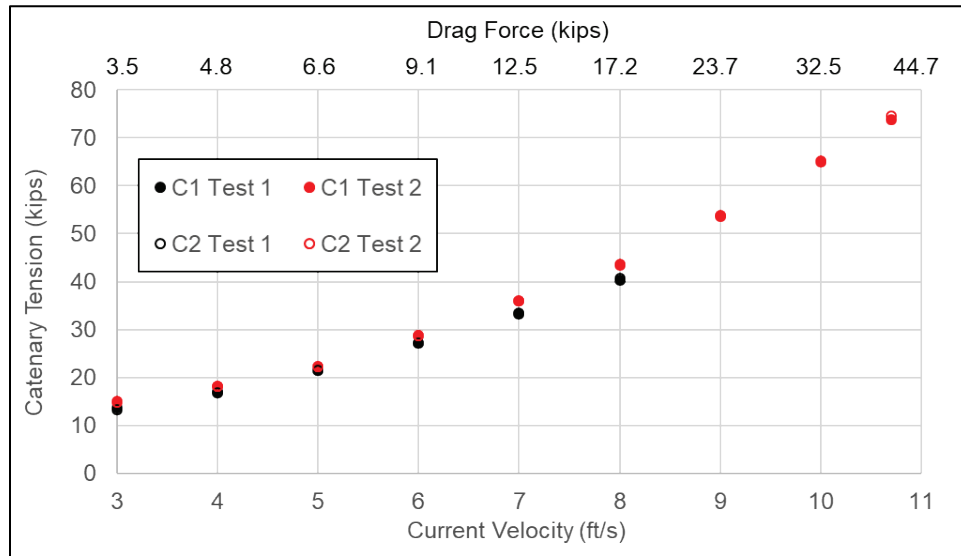


Figure 52 shows the tension measurements from the two load cells in-line with the catenary (gauges 'C1' and 'C2') for the two tests. Because the 'C1' and 'C2' gauges are symmetrically oriented on the catenary, their readings should be similar, i.e., the filled and hollow circles in Figure 52 should fall on top of each other. And, that is exactly what is observed. The tension in the catenary when the failure occurred was 74 kip. This is well below the 306-kip breaking strength of the 1.75-in.-diam Eversteel™-X synthetic catenary rope.

Looking at the loads on the tower guys in Tables 7 and 8, 'G1-3,' 'G1-4,' 'G2-3,' and 'G2-4' remained slack regardless of how much load was applied. These '#3' and '#4' guy lines, which are the guys closest to the crossing (see Figure 46), only help stabilize the towers during assembly. The drag load tends to pull the top of each tower toward the IRB. Therefore, only the guys in the #1 and #2 position, i.e. 'G1-1,' 'G2-1,' 'G1-2,' and 'G2-2,' resist the overturning moment on the tower.

Figure 53. Tower guy anchor load data: (a) guy #1 for tower 1 and 2, (b) guy #2 for tower 1 and 2. Guys #3 and #4 are not plotted as they remained slack (tension=0).

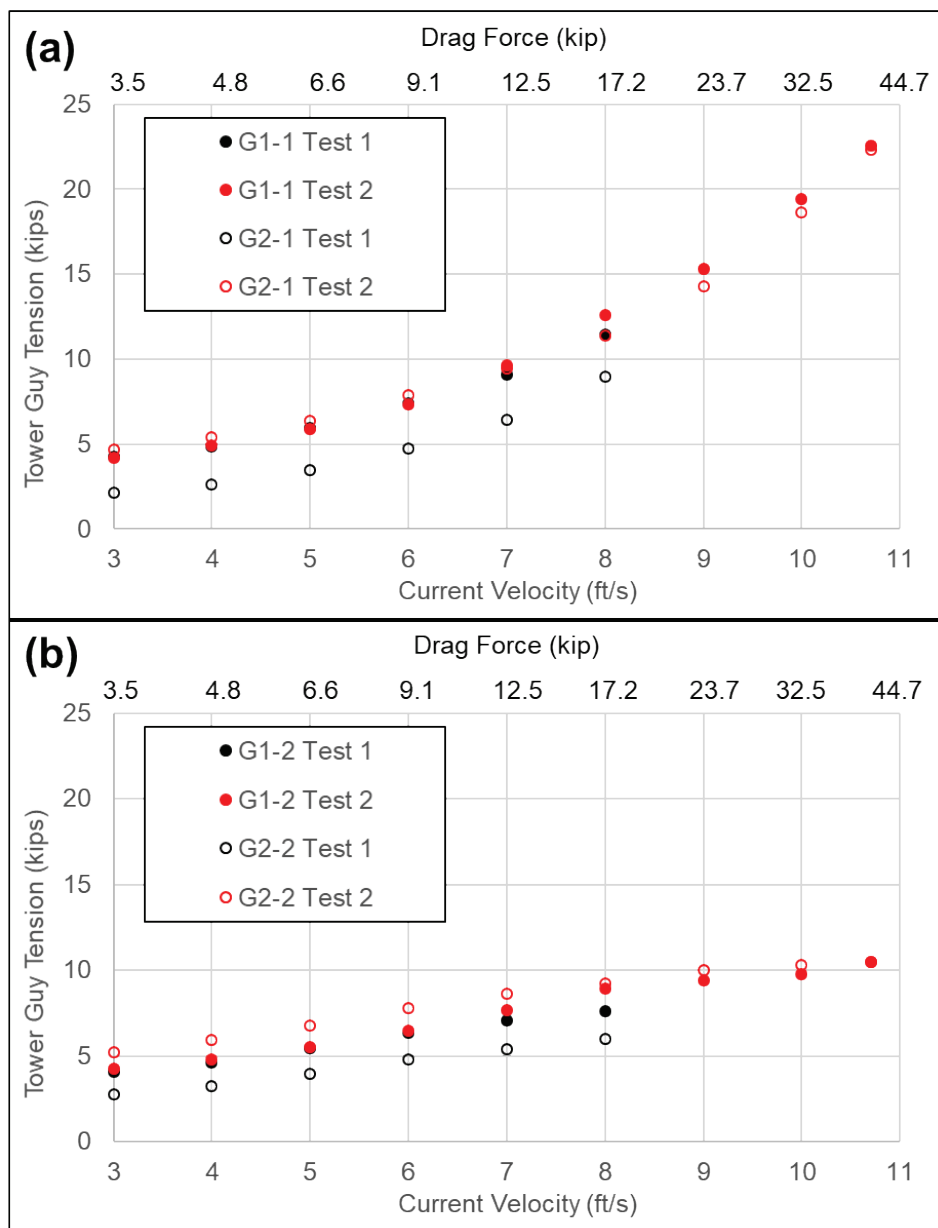


Figure 53 plots the tension in the non-slack tower guys. Figure 53(a) shows the guys in the '#1' position, which are located upstream of the towers. Figure 53(b) shows the guys in the '#2' position, which are downstream of the towers. The downstream '#2' guy lines experienced lower tension compared to the upstream ('#1') guys. The maximum guy line tension (22.6 kips) was experienced by 'G1-1.' This occurred at the time of failure during test 2. The 'G1-1' helical anchor actually pulled out of the ground at this load, which allowed tower 1 to overturn. At tower 2, the load on 'G2-1' was almost identical (22.3 kips); however,

the helical anchor attached to ‘G2-1’ did not fail. The soil at that anchor location potentially had a higher pullout resistance.

The anchor array load data are shown in Figure 54. The load on anchor ‘#1’ in each array is plotted in Figure 54(a). Anchor ‘#2’ load is plotted in Figure 54(b) and so on up to the final anchor in each array (‘#8’), shown in Figure 54(h). An issue with one of the gauges (A2-5) prevented data collection during test 1. The issue was corrected prior to the second pull test. The largest load of the array anchors was experienced by A2-7, which peaked at 14.1 kips just prior to failure. Overall, the load was fairly well-distributed amongst the eight anchors in each array.

The data from the inclinometers attached to the towers are plotted in Figure 55. Tilt in the x -direction (perpendicular to current flow) is shown in Figure 55(a). And, tilt in the z -direction (parallel to current flow) is plotted in Figure 55(b). In these plots, a tilt of 0° indicates the tower is perfectly plumb (vertical). The angle at which Tower 1 overturned, θ , was calculated using the dot product theorem

$$\mathbf{a} \cdot \mathbf{b} = |\mathbf{a}| |\mathbf{b}| \cos (\theta) \quad (10)$$

where, \mathbf{a} is a vector pointing from the point of rotation near the base of the tower to an initial point at the top of the tower prior to tower movement, i.e., $\mathbf{a} = \begin{pmatrix} 0 \\ 300.6 \\ 0 \end{pmatrix} \text{ in.}$ \mathbf{b} also starts at the point of rotation near the base, but points to the top of the tower after the tilt reached its maximum (5.4° in the x -direction and 1.6° in the z -direction), i.e., $\mathbf{b} = \begin{pmatrix} 28.1 \\ 298.6 \\ 8.5 \end{pmatrix} \text{ in.}$ Solving Eq. 10 for θ shows that the tower overturned when the total tilt reached 5.6° off-vertical. For the 25.4-ft tall tower, this resulted in the top of the tower having a horizontal offset of $25.4 \text{ ft} \cdot \sin (5.6^\circ) = 2.5 \text{ ft}$ relative to the tower base.

Figure 55 shows that the lean of tower 2 was not nearly as severe as that of tower 1. Recall that the soil around the base of tower 2 was compacted prior to tower erection. However, the soil beneath tower 1 was left undisturbed. The vertical compressive load on the tower eventually exceeded the bearing capacity of the soil underneath. Consequently, tower 1 compressed into the ground approximately 6 in. This likely contributed to the failure, which is discussed in the following section.

Figure 54. Anchor array load data: (a) A1-1 and A2-1, (b) A1-2 and A2-2, (c) A1-3 and A2-3, (d) A1-4 and A2-4, (e) A1-5 and A2-5, (f) A1-6 and A2-6, (g) A1-7 and A2-7, (h) A1-8 and A2-8.

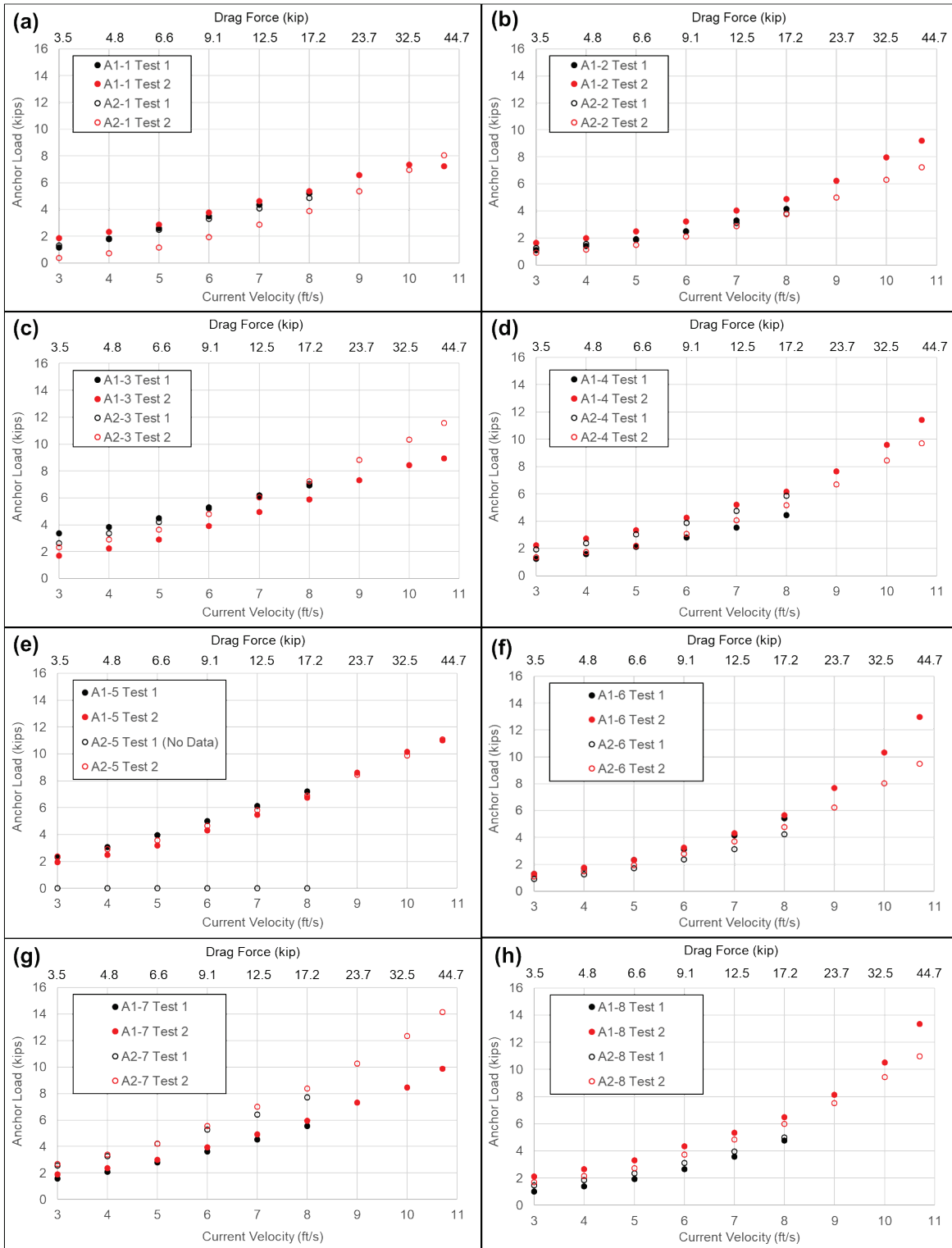
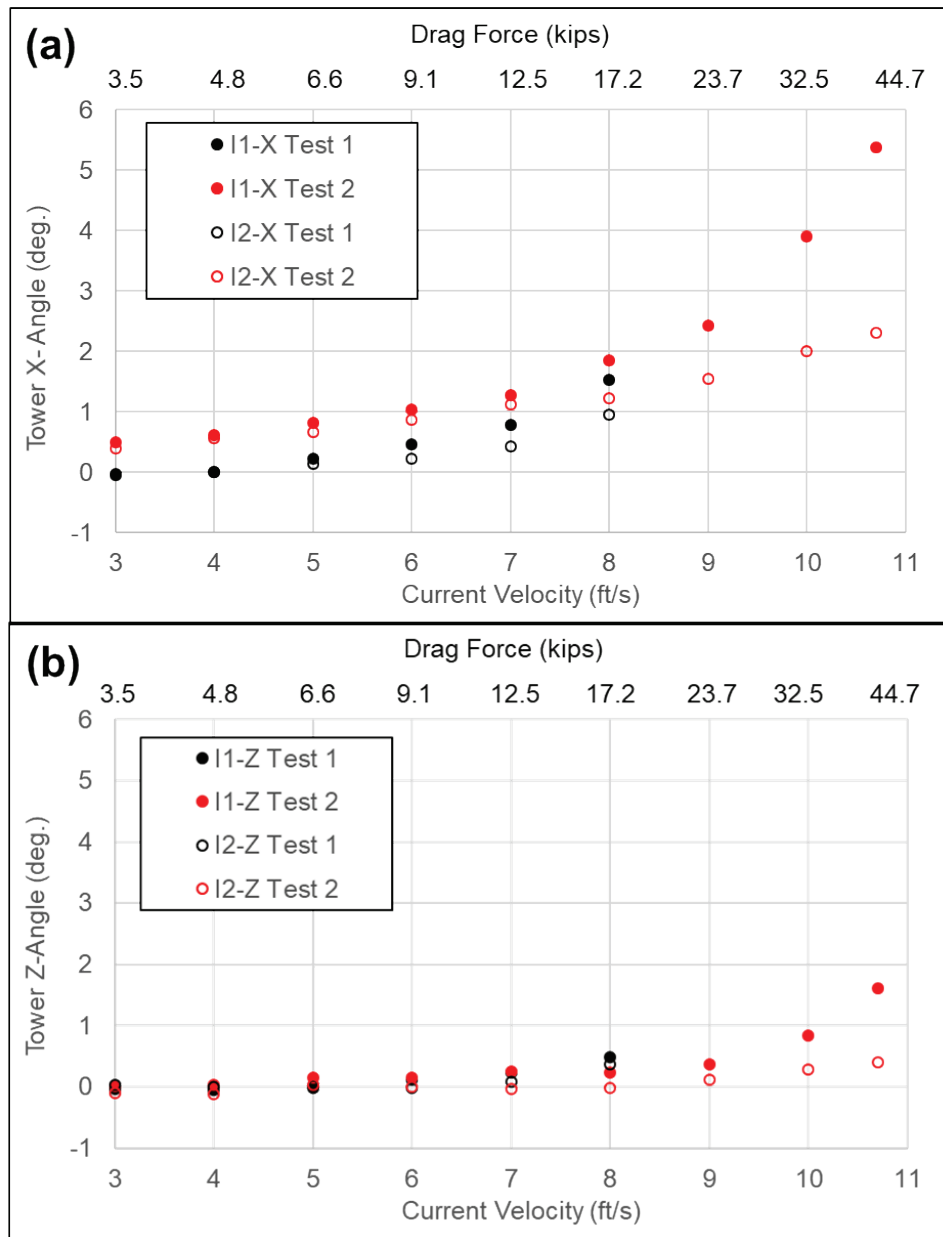


Figure 55. Tower tilt angle data: (a) tower 1 and 2 tilt in X- (crossing) direction, and (b) tower 1 and 2 tilt in Z- (downstream) direction.

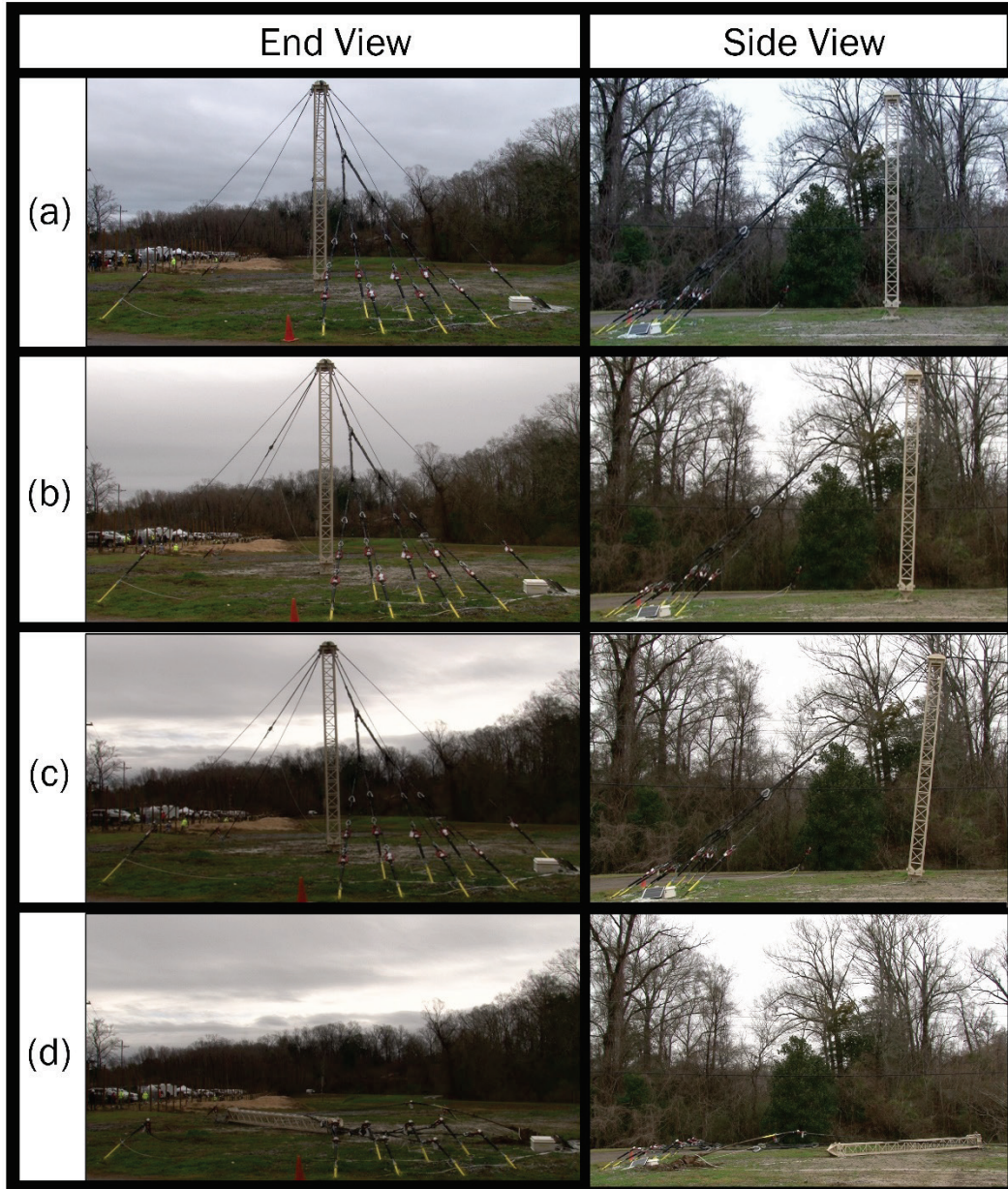


4.2.1 Failure mode

Figure 56 shows tower 1 as viewed from the end (parallel to the crossing direction) and the side (perpendicular to crossing direction) over the course of pull test #2. Figure 56(a) shows the initial state prior to any drag load being applied. In Figure 56(b), the total applied load was 23.7 kips, which corresponds to 9 ft/s of uniform current. By that point, the tower had developed a significant lean, measuring 2.4° according to inclinometer I1-X. Figure 56(c) shows the tower at a simulated velocity

of 10 ft/s (~ 32 kips of applied loading); there the tower lean had increased to about 4° out of plumb. The tower eventually toppled, as shown in Figure 56(d). Just prior to failure, the applied load totaled 40.5 kips, which corresponds to a uniform current velocity of 10.7 ft/s.

Figure 56. Tower 1 failure progression: (a) initial state, $v=0$ ft/s, (b) $v=9$ ft/s, (c) $v=10$ ft/s, and (d) failure at $v=10.7$ ft/s.



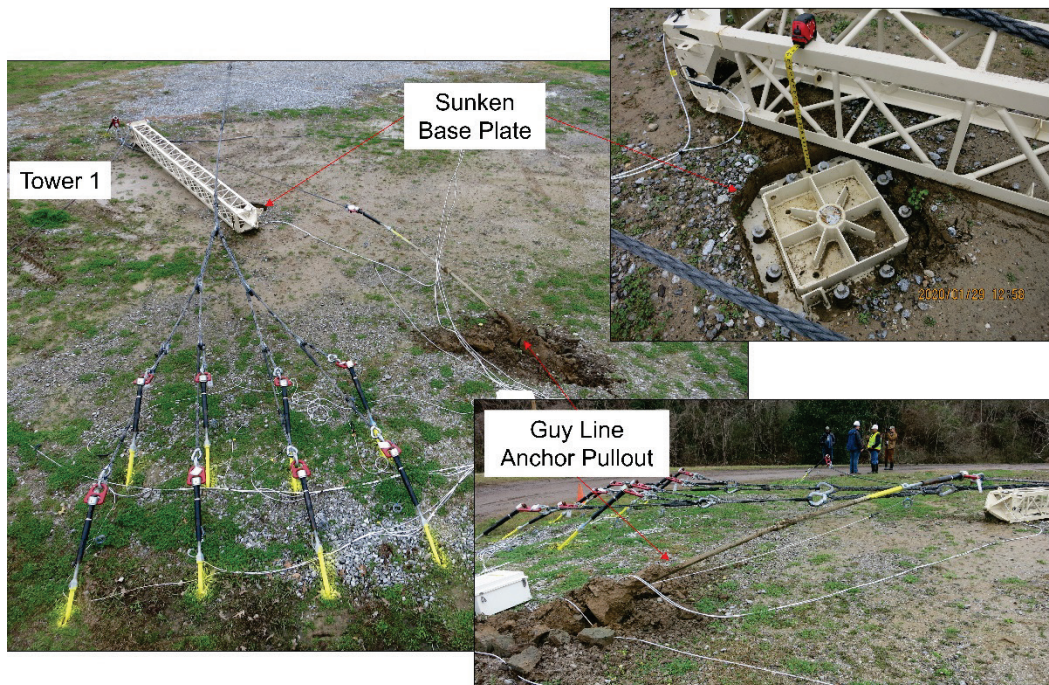
The resultant load on the tower 1 caused guy line #1 to experience the highest level of tension. The 'G1-1' anchor pulled out of the ground; this is

what ultimately allowed the tower to overturn. The load on the ‘G1-1’ anchor when pullout occurred was 22.6 kips.

The baseplate of the tower also gradually sank into the ground due to the bearing pressure exceeding the soil’s capacity. This is visible with a close look at the base of the tower, especially from the side views in Figure 56. The baseplate depressed about 6 in. into the ground in total. The edge nearest the crossing embedded slightly more than the far edge (closest to the anchor array), likely exacerbating the tilt of the tower.

Figure 57 provides additional views of the overturned tower, sunken baseplate, and uprooted guy line anchor. There was a light rain the morning of the test, which softened the ground and probably influenced the failure to some extent. Recall that the soil underneath tower 2 was compacted prior to tower placement. However, no soil preparation was performed for tower 1. The stronger foundation underneath tower 2 prevented the baseplate from sinking into the earth and ultimately made tower 2 more stable than tower 1. This attests to the importance of soil conditions at the OCS site. OCS capacity strongly depends on the soil conditions present.

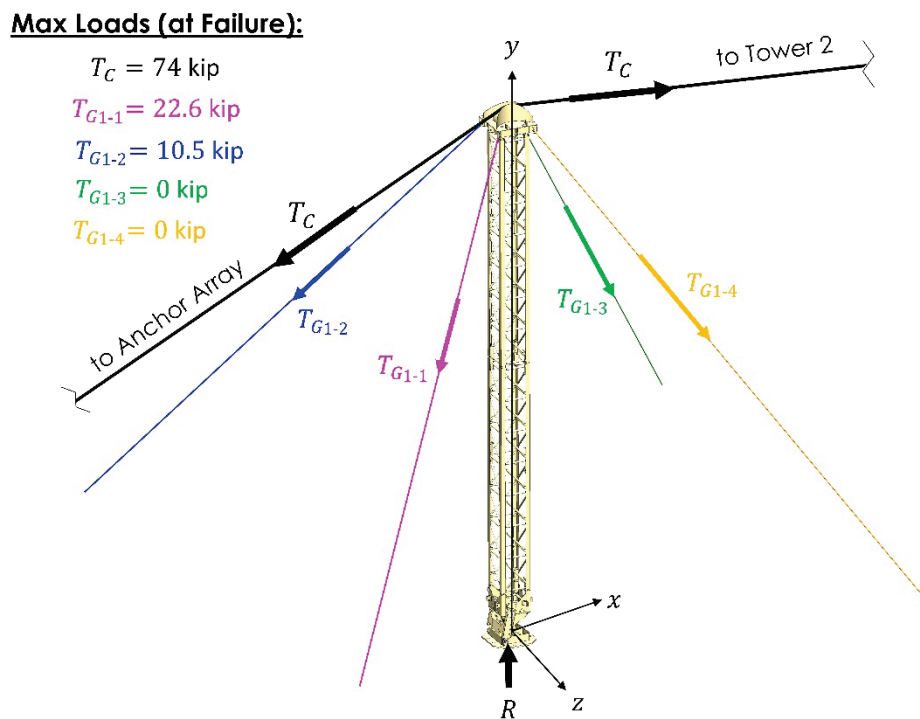
Figure 57. Tower 1 failure photographs.



4.2.2 BSS tower load analysis

An analysis of tower 1 was performed to estimate the factor of safety against buckling under maximum tower loading. Figure 58 is a free-body diagram (FBD) showing the maximum forces on tower 1 (just prior to failure). Note that the tension in 'G1-3' and 'G1-4' was zero, so those guys did not place any load on the tower. Also note that friction over the top of the tower was neglected.

Figure 58. Maximum forces on tower 1.



The first step in the analysis was to combine the catenary tension, T_C , load vectors to determine the resultant catenary load, $T_{C,R}$. Figure 59 shows the diagram used to add the T_C vectors. The resultant load vector, $T_{C,R}$, is given by

$$\mathbf{T}_{C,R} = T_C \begin{pmatrix} \cos(\theta) - \cos(\alpha) \\ -\sin(\theta) - \sin(\alpha) \end{pmatrix} \quad (11)$$

where, the angles were measured as $\theta = 5.6^\circ$ and $\alpha = 39.4^\circ$. The maximum stable tension in the catenary was $T_C = 74$ kip. Thus, the x' and y components of $\mathbf{T}_{C,R} = \begin{pmatrix} 16.5 \\ -54.2 \end{pmatrix}$ kip, and the magnitude, $|\mathbf{T}_{C,R}| = 56.7$ kip.

Figure 59. Diagram showing the resultant catenary load on tower 1 obtained by vector addition.

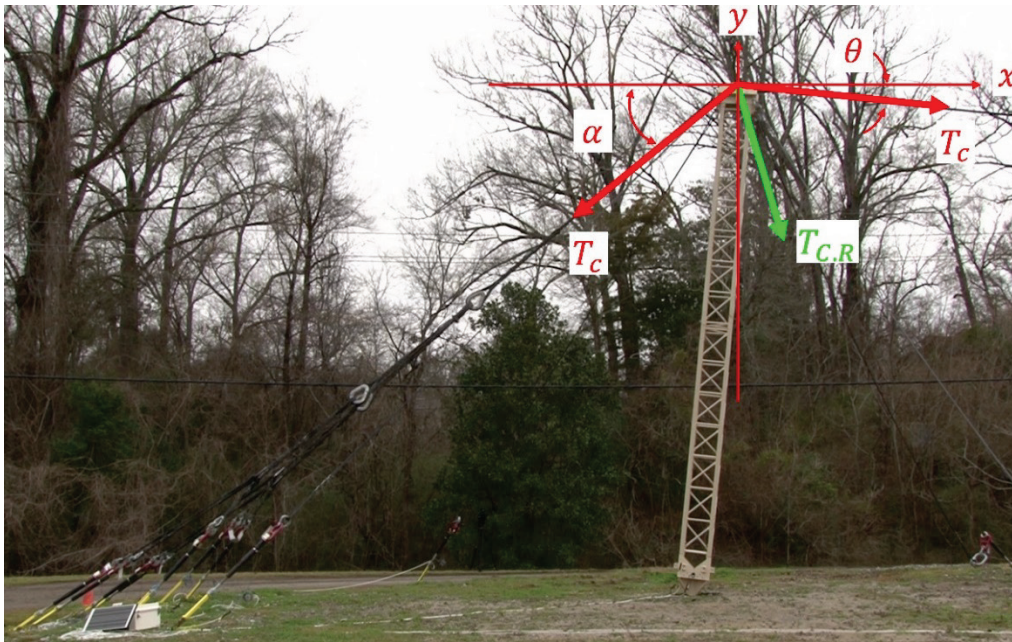


Figure 60 shows the resulting FBD of tower 1 after replacing the T_c vectors with their equivalent resultant. Note that guy wires 'G1-3' and 'G1-4' were omitted since they were not under tension. The reaction force, R , at the base of the tower was determined by summing the forces in the x , y , and z directions using vector algebra, i.e.,

$$\mathbf{R} + \mathbf{T}_{C,R} + \mathbf{T}_{G1} + \mathbf{T}_{G2} = \mathbf{0} \quad (1)$$

The force components for \mathbf{T}_{G1} and \mathbf{T}_{G2} were calculated using

$$\mathbf{T}_{G1,2} = T_{G1,2} \lambda_{G1,2} \quad (2)$$

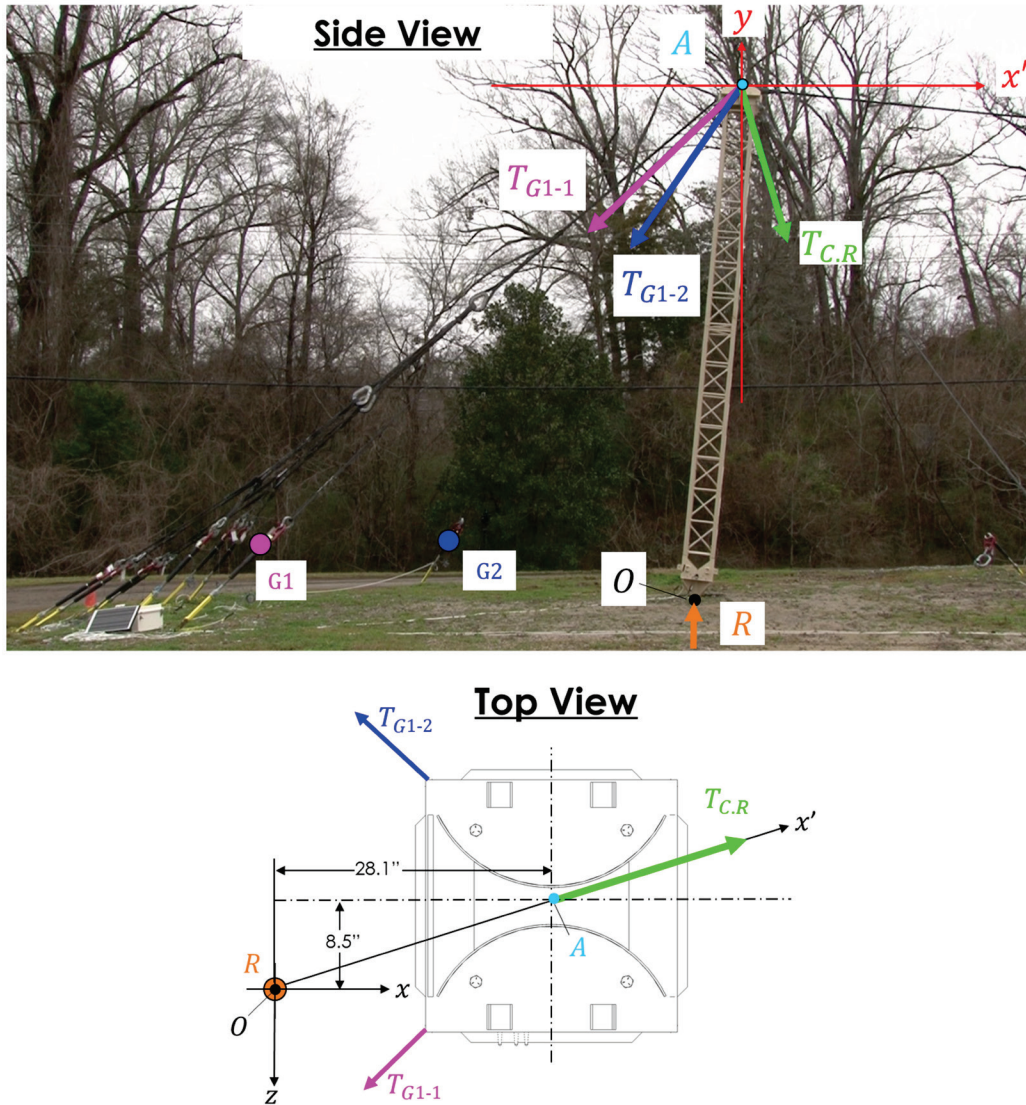
where, the magnitudes, $T_{G1} = 22.6$ kips and $T_{G2} = 10.5$ kips. And, $\lambda_{G1,2}$ represents unit vectors from point A to points $G_{1,2}$, i.e.,

$$\lambda_{G1,2} = \frac{\mathbf{AG}_{1,2}}{|\mathbf{AG}_{1,2}|} \quad (3)$$

Once $\mathbf{T}_{C,R}$, \mathbf{T}_{G1} , and \mathbf{T}_{G2} were calculated, Eq. 12 was solved for \mathbf{R} , which yielded $\mathbf{R} = \begin{pmatrix} -3.8 \\ -72.6 \\ 7.1 \end{pmatrix}$ kips, with magnitude $|\mathbf{R}| = 73$ kips. Recall from section 3.3.2 that the compressive load capacity of the tower was

determined to be 102 kips. Therefore, the factor of safety against tower buckling under maximum load is about 1.4 (102 kips/73 kips).

Figure 60. Free-body diagram used to determine the reaction force at the base of the tower 1.

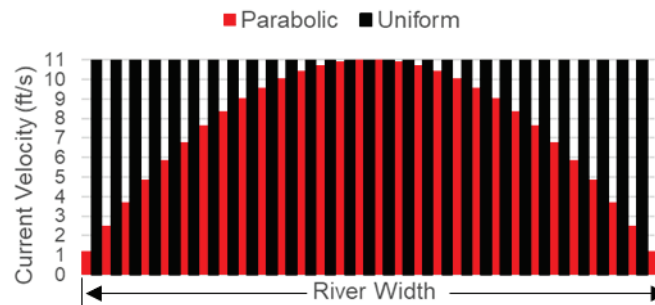


4.3 Loading equivalents for uniform versus parabolic river current distributions

The BSS CPD (MSCoE 2014) threshold requirement states that the OCS must anchor 210 m of IRB in currents up to 11 ft/s. The requirement does not specify how the velocity is distributed across those 210 m. The ‘worst-case’ interpretation of the requirement is to assume a constant 11 ft/s velocity across the entire width. In actuality, river currents tend to flow fastest in the center, and the velocity slows toward the banks, following a parabolic distribution.

Figure 61 illustrates the difference between a parabolic and uniform velocity profile. The parabolic distribution is shown in red and the uniform distribution is shown in black. The peak current speed for both profiles is 11 ft/s. However, for the parabolic distribution, the velocity reaches its maximum at the center and tapers off toward the river banks unlike the uniform profile, where the 11 ft/s velocity is constant across the entire width of the river. The uniform velocity profile will produce more drag force compared to the parabolic profile.

Figure 61. Parabolic and uniform velocity profiles for an 11 ft/s current.



The difference in the total drag load for a uniform versus parabolic current profile can be calculated using the empirical drag function of Eq. 1. The second term in Eq. 1 gives the drag force on a single IRB bay as a function of current velocity. For design and testing purposes, we assumed a constant, uniformly distributed 11 ft/s current speed. The total drag force produced on a 210 m IRB for that ‘worst-case’ current profile was calculated using Eq. 1 with $n_{\text{bays}} = 30$, i.e.,

$$F_{\text{drag}} = n_{\text{bays}} \times 44.9e^{0.3184v(\text{ft/s})} = 30 \times 44.9e^{0.3184(11 \text{ ft/s})} = 44,714 \text{ lbf} = 44.7 \text{ kip}$$

For a non-uniform flow distribution, the second term in Eq. 1 can still be used to find the drag force on a single IRB bay. But, since the velocity is not constant, the drag force has to be calculated separately for each bay, using Eq. 1. The total drag force on the bridge is found by summing the forces on the 30 individual bays. Table 9 provides the results of those calculations for 210 m of IRB in an 11 ft/s current based on a parabolic velocity profile.

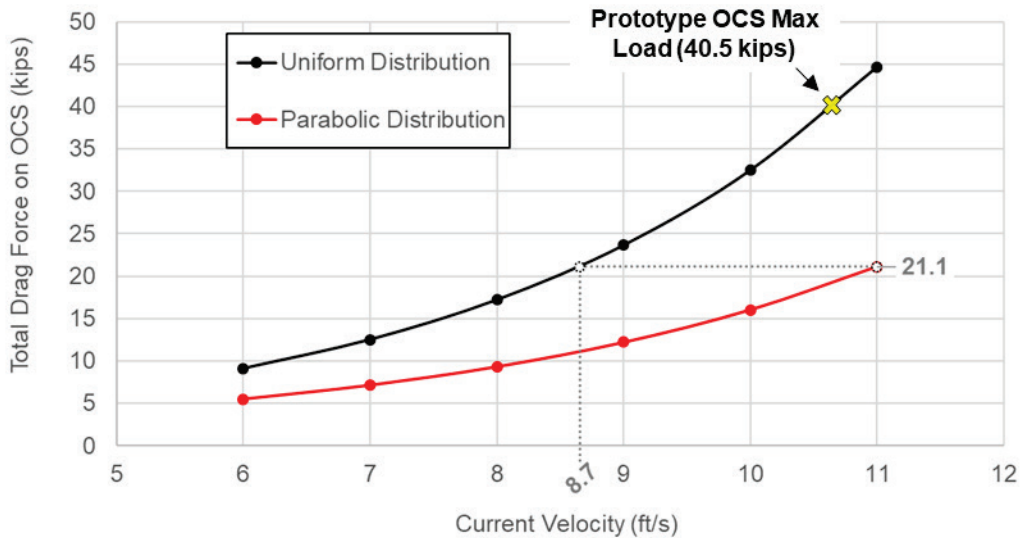
Table 9. Drag force on each IRB bay for a 689 ft (210 m), 11 ft/s crossing assuming the river has a parabolic velocity profile.

IRB Bay #	Current Velocity, v (ft/s)	$F_{\text{drag,bay}}$ (lbf)
1	1.2	64.0
2	2.5	97.1
3	3.7	143.1
4	4.8	204.6
5	5.9	284.1
6	6.8	382.7
7	7.6	500.5
8	8.4	635.4
9	9.0	782.9
10	9.6	936.2
11	10.1	1,086.7
12	10.4	1,224.4
13	10.7	1,338.9
14	10.9	1,421.2
15	11.0	1,464.2
16	11.0	1,464.1
17	10.9	1,421.1
18	10.7	1,338.8
19	10.4	1,224.2
20	10.1	1,086.5
21	9.6	936.0
22	9.0	782.7
23	8.4	635.2
24	7.6	500.4
25	6.8	382.6
26	5.9	283.9
27	4.8	204.5
28	3.7	143.0
29	2.5	97.1
30	1.2	63.9
Total Drag Force, $\sum F_{\text{drag,bay}}$:		21.1 kip

Figure 62 compares the total drag force on the OCS for a 210-m (30 IRB bay) crossing based on currents with uniform and parabolic velocity profiles. From the chart, a 210-m river with a peak current velocity of 11 ft/s and a parabolic velocity profile produces 21.1 kips of drag-induced loading. This was the calculation carried out in Table 9. A uniform velocity profile produces that same 21.1-kip load at just 8.7 ft/s. Thus, the velocity distribution has a significant effect on the drag loading.

A uniform load distribution was used for OCS testing and failure occurred when 40.5 kips of drag load was applied. This is almost twice the drag load produced by an 11 ft/s parabolic current (21.1 kips). Therefore, whether or not the OCS meets the CPS requirement depends on the velocity distribution assumed.

Figure 62. Equivalent drag forces for uniform versus parabolic current distributions.



A temptation might exist to extrapolate the parabolic distribution curve in Figure 62 to determine what current velocity corresponds to 40.5 kips of drag load. This should be avoided as the results would be nonphysical. Above 11 ft/s, the exponential at which the drag force increases, changes nearly asymptotically. The IRB becomes unstable above 11 ft/s as the bow wave begins to flow over the deck, causing a significant downforce. In regards to the IRB, current velocities above 11 ft/s should be avoided at all costs.

4.4 System-level testing summary and conclusions

Key conclusions from full-scale, system-level testing of the improved OCS include:

- A prototype of the improved OCS (described in Chapter 2) was constructed at the ERDC in Vicksburg.
- A 689-ft (210-m) crossing was simulated using 30 winches to apply a mechanical load to the OCS. The applied loading was equivalent to that of a 30 bay IRB hydraulic drag loading.
- For testing purposes, a uniform current velocity profile was assumed, i.e., the applied load was distributed uniformly amongst the 30 winches. This was a very conservative assumption, as most rivers have faster currents in the middle and slower flow slower near the banks. A typical river velocity profile has a parabolic (as opposed to uniform) distribution.
- For a river velocity of 11 ft/s, the total drag load on a 689-ft (210-m) IRB is 44.7 kips, assuming the velocity is constant across the entire river. For that same IRB, if the river current decreases parabolically toward the banks, the total drag load is only 21.1 kips. Note these values are only valid when no vehicles are on the bridge. Vehicular weight will cause the drag loads on the IRB to increase.
- The OCS was conservatively assumed to resist the entire drag load on the IRB. Any support provided by the ramp bays and/or approach guys has been neglected. Additional supports at each end of the IRB will also resist the downstream drag force, reducing the overall load on the OCS.
- The improved OCS prototype performed well up to 40.5 kips of simulated drag load, which corresponds to a uniformly distributed current velocity of 10.7 ft/s.
- At 40.5 kips of simulated drag load, the improved OCS prototype failed when one of the tower guy anchors pulled out of the ground, allowing that tower to overturn. The load on that anchor when pullout occurred was 22.6 kips. This pullout load is highly dependent on soil conditions so it will vary with location. The design manual published by the helical anchor manufacturer (Hubbell Power Systems 2018) contains additional information related to soil classification, probing, and capacity estimations.

While the improved OCS prototype was largely successful in demonstrating its ability to anchor 689 ft (210 m) of IRB in currents up to 11 ft/s, there is certainly room for improvement in the design. Several issues were identified with the prototype during testing. Section 5.1 covers these issues.

5 Summary and conclusions

In summary, an improved OCS prototype was developed and structurally evaluated via full-scale testing. While the improvements implemented to the OCS expanded its functionality, there is certainly room for additional improvement to the design. Section 5.1 describes several unresolved issues with the improved OCS prototype. Finally, key conclusions from this work are garnered in section 5.2.

5.1 Summary of unresolved issues with the improved OCS prototype

5.1.1 Helical anchors unable to penetrate all soil types

During helical anchor installation near tower #2, a subsurface layer of crushed limestone prevented helical penetration. The area had to be excavated and re-compacted, which caused a significant delay during installation. The anchor manufacturer recommends using their ROCK-IT™ helical anchor lead sections with carbide tips for such applications (https://hubbellcdn.com/literature/SF04112E_Rock-It_HelicalPileLeadSection.pdf). These special purpose anchors, shown in Figure 63, have not been tested by ERDC. The anchor manufacturer also recommends soil probe testing prior to installation to identify subsoil conditions. More work is needed to ensure the helicals can be installed in ‘all soil conditions,’ as defined in the BSS CPD.

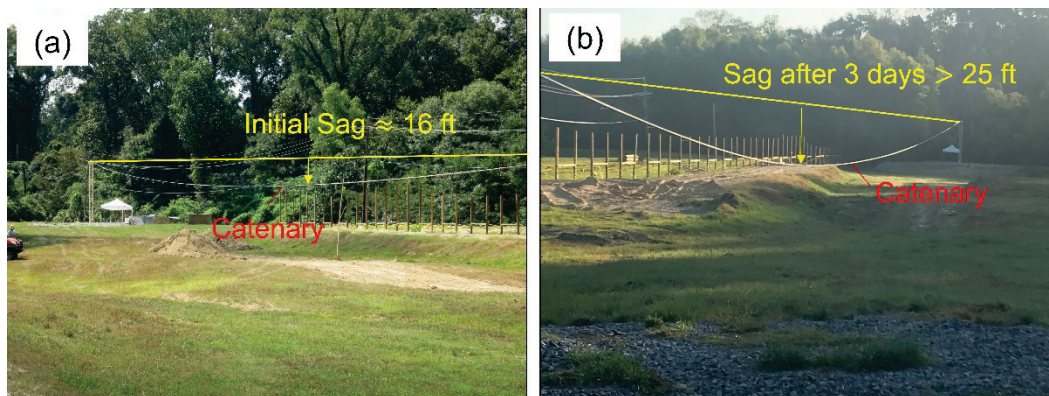
Figure 63. Chance ROCK-IT™ helical lead section designed to penetrate rocky soils.



5.1.2 Synthetic rope constructional elongation

During assembly of the prototype OCS, the catenary rope was tensioned and left to hang under its own weight. Over time, the tension decreased, causing excessive catenary sag, as shown in Figure 64. If too much initial sag is present, tension cannot develop in the OCS, rendering it ineffective for anchorage. This issue was determined to result from the synthetic rope undergoing constructional elongation.

Figure 64. Loss of catenary tension: (a) initial sag and (b) sag after 3 days.



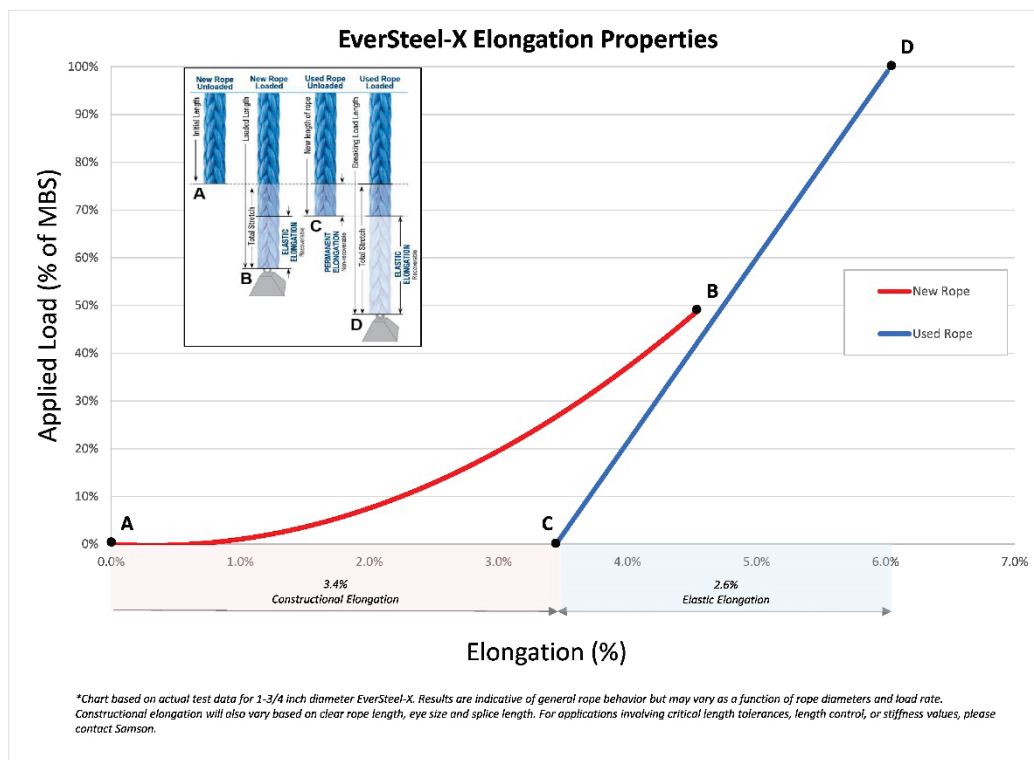
Constructional elongation (or stretch) is an inherent property of all multi-strand wound and/or braided cables. The phenomenon occurs in newly constructed steel and synthetic cables when tension is applied. As load is applied, gaps between the individual wires and strands close. This causes the cable to permanently elongate, producing a rope that is longer than it was initially.

Figure 65 is a plot showing load (percent of minimum breaking strength [MBS]) versus elongation for 1.75-in.-diam EverSteel™-X rope, i.e., the catenary rope used in the improved OCS prototype. The chart was provided by the rope manufacturer, Samson Inc. The new rope exhibits more stretch due to constructional elongation as the fibers reorient and compress together. After several load cycles, the used rope is longer and also stiffer.

Constructional elongation was considered during design of the improved OCS prototype. When the new rope for the prototype was purchased, a specification was included stating that the vendor was to remove constructional elongation via pre-stretching prior to shipment. The vendor did pre-stretch the rope, which apparently removed some but not all of the construction elongation. Some residual constructional elongation remained

in the 1,100-ft-long spool of rope used for the catenary. The vendor stated that their facility did not have the capability to tension the entire 1,100-ft-long, 1.75-in.-diam rope at one time. Instead, they had to tension the rope in sections. Furthermore, they were only able to load the rope to 50 percent of its minimum breaking strength (MBS). This likely contributed to residual construction elongation remaining in the rope. This lesson learned prompted a stricter constructional elongation removal specification given in Table 1 note 3. Team researchers believe that tensioning all new rope to 70 percent MBS for minimum of 10 cycles will remove all of the constructional elongation. However, this has not been confirmed. Additional laboratory testing would be required to fully understand constructional elongation and determine the optimal method for its removal.

Figure 65. Load versus elongation chart for 1.75-in.-diam EverSteel™-X rope provided by Samson Inc.



5.1.3 BSS tower modifications

Due to time and budget constraints, significant redesign of the legacy BSS tower was not feasible. However, some minor modifications were required to make the tower work with the improved OCS. Prior to fielding of the final modernized BSS kit, researchers recommend the following issues be

addressed with the tower baseplate and tower cap, both of which are described in the fabrication drawings by (Amato 2012).

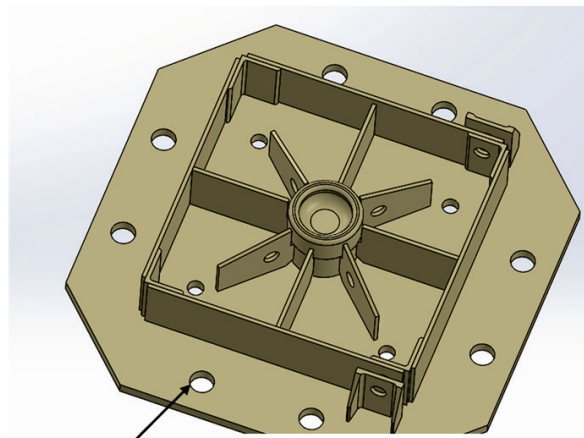
5.1.3.1 Tower baseplate

Two issues were identified with the tower baseplate. First, the diameters of the 8x thru holes had to be enlarged from 1.5 in. to 1.875 in. to accommodate the PE18 screw anchors

(<https://americaneearthanchors.com/products/ground-anchors-penetrators/>) used to anchor the baseplate to the ground. This modification is illustrated in Figure 66.

Figure 66. BSS tower baseplate modification.

Tower Baseplate



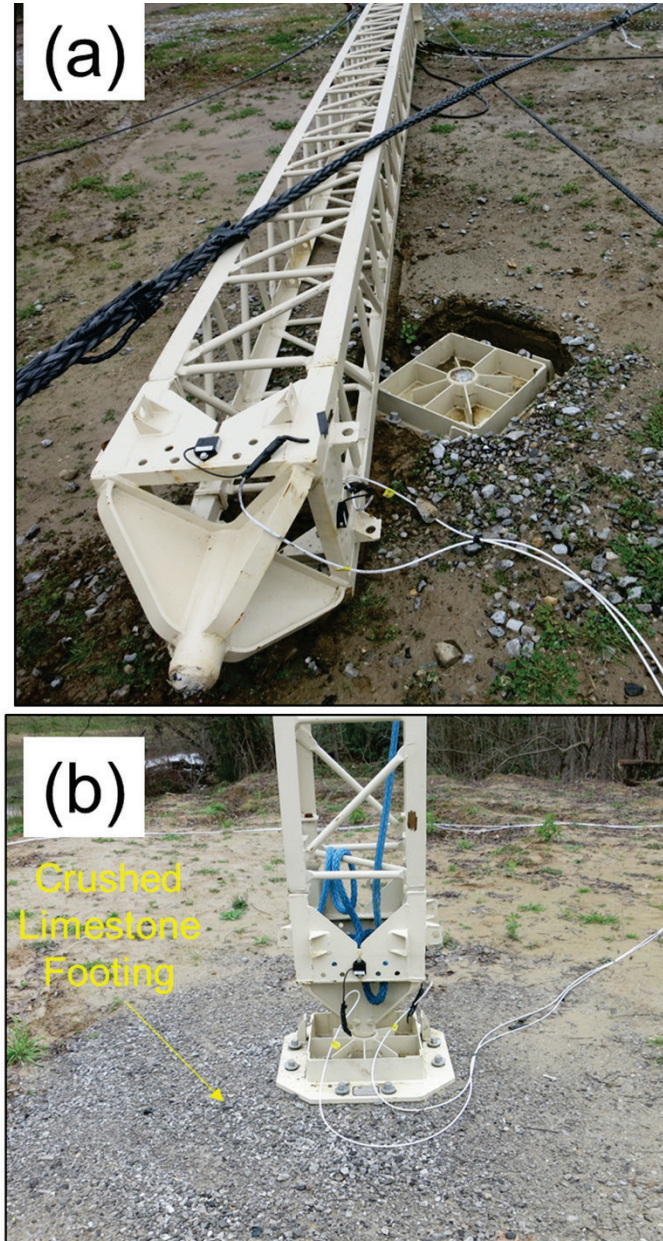
8x thru hole diameters enlarged from 1.5" to 1.875" to accommodate PE18 screw anchors

The second issue with the tower baseplate is related to the bearing pressure it exerts on the ground beneath. The tension in the OCS transmits a vertical, compressive force through the tower and onto the baseplate. The bearing pressure imposed on the soil beneath the baseplate equals that compressive force divided by the area over which it is distributed. As currently designed, the tower baseplate has a footprint of approximately 4.5 ft². The tower was found to have a compressive load capacity of about 100 kips (refer to section 3.3.2). Thus, the bearing pressure exerted on the ground through the baseplate could be as much as 155 psi (100 kips/4.5 ft²). This exceeds the bearing capacity of most soil types.

The baseplate may need to be enlarged or a footer and/or piling may be required to prevent the tower from sinking into the ground. This issue contributed to the improved OCS prototype failure mode. Recall from

section 4.2.1 the baseplate of tower #1, which was placed on virgin ground, sunk into the ground during prototype testing. However, the baseplate of tower #2, which was placed on a compacted crushed limestone footer, did not appreciably embed into the ground. Post-test photographs of the tower baseplates are shown in Figure 67.

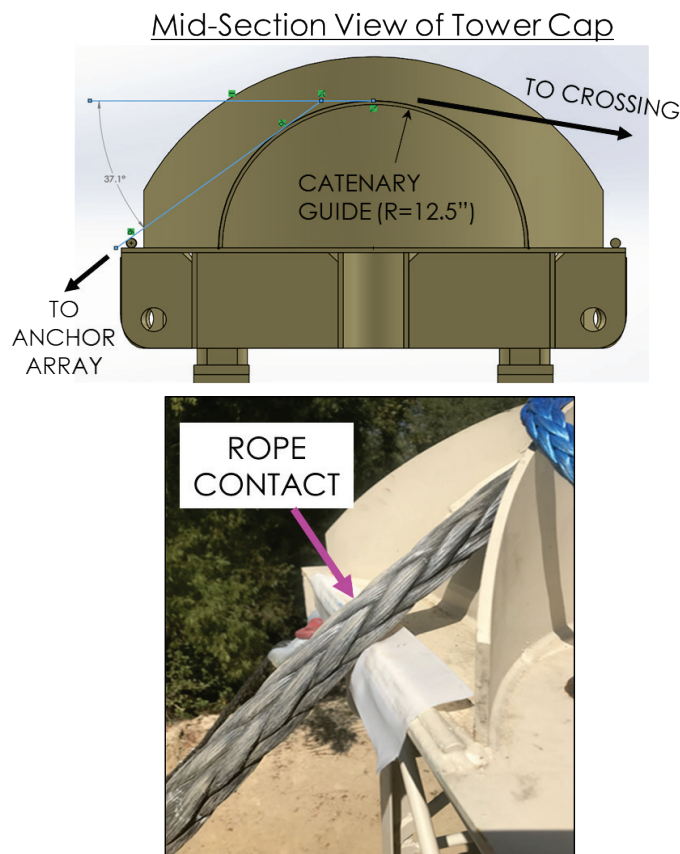
Figure 67. Post-test photographs of (a) tower 1 and (b) tower 2 baseplates.



5.1.3.2 Tower cap

Two issues with the legacy BSS tower cap were identified during prototype testing. The first involves the rope guide, which guides the catenary over the top of the tower and down to the anchor array. Per the legacy drawings, the rope guide is a 3/16" x 8.5" x 24.5" steel plate bent to a radius of 12.5". As currently designed, any rope departure angle in excess of $\sim 37^\circ$ causes the rope to contact the lip of the tower cap, which will produce undesirable eccentric loading on the tower. Figure 68 illustrates this issue.

Figure 68. Tower cap rope departure angle issue.

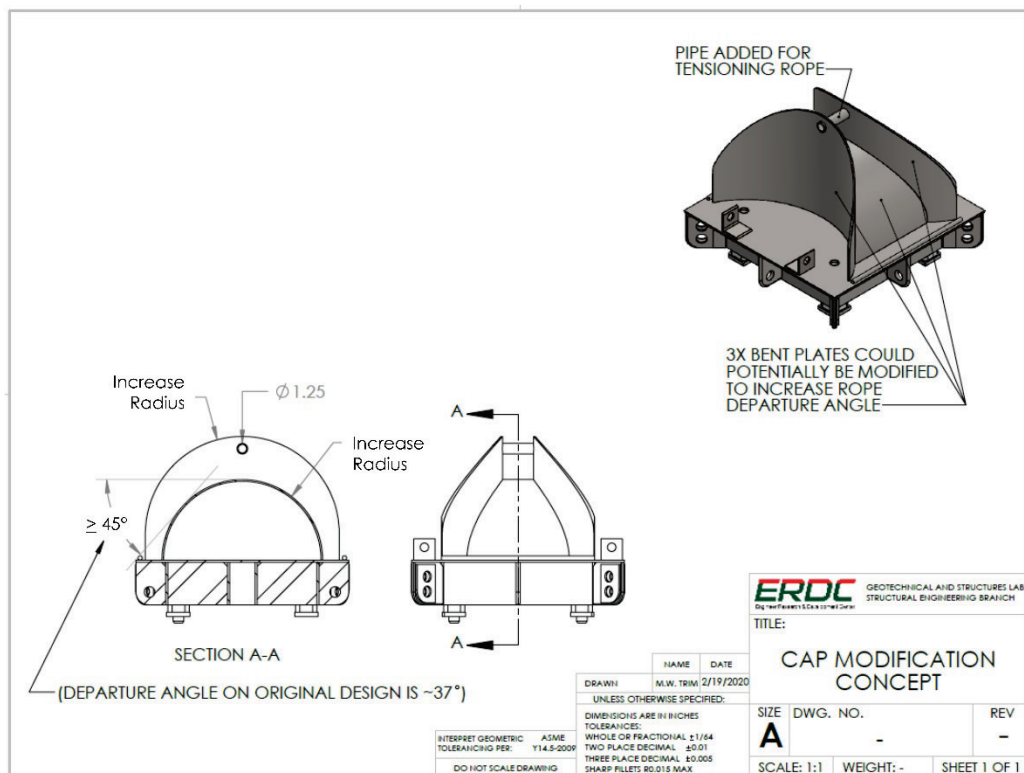


For the improved OCS prototype test, the anchor arrays were offset from the towers to achieve a 45° catenary departure angle. This is the maximum angle allowed in the Operator's Manual and was chosen because it represents a 'worst-case' condition. A shallower departure angle (with respect to the horizontal) will transmit less compressive force into the tower. The tradeoff is the footprint of the system is increased, since the anchors have to be placed farther from the tower to achieve the reduced angle. During field installations of the OCS, if the terrain can accommodate

an increased footprint, it is recommended to use as shallow of a departure angle as feasible. Decreasing the departure angle from 45° to 30° reduces the vertical force on the tower by a factor of 1.7 ($\tan(45^\circ) / \tan(30^\circ)$).

Decreasing the angle on the tower guys has similar benefits, as it allows the guys to carry a larger horizontal force component. In the prototype test, the tower guys had a 45° angle. For the 25.4-ft-tall tower, this corresponds to the anchor being 25.4 ft away (assuming perfectly flat ground). If the anchors were instead located 44 ft away, a 30° angle would result. This would significantly reduce the tension in the guy wires. If feasible, the final BSS kit should include ropes to accommodate 30° tower guys in addition to the ropes required for 45° guys. If increasing the footprint of the OCS to allow for smaller departure angles is deemed impractical, the tower cap may need to be redesigned so that the catenary rope does not contact the edge of the cap. This could be accomplished by increasing the bend radius on the plates forming the rope guide to make it taller. The concept is illustrated in Figure 69.

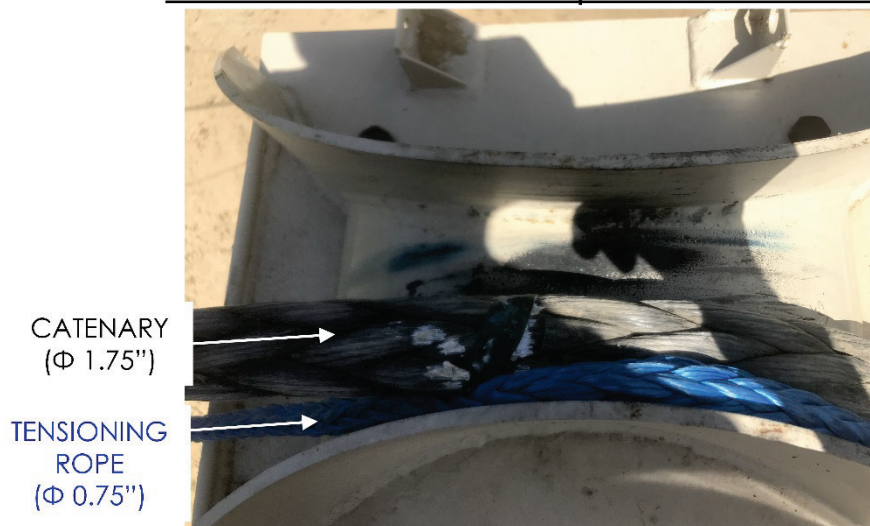
Figure 69. BSS tower cap modification concept.



The concept drawing in Figure 69 also shows the addition of a 1.25-in.-diam pipe above the rope guide. This feature addresses the second issue

related to the legacy tower cap -- the design is not ideal for the newly devised catenary tensioning method. The improved OCS catenary tensioning method was described in section 2.1 and illustrated in Figure 24. The tensioning rope is used to hold the tension due to the weight of the rope until the catenary can be connected to the anchor array. As currently designed, the tensioning rope and catenary have to go through the same rope guide. Since the two ropes follow the same path, the ropes get pinched, as shown in Figure 70. The modification shown in Figure 69 allows the tensioning rope to be routed over the 1.25-in-diam pipe, while the catenary is routed below the pipe, thus preventing interference. Redesign of the tower cap was beyond the scope of this work but is recommended prior to fielding of the final modernized BSS kit.

Figure 70. Catenary tensioning issue.
View of Tower Cap from Above



5.1.4 Differing bank heights

The bank height on each side of a river is an important factor in float bridge anchorage design. In the improved OCS prototype design, concentration was focused on meeting the requirements identified in the BSS CPD, i.e., a 689-ft (210-m) crossing and 11-ft/s current velocity. Due to the accelerated schedule and since no specific CPD requirement existed for differing bank heights, the issue was not initially addressed.

It is unknown whether the improved OCS prototype will work with uneven banks. During prototype evaluation, only equal bank heights were tested. Adding tower sections to increase tower height will produce a larger

eccentricity for a given angle of tilt. This will increase the load requirement on the guy cables. These effects have not been studied.

5.1.5 Approach guys and downstream anchorage

The OCS is the upstream anchorage system for the IRB, which holds the bridge in position against the force of the normal river current. This is the primary anchorage system, and its design is the most critical. The improved OCS prototype focused on this critical upstream anchorage design. However, two additional types of anchorage may be required to fully anchor the IRB, i.e., approach guys and downstream anchorage.

Approach guys are cables that prevent the bridge from being pushed away from the shore as a result of the impact of vehicles driving onto the ramps of the bridge. One end of each approach guy is attached to each side (upstream and downstream) of the first bay at both ends of the bridge. The other end of each approach guy is secured on the shore. Helical ground anchors similar to those used for the OCS could potentially be used to secure the approach guys to the shore. The approach guy cables should be made from the same lightweight synthetic rope used in the OCS.

Reverse currents, tidal conditions, eddies, and high winds may temporarily alter or reverse the natural flow of a river. In these conditions, a downstream solution is needed. Per the current IRB Operator Manual, shore guys should be attached to the bridge at regular intervals, and/or BEBs should be used to oppose these forces.

Approach guys and downstream anchorage solutions were beyond the scope of the current effort. However, we recommend the materials needed to implement these additional types of anchorage be included in the final modernized BSS kit. Also, better installation procedures for approach guys and downstream anchorage need to be developed. The manual provides very little information regarding the items.

5.1.6 Optimal OCS configurations for various crossings

The improved OCS prototype that was developed in this work was optimized for a 689-ft (210-m) crossing with river currents up to 11 ft/s. Developing optimal OCS configurations was beyond the scope of the current effort. A new table (similar to Figure 6) needs to be developed. Work will need to be done to determine the optimal number of helical anchors and the

optimal rope sizes for various crossing spans and current flows. A 1.75-in.-diam main anchor cable was chosen for the prototype, which was sized based on the 689-ft (210-m), 11-ft/s crossing conditions. The optimal rope size for other crossing conditions will vary. Longer spans will require larger rope. For shorter spans, smaller ropes may aptly carry the load.

5.1.7 Effects of vehicular loading on the OCS

Vehicular weight on the IRB increases the draft of the bridge and drag is directly related to the draft of the bridge. The effect of vehicles was not included in the BSS CPD requirements, so it was beyond the scope of the current work; however, future work is recommended. The work previously conducted by Trim and Padula (2020) could be leveraged. That study examined only the IRB; however, it could be expanded upon to include the OCS. Ideally, a table could be developed that lists permissible crossing conditions of the IRB with OCS for various crossing spans, river current velocities, and vehicular loading scenarios.

5.1.8 OCS scalability

A major shortcoming of the OCS is that it does not scale well. The prototype OCS design was optimized for a 689-ft (210-m) crossing and 11-ft/s current. The design is not as functional for longer or shorter spans with faster or slower currents. The issue stems from the fact that each individual IRB bay collects drag load; therefore, the addition or removal of bays directly affects OCS loading. A more universally applicable, scalable anchorage solution would be more modular, where the addition or removal of anchorage corresponds to the addition or removal of IRB bays.

One alternative to the OCS could possibly use spud anchors directly affixed to each IRB bay. Another alternative would be to add waterjet propulsion to the IRB itself. For extremely wide gaps greater than 210 m with relative fast-moving currents, a possible crossing solution might be to combine IRB bays with M3 amphibious bridges, where the propulsion of the M3s could be used to resist drag.

5.2 Conclusions

Key conclusions from this work include the following.

- An improved OCS prototype for a 689-ft (210-m) IRB crossing was designed, assembled, and structurally tested. During system-level testing, the improved OCS prototype performed well up to 40.5 kips of simulated drag load, which corresponds to a uniformly distributed current velocity of 10.7 ft/s. Under this load, the tension in the catenary measured 74 kips, and the compressive load on the tower was 73 kips.
- If a more realistic parabolic velocity distribution is assumed instead of a uniform distribution, the drag load for an 11-ft/s current is 21.1 kips. Under this assumption, the improved OCS prototype has a factor of safety of 1.9 based on a 689-ft (210-m) crossing and 11-ft/s current.
- An assembly schematic of the improved OCS prototype was provided in Figure 25. Tables 1-3 comprise the bill of materials.
- A component-level compression test of the legacy BSS Class 60 tower was executed to determine its load capacity and failure mode. Under simple, quasi-static, compressive loading, the BSS tower capacity was determined to be 102 kips. The failure mode was localized buckling in the legs of the tower section.
- During system-level prototype testing, the upstream, outermost tower guy lines ('G1-1' and 'G2-1' in Figure 46) experienced the highest loads and ultimately dictated the failure mode of the system. The 'G1-1' anchor pulled out when the tension on that cable reached 22.6 kips. This pullout load is highly dependent on soil conditions so it will vary by location. Helical anchor load capacity is related to installation torque. The relationship can be found in Hubbell Power Systems (2018). During field OCS installations, we recommend measuring installation torque and documenting the estimated pullout load for each helical anchor.
- The following issues with the OCS prototype were identified. Researchers recommend addressing these issues prior to fielding the modernized BSS.

- Helical anchors were unable to penetrate all soil types (refer to section 5.1.1).
- Synthetic rope exhibited excessive constructional elongation (refer to section 5.1.2).
- The legacy BSS tower cap and baseplate required modifications (refer to section 5.1.3).
- The soil under tower 1 lacked sufficient bearing capacity to prevent the tower from sinking into the ground. Development of a procedure to test soil-bearing capacities in the field is recommended. Certain sites might require footings be prepared prior to tower erection (refer to section 5.1.3.2).
- Differing bank heights were not addressed (refer to section 5.1.4).
- Approach guys and downstream anchorage solutions were not developed (refer to section 5.1.5).
- Optimal OCS configurations for various crossings were not determined (refer to section 5.1.6).
- Effects of vehicular loading on the OCS were not quantified (refer to section 5.1.7).
- The OCS has inherent scalability issues (refer to section 5.1.8).
- The IRB Operator's Manual Work Package WPO035 needs a thorough revision prior to fielding the final modernized BSS kit. The following issues are not currently addressed in the manual.
 - Detailed assembly and installation procedures for the improved OCS prototype need to be developed.
 - A method needs to be developed to accurately measure current velocity in the field. Tossing an empty bottle into a river and measuring the time, t , it takes the bottle to travel a distance, d , downstream can technically be used to calculate a velocity ($v = d/t$). However, this rudimentary method can give grossly inaccurate results. It is unlikely that the current velocity at the location of the bottle toss is constant across the entire river. The total drag force on an IRB is a function of the velocity profile across the river.
- A bridge protection device for the IRB needs to be developed. Without protection, any debris floating downstream will collect along the leading edge of the IRB. This will likely lead to increased drag, which could cause premature OCS failure.

- Due to time and budget constraints, the improved OCS prototype had to make use of the legacy BSS Class 60 towers. If a future OCS redesign is feasible, perhaps the legacy towers can be redesigned or potentially removed from the system all together. Such a redesign would require significantly more work, but it would greatly simplify OCS installation while also negating the need to cut and splice a specific length of the 1.75-in.-diam catenary rope.

References

- Amato, J. 2012. *U.S. Army Tank Automotive & Armaments Command*. DWG No. 12565632 - Class 60 bridge support. Warren, MI: TACOM..
- ATEC. 2002. *Test report for the Improved Ribbon Bridge Limited User Test (IRB LUT)*. 2002-LU-E/CS-1966. Fort Hood, TX: U.S. Army Operational Test Command.
- _____. 2003. *System evaluation report of the Improved Ribbon Bridge (IRB)*. Alexandria, VA: U.S. Army Test and Evaluation Command.
- Bryant, D. B., J. Sharp, and C. Kees. 2019. *Hydrodynamics of the Improved Ribbon Bridge: Physical model testing*. ERDC/CHL TR-19-24. Vicksburg, MS: U.S. Army Engineer Research and Development Center.
- Headquarters, Department of the Army. 1988. *Military float bridging equipment, TC 5-210*. TC5-210. Washington, D.C.: Department of the Army.
- _____. 2003a. *Operator's manual for Improved Ribbon Bridge (IRB), change No. 1, TM 5-5420-278-10*. TM 5-5420-278-10. Washington, D.C.: Department of the Army and the Air Force.
- _____. 2003b. *Operator's manual for Improved Ribbon Bridge (IRB), change No. 1, TM 5-5420-278-10, Work Package WP 0035: Bridge anchorage*. TM 5-5420-278-10. Washington, D.C.: Department of the Army and the Air Force.
- Hubbell Power Systems Inc. 2018. *CHANCE technical design manual*. Centralia, MO: HPS.
- Mejias-Santiago, M. 2018. *ENDEX - Evaluation of ground anchorage for Improved Ribbon Bridge (iRB) Overhead Cable System (OCS)*. Memorandum for record. Vicksburg, MS: U.S. Army Engineer Research and Development Center.
- MSCoE, U.S. Army. 2014. *Capability production document for (U) Bridge Supplementary Set (BSS), Increment I*. Catalog of Approved Requirements Documents (CARDS) # 06095. Fort Leonard Wood, MO: Maneuver Support Center of Excellence.
- Samson Rope Technologies EverSteel-X. 2020.
<https://www.samsonrope.com/mooring/eversteel-x>.
- Trim, M. W., and J. A. Padula. 2020. Structural analysis of an Improved Ribbon Bridge subjected to hydrodynamic and vehicular loading. ERDC/GSL TR-20-13. Vicksburg, MS: U.S. Army Engineer Research and Development Center.

Unit Conversion Factors

Multiply	By	To Obtain
degrees (angle)	0.01745329	radians
feet	0.3048	meters
foot-pounds force	1.355818	joules
inches	0.0254	meters
inch-pounds (force)	0.1129848	newton meters
kip (force)	4448.2216	newtons
microinches	0.0254	micrometers
microns	1.0 E-06	meters
pounds (force)	4.448222	newtons
pounds (mass)	0.45359237	kilograms
square inches	6.4516 E-04	square meters
tons (2,000 pounds, mass)	907.1847	kilograms

REPORT DOCUMENTATION PAGE

Form Approved
OMB No. 0704-0188

Public reporting burden for this collection of information is estimated to average 1 hour per response, including the time for reviewing instructions, searching existing data sources, gathering and maintaining the data needed, and completing and reviewing this collection of information. Send comments regarding this burden estimate or any other aspect of this collection of information, including suggestions for reducing this burden to Department of Defense, Washington Headquarters Services, Directorate for Information Operations and Reports (0704-0188), 1215 Jefferson Davis Highway, Suite 1204, Arlington, VA 22202-4302. Respondents should be aware that notwithstanding any other provision of law, no person shall be subject to any penalty for failing to comply with a collection of information if it does not display a currently valid OMB control number. **PLEASE DO NOT RETURN YOUR FORM TO THE ABOVE ADDRESS.**

1. REPORT DATE (DD-MM-YYYY) March 2021		2. REPORT TYPE Final		3. DATES COVERED (From - To)	
4. TITLE AND SUBTITLE Modernization and Structural Evaluation of the Improved Overhead Cable System				5a. CONTRACT NUMBER	
				5b. GRANT NUMBER	
				5c. PROGRAM ELEMENT NUMBER	
6. AUTHOR(S) M. Wesley Trim, Matthew P. Murray, and C. Kennan Crane				5d. PROJECT NUMBER	
				5e. TASK NUMBER	
				5f. WORK UNIT NUMBER	
7. PERFORMING ORGANIZATION NAME(S) AND ADDRESS(ES) Geotechnical and Structures Laboratory U.S. Army Engineer Research and Development Center 3909 Halls Ferry Road Vicksburg, MS 39180-6199				8. PERFORMING ORGANIZATION REPORT NUMBER ERDC/GSL TR-21-4	
9. SPONSORING / MONITORING AGENCY NAME(S) AND ADDRESS(ES) U.S. Army, PdM Bridging 6501 East 11 Mile Road Warren, MI 48397-5000				10. SPONSOR/MONITOR'S ACRONYM(S)	
				11. SPONSOR/MONITOR'S REPORT NUMBER(S)	
12. DISTRIBUTION / AVAILABILITY STATEMENT Approved for public release; distribution is unlimited.					
13. SUPPLEMENTARY NOTES MIPR 11326139					
14. ABSTRACT A modernized Overhead Cable System (OCS) prototype for a 689 ft (210 m) Improved Ribbon Bridge (IRB) crossing was designed, assembled, and structurally tested. Two independent structural tests were executed, i.e., a component-level compression test of the BSS tower was performed to determine its load capacity and failure mode; and a system-level 'dry' test of the improved OCS prototype was conducted to determine the limit state and failure mode of the entire OCS. In the component-level compression test of the BSS tower, the compressive capacity was determined to be 102 kips, and the failure mode was localized buckling in the legs of the tower section. During system-level testing, the prototype performed well up to 40.5 kips of simulated drag load, which corresponds to a uniformly distributed current velocity of 10.7 ft/s. If a more realistic, less conservative parabolic velocity distribution is assumed instead, the drag load for an 11 ft/s current is 21.1 kips. Under this assumption, the improved OCS prototype has a factor of safety of 1.9, based on a 689-ft crossing and 11-ft/s current. The OCS failed when one of the tower guy wires pulled out of the ground, causing the tower to overturn.					
15. SUBJECT TERMS					
Military bridges		Structural analysis (Engineering)		Anchorage	
Stream crossing		Transportation		Bridge Supplemental Set	
Stream crossing, Military		Transportation, Military		Overhead Cable System	
		Improved Ribbon Bridge		Military bridges—Cables	
		Anchorage (Structural engineering)			
16. SECURITY CLASSIFICATION OF:			17. LIMITATION OF ABSTRACT	18. NUMBER OF PAGES	19a. NAME OF RESPONSIBLE PERSON
a. REPORT	b. ABSTRACT	c. THIS PAGE			19b. TELEPHONE NUMBER (include area code)
Unclassified	Unclassified	Unclassified	SAR	97	

